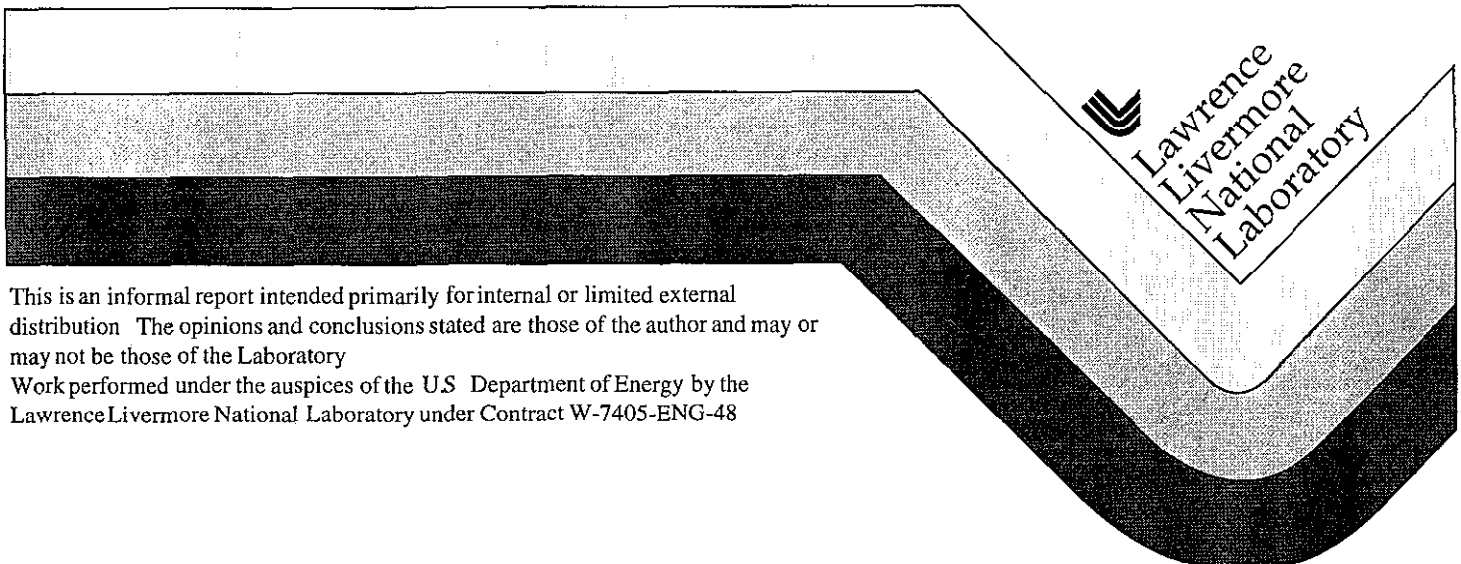


New Monte Carlo Simulations of the LLNL Pulsed-Sphere Experiments

A A Marchetti
G W Hedstrom

July 1, 1998



This is an informal report intended primarily for internal or limited external distribution. The opinions and conclusions stated are those of the author and may or may not be those of the Laboratory.

Work performed under the auspices of the U.S. Department of Energy by the Lawrence Livermore National Laboratory under Contract W-7405-ENG-48

DISCLAIMER

This document was prepared as an account of work sponsored by an agency of the United States Government. Neither the United States Government nor the University of California nor any of their employees, makes any warranty, express or implied, or assumes any legal liability or responsibility for the accuracy, completeness, or usefulness of any information, apparatus, product, or process disclosed, or represents that its use would not infringe privately owned rights. Reference herein to any specific commercial product, process, or service by trade name, trademark, manufacturer, or otherwise, does not necessarily constitute or imply its endorsement, recommendation, or favoring by the United States Government or the University of California. The views and opinions of authors expressed herein do not necessarily state or reflect those of the United States Government or the University of California, and shall not be used for advertising or product endorsement purposes.

This report has been reproduced
directly from the best available copy.

Available to DOE and DOE contractors from the
Office of Scientific and Technical Information
P.O. Box 62, Oak Ridge, TN 37831
Prices available from (615) 576-8401, FTS 626-8401

Available to the public from the
National Technical Information Service
U.S. Department of Commerce
5285 Port Royal Rd.,
Springfield, VA 22161

NEW MONTE CARLO SIMULATIONS OF THE LLNL PULSED-SPHERE EXPERIMENTS

Alfredo A. Marchetti and Gerald W. Hedstrom

Nuclear Data Group
Lawrence Livermore National Laboratory

July, 1998



INTRODUCTION

From the late 1960s to about 1985, the Pulsed-Sphere Program¹⁻³ at Lawrence Livermore National Laboratory (LLNL) was carried out to measure 14-MeV neutron leakage spectra from target spheres made out of various elements, compounds, and mixtures. Data from these experiments have been and continue to be fundamental in the evaluation of neutron Monte Carlo transport codes and cross section data libraries. In addition, the data provide important integral information for stockpile stewardship, fusion technology, neutron therapy, and other applications. Therefore, comparisons between computer Monte Carlo simulations and the results of these experiments are pivotal for the integral testing of processed nuclear data libraries and transport codes.

Fortunately, a large subset of data from the pulsed-sphere program (some 70 experiments) is available as a computer file called *disp93in*. Furthermore, in the past few years, there has been a remarkable improvement in computer performance that allows for more realistic simulations by Monte Carlo codes such as TART.⁴ Previous TART simulations of the pulsed-sphere experiments were performed using simplified models with relatively small numbers of histories and very large solid angle detectors to offset the limitations in computer power. Also, not all the TART input files were created with the same level of detail. For example, some input files included the air around the sphere while others did not. These factors prompted a study to simulate in more detail all of the available pulsed-sphere experiments using the Monte Carlo transport code, TART, and the LLNL evaluated neutron data library, ENDL. The timing of this study is significant because many years have passed since those experiments were done, and only a few people who participated in them are still working at LLNL. Their help has been essential for an accurate documentation of the experiments. For the Stewardship Program it is important to preserve and make use of as much

of the data as possible, because it represents a unique resource and an enormous effort that would be very costly to reproduce

The initial part of this study consisted of an analysis of the experimental setup and neutron source characteristics necessary to create the foundation for a TART input file. The next task was to create the input files for the various experiments by incorporating particular settings, such as flight path, sphere materials and dimension, etc., to the basic TART input. The results of the TART simulations of these experiments will be used to help assess the quality of evaluated data currently in ENDL. Further, other nuclear libraries, e.g., ENDF/B-VI, JENDL-3, and JEF-2, will be used in the Monte Carlo simulations after being reformatted for TART and other Laboratory codes. Finally, this work will be part of the integral check of the new evaluations being prepared for the Stewardship Barn Book by the LLNL Nuclear Data Group.

EXPERIMENTAL AND SIMULATED SETUP

The pulsed-sphere experiments were performed at the now-decommissioned ICT (Insulated Core Transformer) accelerator at LLNL. The facility consisted of a 12.2-m cubic target pit with ~2-m thick concrete walls connected to a separate detector room by a tunnel in which a cylindrical collimator was inserted. The target sphere was located close to the center of the target pit. Mass near the sphere and detector was kept to a minimum to reduce background scattering. The spheres had conical openings to allow the neutron source to be centered in the sphere. Neutrons at a nominal energy of 14 MeV were generated via the $^3\text{H}(\text{d},\text{n})^4\text{He}$ reaction by a 400-keV deuteron beam impinging on a tritiated titanium target. The deuteron beam line formed a 26° angle with the floor. Therefore, the detector was situated 26° from the deuteron beam line as shown in Fig. 1. Further details are given in Ref. 1.

In the TART calculations the deuteron beam axis was chosen as the reference z-axis with the

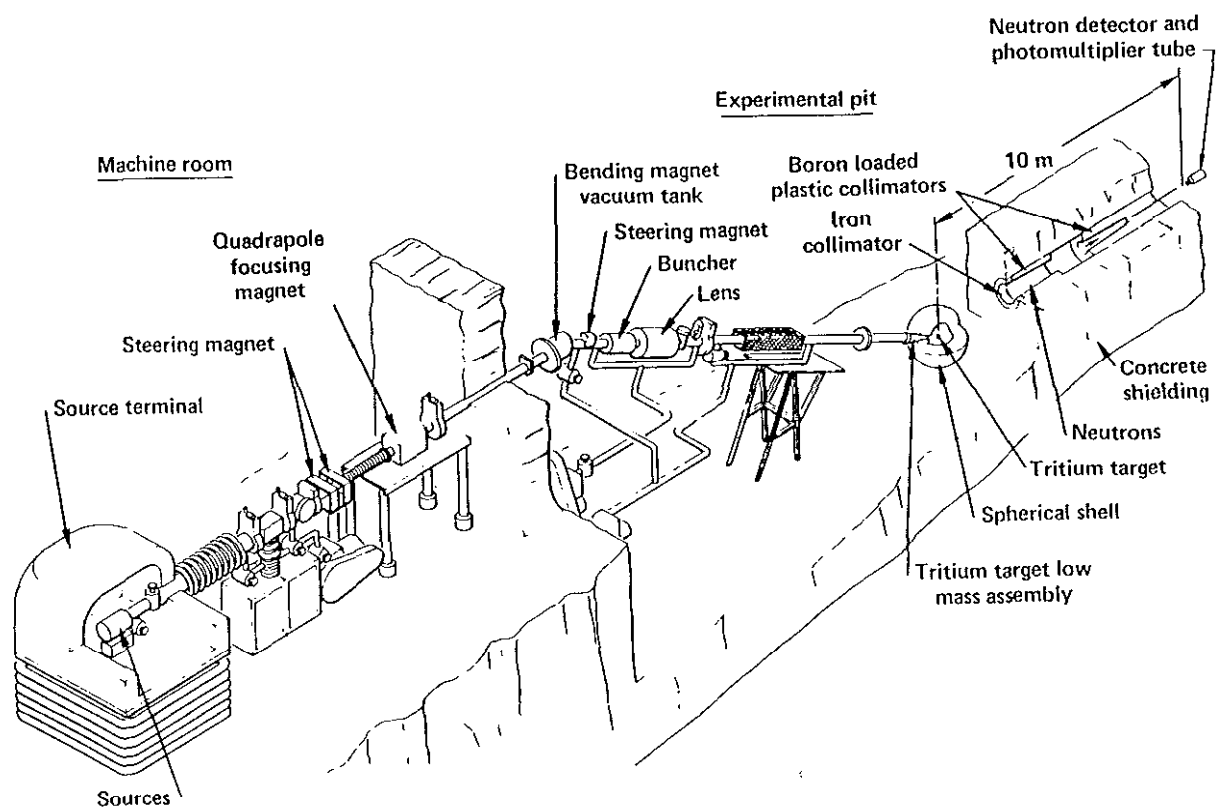


Fig. 1. Schematic view of accelerator, beam transport, target sphere, collimator, and detector assembly—not to scale

origin at the center of the sphere (and source) The detector was defined as the intersection volume between two forward cones and two spheres, all centered at the target sphere, thereby making a conical ring. The inner spherical surface of this ring had its radius equal to the flight path, and the outer one had a 5-cm longer radius The conical surfaces of the detector ring formed 25° and 27° angles with the z-axis, respectively The concrete wall that separated the target pit from the detector room was simulated as a hemisphere with thickness equal to the wall thickness This concrete hemisphere had a conical slot to simulate the collimator aperture, with an air gap from 25° to 27° from the z-axis. The collimator was modeled as two conical rings astride this air gap. The details of the collimator were taken from Fig 3 of Ref 1, keeping the radial lengths presented in the figure but replacing the cylinder with cones to match the symmetry of the ring detector The back wall of the detector room was also represented by a hemispherical concrete shell

The reason for using a conical ring detector was that initial test computations with a more realistic cylindrical detector required an exorbitant amount of computer time because of the small solid angle subtended by the detector used in the experiments. One disadvantage of our conical ring collimator is that it accepts all neutrons which are nearly tangent to the ring We therefore implemented a filter to reject neutrons coming into the detector from those directions The main effect of the filter is to eliminate neutrons scattered by the air in the target room.

Also, for the TART calculations, an idealized tritium target assembly was included to represent the mass close to the target sphere This assembly was taken from Fig. 6 of Ref 1 as interpreted by E. F. Plechaty. A diagram of this model setup is presented in Fig 2

In an effort to evaluate the differences between the conical ring collimator and detector used in TART and the cylindrical ones actually used in the experiment, we made computations for tantalum and beryllium spheres using the collector-surface option in TART. Using this option, the

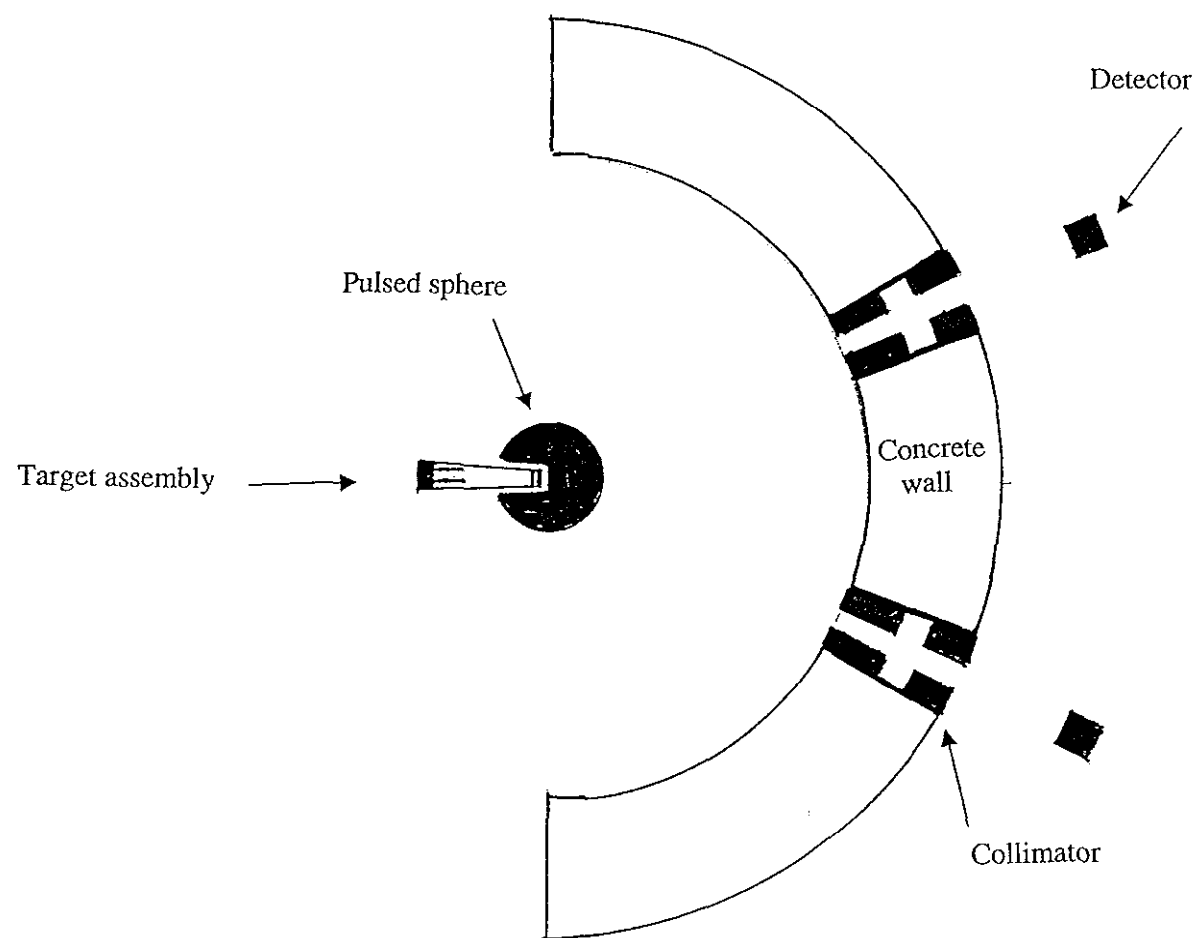


Fig. 2. Schematic view of a z-y section of the model setup—not to scale

code collected the neutrons entering a conical ring and moved them to the front of a cylindrical collimator. Thus, we took advantage of the symmetry of the problem to get a very realistic representation of the experimental collimator and detector while sampling a much larger solid angle. The differences collector-surface calculations and the ring setup were not statistically significant. In addition, the computation time for the collector-surface option was too long to justify its use for all of the spheres.

Specifically, for the Ta sphere with a radius of 1.0 mean free path ($r=3.4$ cm), the detector was located about one meter from the back of the concrete wall. Computations based on the conical ring collimator and detector without filter showed that around 0.4% of the neutrons scattered from the collimator. On the other hand, the calculation with the collector-surface option showed approximately 0.1% of the neutrons scattering from the cylindrical collimator. Scattering from the air in the target room contributed about 1% in the case of the ring collimator, but the collector-surface option did not allow this comparison. Overall, the difference between a ring and a cylindrical setup seems a minor effect, particularly since about 2.5% of the neutrons counted come from scatters in the target assembly, which is a gross simplification of the apparatus used in the experiment. However, we implemented a filter to correct for this effect.

We made an analogous comparison in the case a beryllium sphere with radius of 3.5 mean free path ($r=27.94$ cm). This case differs from the tantalum one, because the detector was situated very close to the concrete wall and collimator. The collector-surface calculation showed that about 10% of the neutrons counted came from scatters in the collimator, evidently because the detector was practically right next to it. In this case, the computation with the conical ring detector estimated the number of neutrons arriving from the collimator at about 3%. Fortunately, the tantalum

experiment is more representative, because for most of the spheres the detector was situated well back from the concrete wall

CALCULATION OF THE NEUTRON ENERGY SPECTRUM

The experimental neutron source was a tritium-loaded titanium target bombarded with 400-keV deuterons. The tritium was absorbed in a titanium disk that was thick enough to stop all the deuterons. For the case of a thin target where there is negligible beam attenuation, the neutron generation rate (R) is given by the equation

$$R = \phi \sigma N_t \quad (1)$$

where ϕ is the deuteron flux, σ is the reaction cross section, and N_t the number of tritium nuclei. In the pulsed-sphere experiments, the deuteron beam lost energy and intensity in the target until it was stopped completely. Therefore, the cross section and flux terms in (1) were not constant and had to be integrated for modeling purposes

The approach used was to divide the target into thin slices where Eq. 1 should be valid and to determine the number and energies of a given initial number of deuterons as they pass through consecutive slices. A relative spectrum could then be calculated using the cross section and angular distribution as weight factors for the neutron production corresponding to the deuterons in each slice. For this calculation, it was assumed that the tritium distribution in the target was homogeneous and remained constant

The Monte Carlo code TRIM⁵ was used to determine the energy and number of deuterons transported through targets of systematically-increasing thickness. The target was defined as a mixture of titanium and hydrogen in an atomic ratio 1:1, hydrogen was used in place of tritium that was not available as target material in the TRIM code. The code calculated a density of 2.295 g/cm³ for this material. The target thickness was varied from 0.05 to 485 μm in increments of 0.05

μm . For each thickness, 1000 particle histories were run and a file was created containing the space coordinates and energy for each deuteron transmitted. Because the density of the target was arbitrarily estimated by the code, the location given by the thickness along the beam axis was arbitrary. However, the target thickness was practically zero compared to the dimensions of the experimental setup and, as mentioned above, it was assumed that the tritium was homogeneously distributed in the target. The relevant information to calculate the source spectrum in this case was the relative number and energy of the deuteron particles and not their physical location along the beam axis. The file of transported deuterons created with TRIM contained a total of 88605 deuterons characterized by their space coordinates and energies.

We used these data to calculate the energy spectrum of the neutron source. First, given the energy for each transmitted deuteron, the cross section of the ${}^3\text{H}(\text{d},\text{n}){}^4\text{He}$ reaction was evaluated by search and interpolation in an electronic file obtained from the National Nuclear Data Center.⁶ These cross sections were used as weight factors to estimate the relative neutron yield. For each deuteron, a non-relativistic kinematics calculation⁷ was performed to determine the corresponding neutron energy at all possible laboratory emission angles, i.e., varying the neutron angle cosines between 1 and -1 at 0.1 cosine increments. The relative laboratory angular distribution of the neutrons was included as another weight factor for the relative yield. Published data⁸ for these distributions are displayed in Fig. 3 as a function of the cosine in the laboratory system for 200 and 500 keV deuterons.

For each deuteron energy and neutron cosine, the relative angular distribution was calculated by linear interpolation using the data of Fig. 3 and assuming an isotropic distribution at the zero energy limit. This number multiplied by the corresponding cross section became the final weight factor for that particular neutron. Finally, a routine sorted all the neutron weight factors into 36

Angular distributions for $^3\text{H}(\text{d},\text{n})^4\text{He}$

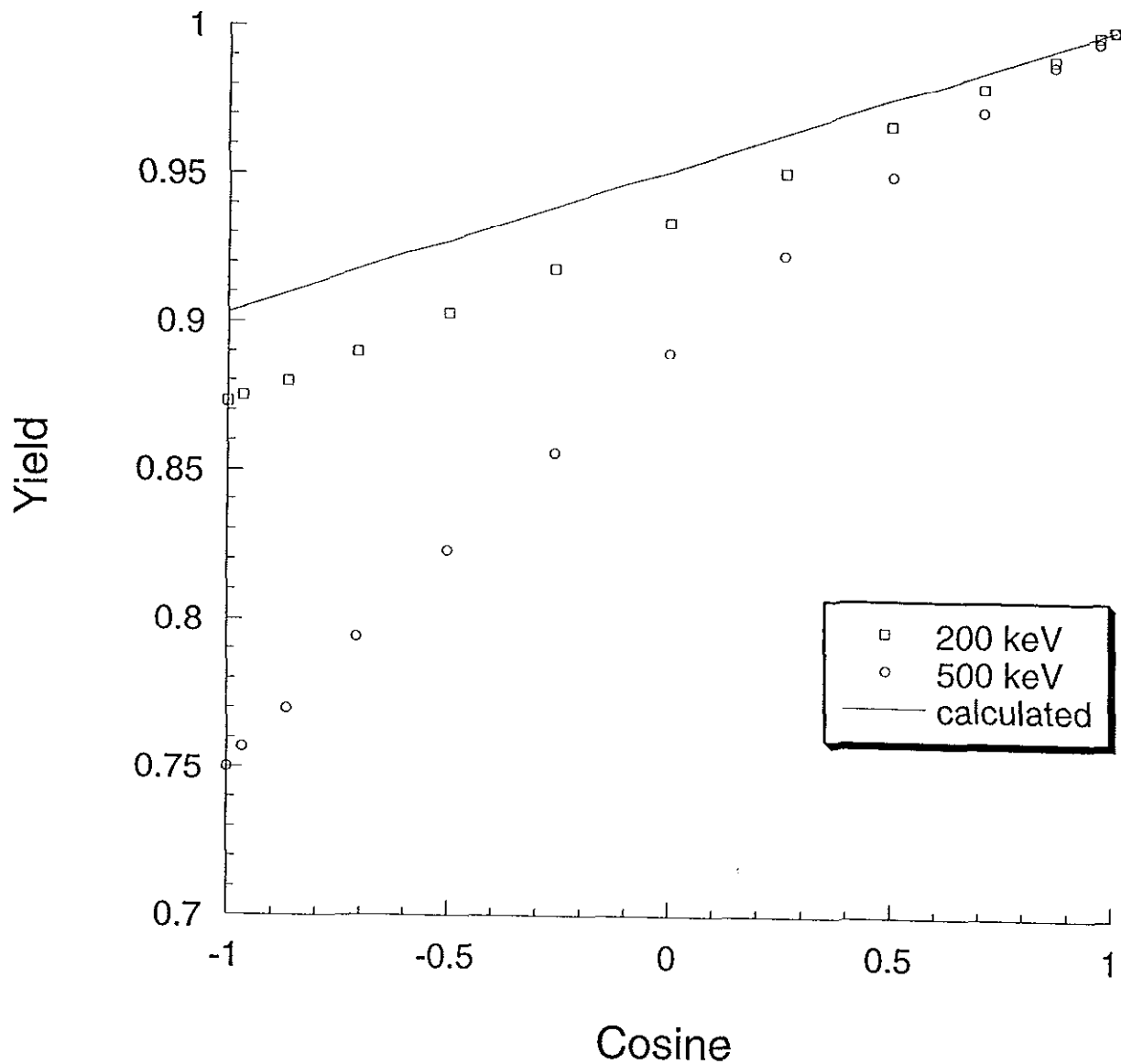


Fig. 3. The circles and squares represent experimental relative angular distributions as a function of laboratory cosine for 200 and 500 keV deuterons, respectively. The solid line represents the calculations presented in this report for 400 keV deuterons impinging on a thick tritiated titanium target. Because of the energy loss in the thick target, the calculations are dominated by the 100 keV resonance cross section

energy bins from 12.4 to 16.0 MeV at 0.1 MeV increments for each of the 21 laboratory cosines. The end result was a 36 by 21 matrix model of the energy spectrum of the experimental source that was later edited for TART input. The angular distribution for this source, calculated relative to 0° , is represented as a solid line in Fig. 3. It would be expected that, at 400 keV of beam energy, the angular distribution should fall between those at 200 and 500 keV. However, because of the kinetic energy loss in the thick target, the yield is dominated significantly by the weight of the cross section that peaks at around 100 keV. To illustrate this point, according to TRIM calculations, the beam intensity remains at about 90% of the original after its average energy has decreased to about 20 keV. Therefore, the flux in Eq. (1) remains more or less constant for most of the energy range and the yield is determined mostly by the cross section function. A surface plot of the calculated neutron spectrum is shown in Fig. 4 and represents the relative yield as a function of energy and laboratory cosine. For each cosine bin, the average neutron energy of the source was calculated as a particle-weighted average and was found to correspond kinematically to a deuteron energy in the range between 150 and 200 keV. This is in fair agreement with experimental measurements that indicated 200 keV as the most probable deuteron reaction energy.¹

MODEL CALCULATION AND ANALYSIS

The model of the experimental setup and neutron source described in the preceding sections was common to all the TART input files. The input for each experiment was prepared by adding the sphere details to this basic file and editing the flight path value. The geometry, composition, and other details necessary to model the spheres were obtained from different sources. A number of them have been diagrammed in Ref. 1. Some of the diagrams had information such as composition, density and/or mass. Other spheres were described in papers or reports. Some of these descriptions included a diagram, geometrical parameters, mass, density and/or composition. Also,

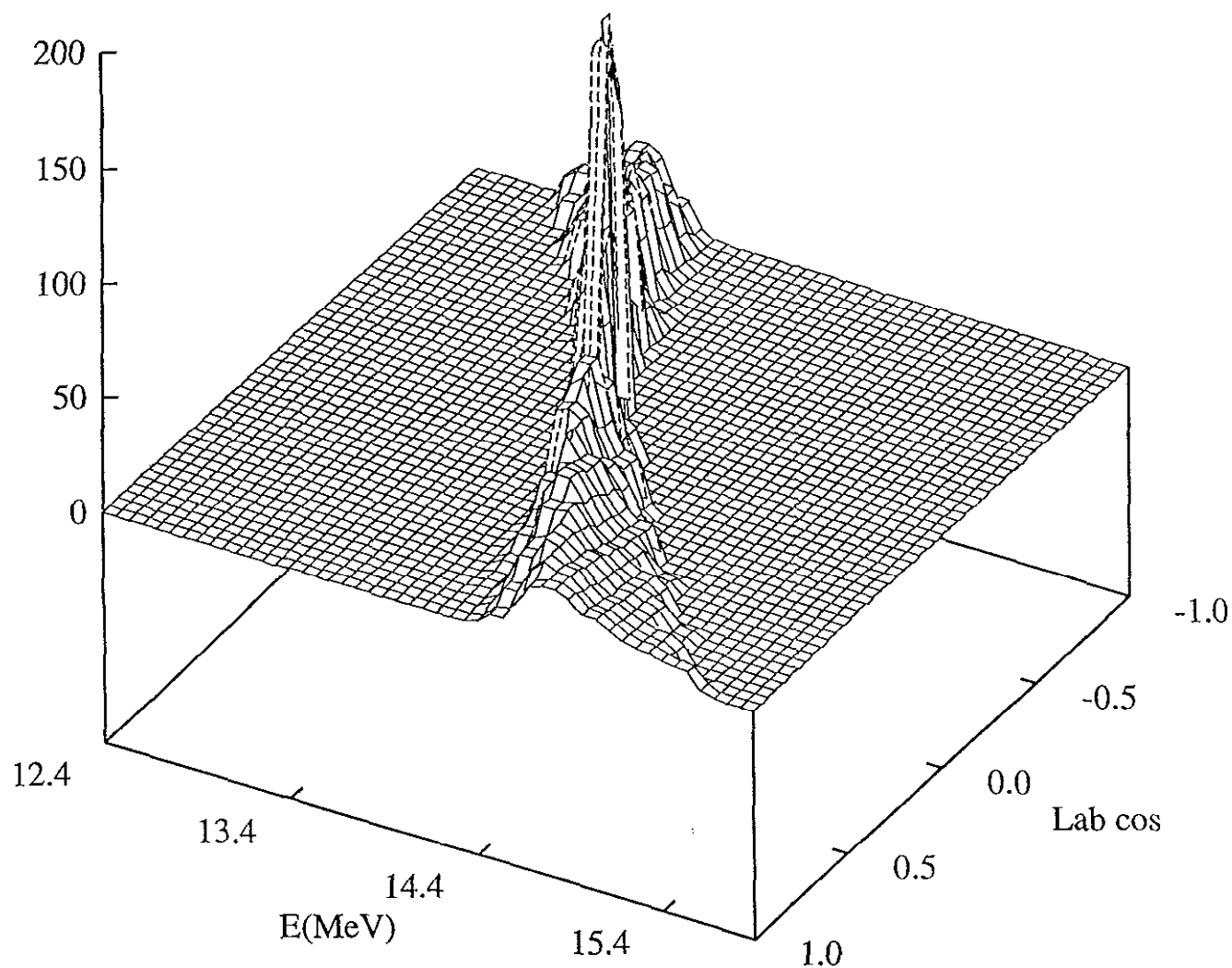


Fig. 4. Surface plot of the calculated neutron spectrum as a function of energy and laboratory cosine for the reaction ${}^3\text{H}(\text{d},\text{n}){}^4\text{He}$ at 400 keV in a thick tritiated titanium target.

earlier input files were used to extract information as needed. Occasionally, reported masses for the spheres were not in agreement with density-volume calculations. In these situations the mass and density of the sphere were assumed correct and, in most cases, very slight adjustments in the geometry were sufficient to reproduce the reported mass.

In January 1997, we held a meeting with most of the investigators who carried out the pulsed-sphere measurements and calculations (J D Anderson, R Bauer, L F Hansen, R J Howerton, E. F Plechaty, and B A. Pohl) We discussed various experimental aspects and to help verify that assumptions made were as reasonable as possible within the limits of “corporate memory” The consensus from this meeting was that the measurements should be reliable to about 7% Regarding the experimental setup, the use of various collimators was discussed and the collimator shown in Fig 3 of Ref 1 can be considered representative, but not necessarily the actual one used in a given experiment The criterion employed to choose a collimator was that the sphere in question should be viewed in its entirety by the detector The collimator representation used in the TART input file fulfills this criterion for all but two of the experiments (liquid air and liquid nitrogen with \sim 1-m radius sphere) In these two cases, the collimator in the TART input file was modified to view the whole sphere according to the diagram shown in Fig. 1 of Ref 9.

A flight path of 722 cm is indicated for several beryllium and polyethylene pulsed-sphere experiments in the *disp93in* file With the TART representation of the wall and collimator common to all the spheres, this flight path would place the detector inside the collimator According to L. Hansen, such arrangement was never implemented At most, the detector could have been placed at close proximity of the collimator back but not inside. The thickness of the collimator (and wall) calculated using Fig 3 from Ref 1 was 202 cm. From the center of the sphere to the face of the collimator the distance was 524 cm, adding to a total of 726 cm Therefore the discep-

ancy is only a few centimeters. However, Ref 10 indicates a flight path of 728 cm for the beryllium experiments. Since this flight path is consistent with the experimental data and setup, we concluded that the header value should be incorrect and changed it from 722 to 728 cm for all the corresponding experiments.

The code PSEdit

Currently, the computer code PSEdit¹¹ is used to analyze the output of the TART calculations of pulsed-sphere experiments. The purpose of this code is to fold the experimental factors into the calculations to allow a direct comparison to the experimental results. First, the PSEdit code reads the *input* file for the user options. One of the options is the header identification number of the experiment that PSEdit uses to read the experimental data from the *disp93in* file. The experimental data consist of the detector counts and standard deviation as a function of time-of-flight in nanoseconds. The counts per nanosecond are normalized per source neutron.

APPENDIX A lists the header identification numbers found in the *disp93in* file. In addition, there is the name of the input file created for the TART simulation and comments and references used to model the particular sphere. Note that APPENDIX A has a **separate list** of references of its own. Each header of the *disp93in* file starts with a 10-digit number that identifies the experiment. The first 2 digits are the atomic number of the element and the next 3 digits the mass number of the particular isotope. If the element consists of a natural mixture of isotopes the mass number is identified by “000”. Compounds have special identification numbers, such as water (01318), lithium deuteride (03010), or polyethylene (06314). The sixth and seventh digits represent the radius of the sphere in quarters of the 14-MeV neutron mean free path of the sphere material. The eighth digit represents the experiment number. In some cases the sixth, seventh and eighth digits do not follow the nomenclature but still the numbers turn out to be unique for each

experiment. Finally, the last two digits represent the year in which the experiment was carried out. For example, 7318104180 represents a ^{181}Ta sphere of radius about 1 mean free path, and this was the first experiment with the target sphere in 1980.

The header contains other information in addition to the identification number. The next line is a title line followed by various parameters required by the PSEdit code. The first parameter is "detector" and can take six values -1, 0, 1, 2, 3, or 4, depending on the scintillator material and the electronic bias used for that particular experiment. The parameter "path" is the length of the neutron flight path in cm and the parameter "tmax" is a cutoff time in nanoseconds. There are other parameters in the header used in previous versions of PSEdit, but they are no longer used. For example, "geometry" gives the radius of the sphere in cm, and it was used in earlier TART simulations to model the effect of a collimator.

Following the experimental and input data, the PSEdit code reads the *ncordxxx* output files from TART and processes the information to simulate the experiment. Since the TART code is non-relativistic, PSEdit makes a relativistic correction to the time of flight from the source to the detector, making use of the "path" parameter. In addition, since the uncertainty of the experimental values includes factors such as electronic noise, beam pulse width, etc., that affect the resolution and are not included in the simulation, PSEdit makes a convolution of the results of the calculations with a resolution function to compensate for these differences. The convolution function is a Gaussian with variance equal to the difference between the variances of the experimental and calculated direct neutron peak. The variances were determined from the calculated and experimental data and the square root of their difference used as one of the user inputs for PSEdit. Rigorously, the variance should be determined after the detector response has been folded in the calculated data. However, the detector response curves are practically flat in the peak region and

do not contribute significantly to the width. Note that in some of the previous TART calculations the convolution was with the sum of a Gaussian plus a decaying exponential, to account for straggling in the deuteron beam. We found no consistent way to choose such an exponential for all of the spheres, and several of them called for none. Therefore we used only a Gaussian.

The PSEdit code also folds in the detector efficiency. Three different scintillators were used in the experiments NE213, stilbene, and Li glass. Most experiments in the *disp93in* file were performed using either the NE213 or stilbene scintillator. The Li glass scintillator was used only in four experiments to measure the low-energy neutrons from a beryllium sphere. There are six different efficiency curves that PSEdit applies to correct the calculated data. The efficiency curves are presented in Figs. 5, 6, and 7 as a function of energy for each scintillator. Stilbene has two curves and NE213 three because these scintillators were used at different energy bias settings, depending on the experiment. Table 1 lists the detector parameter value used by PSEdit with the corresponding scintillator material and an approximate energy bias.

Table 1: Detector settings used in the pulsed-sphere experiments

Detector parameter ^a	Scintillator material	Detector bias ^b
-1	Stilbene	~ 0.8 MeV
0	Stilbene	~ 3.0 MeV
1	NE213	~ 0.8 MeV
2	NE213	~ 1.6 MeV
3	Li glass	
4	NE213	~ 3.0 MeV

a Number used by the PSEdit code to identify the detector and its efficiency curve

b Nominal low energy cutoff for neutrons

Stilbene

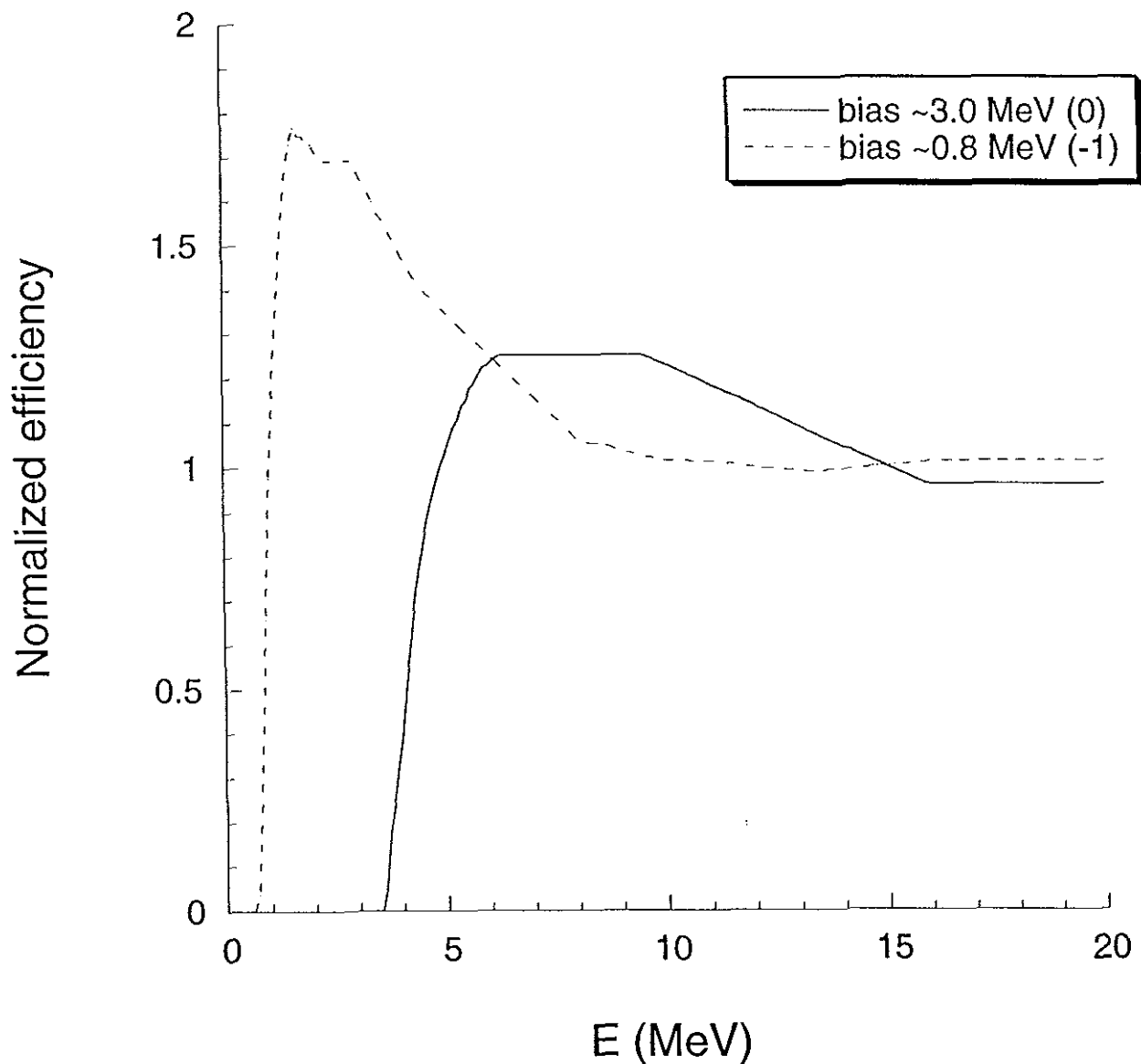


Fig. 5. Detector efficiency as a function of energy for the stilbene scintillator—scaled to 1 at 15 MeV

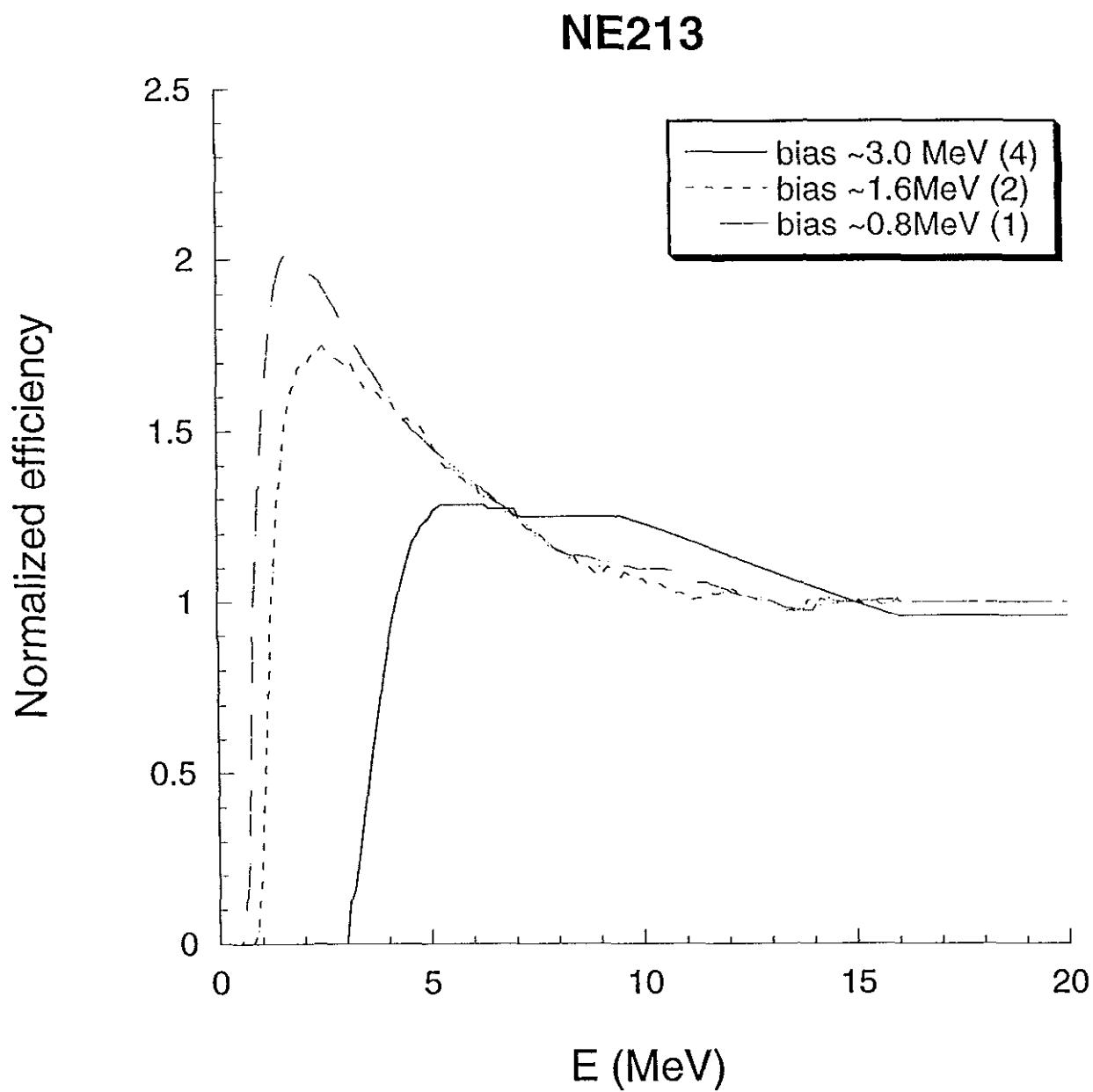


Fig 6. Detector efficiency as a function of energy for the NE213 scintillator—scaled to 1 at 15 MeV

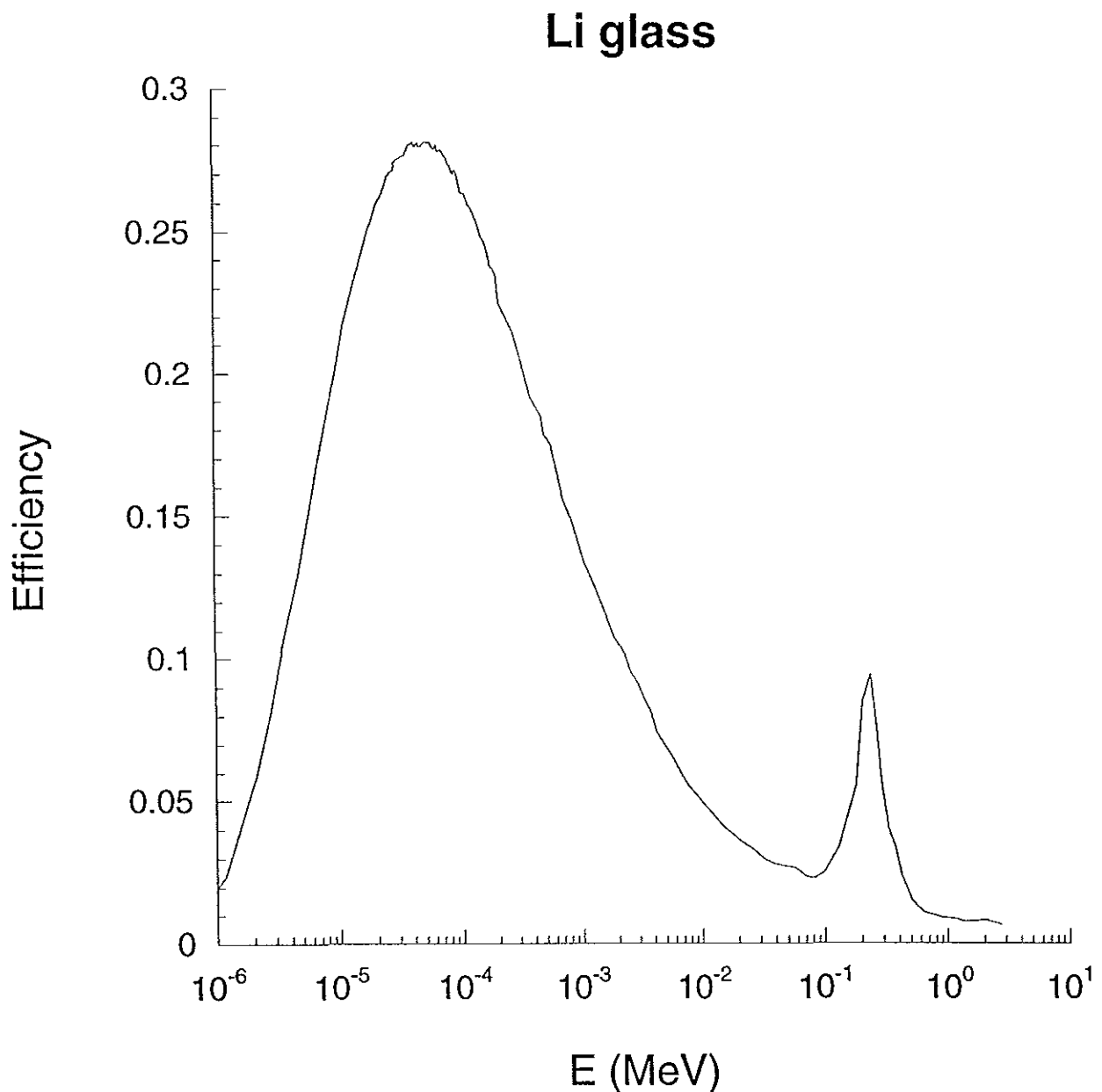


Fig. 7. Detector efficiency as a function of neutron energy for the lithium glass scintillator.

In the initial version of PSEdit, there were no NE213 efficiency curves with approximate bias of 1.6 MeV or 3.0 MeV. With help from E. Plechaty, we found the efficiency curve for NE213 at 3.0 MeV bias in one of the archived versions of the code. We obtained an efficiency curve for NE213 at 1.6 MeV bias by digitizing a plot facilitated by R. Bauer that was calculated using a Monte Carlo code from Physikalisch-Technische Bundesanstalt, Braunschweig, Germany. The PSEdit code scales all the efficiency curves to have a value of 1.0 at 15 MeV and keeps the efficiency constant at the 16-MeV value for energies higher than 16 MeV. We should indicate that previous versions of PSEdit corrected the calculations multiplying by a scale factor that was the ratio of the experimental to the calculated direct peak areas for the 1.8 mean-free-path polyethylene sphere. Also, a constant could be set to shift the time coordinate as needed. The current version of PSEdit does not use these corrections.

As mentioned earlier, the PSEdit code applies a filter to account for the fact that the collimator in the TART calculation was a ring-shaped slot instead of the cylindrical hole used in the experiments. The filter algorithm determines the plane generated by the beam axis and the point of contact of the neutron with the detector surface. The neutron is accepted if its velocity vector forms close to a right angle with the normal to this plane. The measure of this angle is the cosine which is used as input parameter for PSEdit.

RESULTS AND DISCUSSION

Background Calculations

Background contributions to the neutron spectra were evaluated by blank runs, calculations that included the modeled experimental setup but without the sphere. The results of a TART calculation of a blank time spectrum for a 766-cm flight path are presented in Fig. 8 as produced

Background calculation

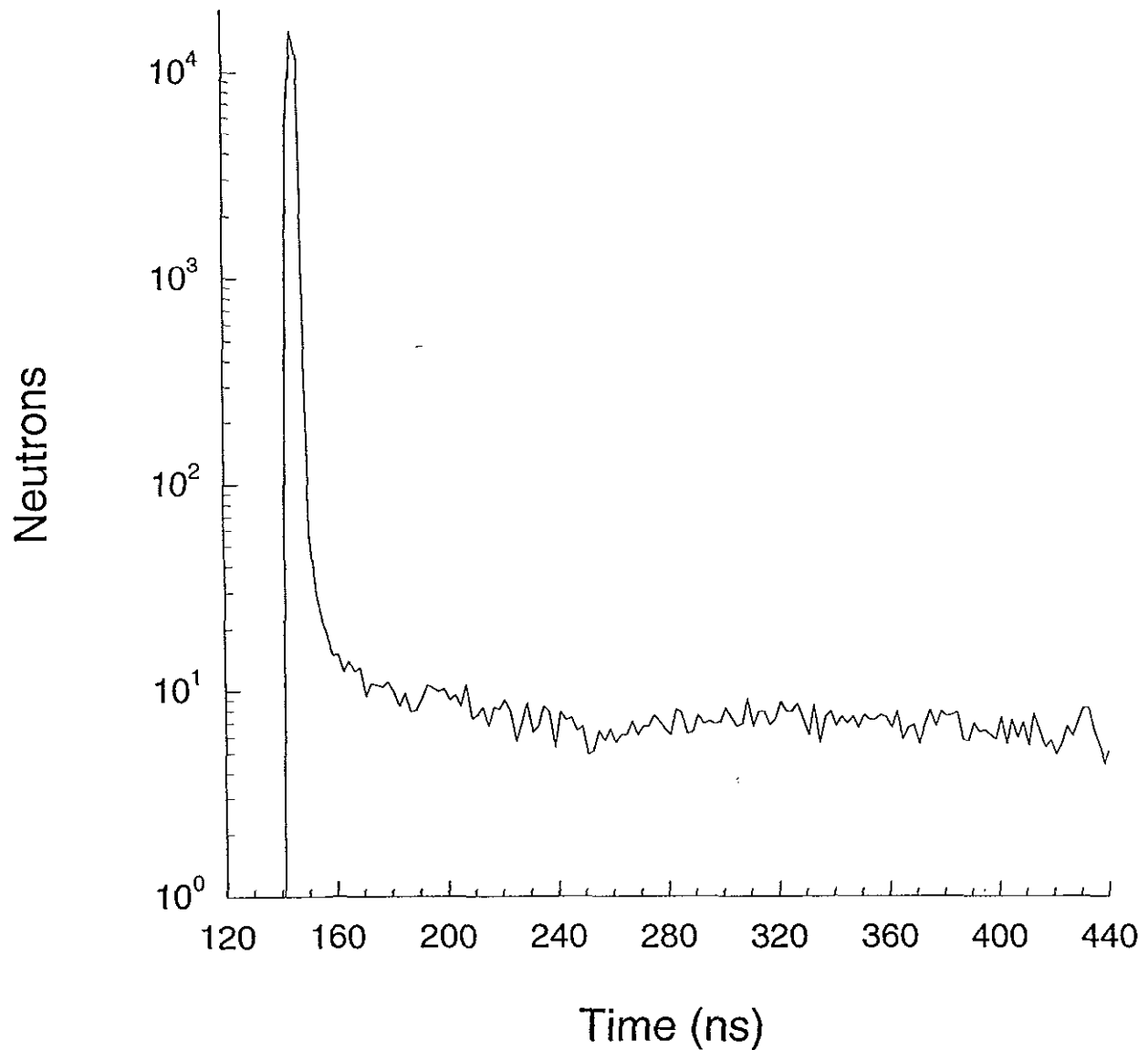


Fig. 8 Neutrons as a function of time for a blank (no sphere) TART run—air, target assembly, concrete wall, and collimator included

without any corrections. The spectrum shows the 14-MeV neutron peak with a tail that quickly drops with time into a more or less constant background. A Gaussian fit to the peak gave a centroid at 145.16 ± 0.01 ns with a standard deviation (width) of 1.552 ± 0.005 ns. The same calculation for a flight path of 852.5 cm resulted in a centroid at 161.47 ± 0.02 ns and a standard deviation of 1.75 ± 0.02 ns. The larger width of this peak can be explained by the longer flight path. To determine how much the neutron source can affect the results, a more coarsely defined source used in previous calculations was tested using the 766-cm setup. The resulting time spectrum was practically identical to that shown in Fig. 8. A Gaussian fit to the peak gave a centroid at 145 ± 0.02 ns and a standard deviation of 1.74 ± 0.02 ns. The slight differences in the elastic parameters are the result of the coarser definition in energy and angle of this source as compared to the previous one. In addition, a test with a source with a completely flat and isotropic distribution between 13.0 and 15.6 MeV resulted in a blank spectrum very similar to that of Fig. 8, beyond the direct peak region. At least in appearance, a precise definition of the source does not seem very critical to the shape of the background spectrum. We investigated the effect of the collimator and wall on the background calculations by replacing them by air in the TART input file. This produced an elevated background spectrum as shown in Fig. 9.

Unfortunately, blank experiments are not available in the *disp93in* file. However, there exist published figures showing the results of blank runs, and we used them for comparison. For example, Fig. 4 from the 1990 paper by Goldberg, et al.¹², shows the blank neutron spectrum for a flight path of 852.5 cm measured with the NE213 scintillator. This figure was scanned and digitized. Figure 10 shows the scanned version along with the TART calculation normalized and corrected for detector efficiency with the PSEDIT filter parameter set large enough to reject no neutrons. The small peak appearing in the experimental data at 350 ns corresponds to 2.81-MeV

Background calculation

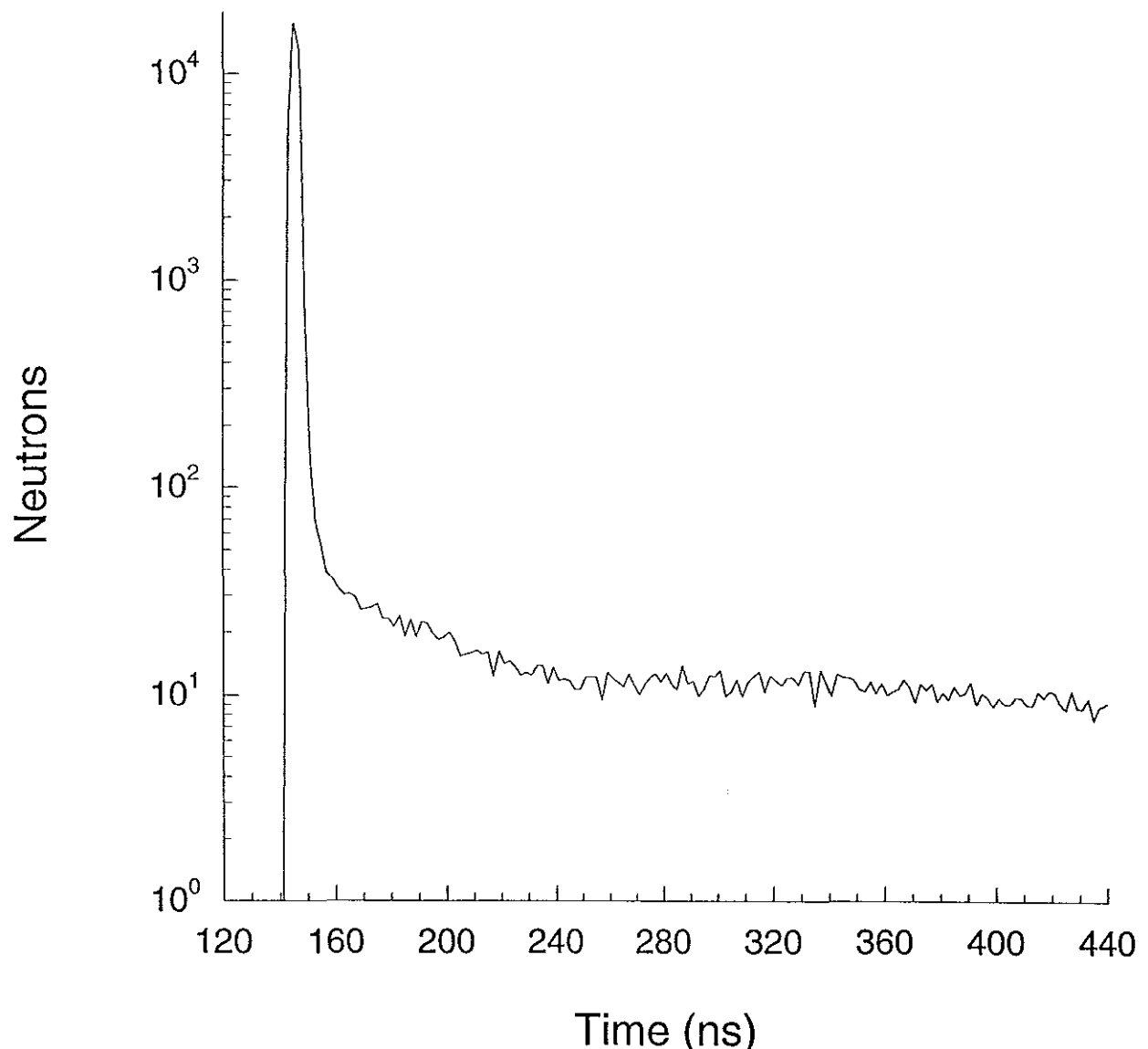


Fig 9 Same as in Fig 8 but without the concrete wall and the collimator which were replaced by air

NE213 background

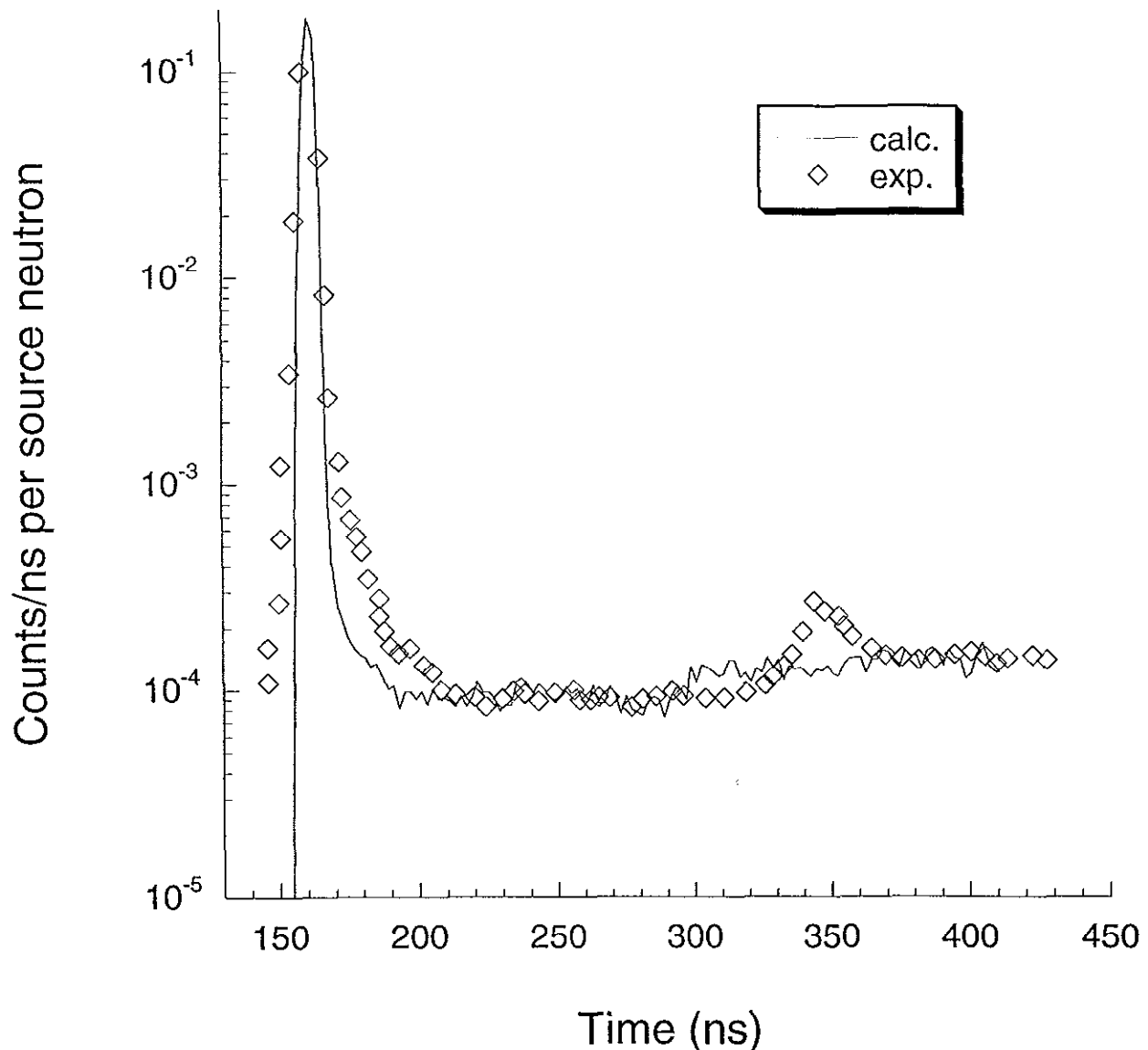


Fig. 10 Comparison between calculated and experimental neutron background spectra using the NE213 scintillator at a bias of ~ 0.8 MeV—experimental data from Ref. 12

neutrons from the reaction $^2\text{H}(\text{d},\text{n})^3\text{He}$ resulting from the deuterium buildup in the tritium target.^{12,13} The experimental and calculated centroids of the peaks coincide very well at 161 ns Overall, there is good agreement between the measured and calculated blank, though the direct peak of the experimental data exhibits a tail that does not appear in the calculation. Another example is Fig. 3 from a 1986 paper by Hansen, et al.,¹³ showing a blank obtained with stilbene scintillator at 878-cm flight path. The peaks agree very well at 166 ns as shown in Fig. 11. As in the previous case, the experimental direct peak has a tail that the calculation does not show and, in addition, this data shows a pronounced dip between ~200 and 360 ns. As before, there is a $^2\text{H}(\text{d},\text{n})^3\text{He}$ peak at around 365 ns. Fair agreement between the experimental and calculated blanks is also found in this case.

The same blank calculations were reanalyzed with PSEdit using a filter parameter of 0.02. The overall decrease in the number of neutrons was only about 2%, even though this filter requires that neutrons arrive at the detector with velocity at least 89° to the reference normal. However, this percentage is not constant but a function of the time of flight and is generally larger in the first 200 ns after the peak. Therefore, even though the neutrons removed by the filter seem relatively few, they could be significant over certain time bins. The TART *ncordxxx* files include the zone where the neutron last scattered for each neutron tallied. With this information, PSEdit generates a file called *fromzone* which gives the number of neutrons tallied per zone and time bin. Analysis of this file allowed us to establish the contributions to the tally from the collimator and other parts of the model setup. For example, with a relaxed filter, the collimator zones contributed about 10% to the background spectra over the first 200 ns after the direct neutron peak. Application of a filter parameter of 0.02 effectively reduces these contributions to about 0.5%. Since the filter in PSEdit is intended to compensate for the geometrical differences between the model and the

Stilbene background

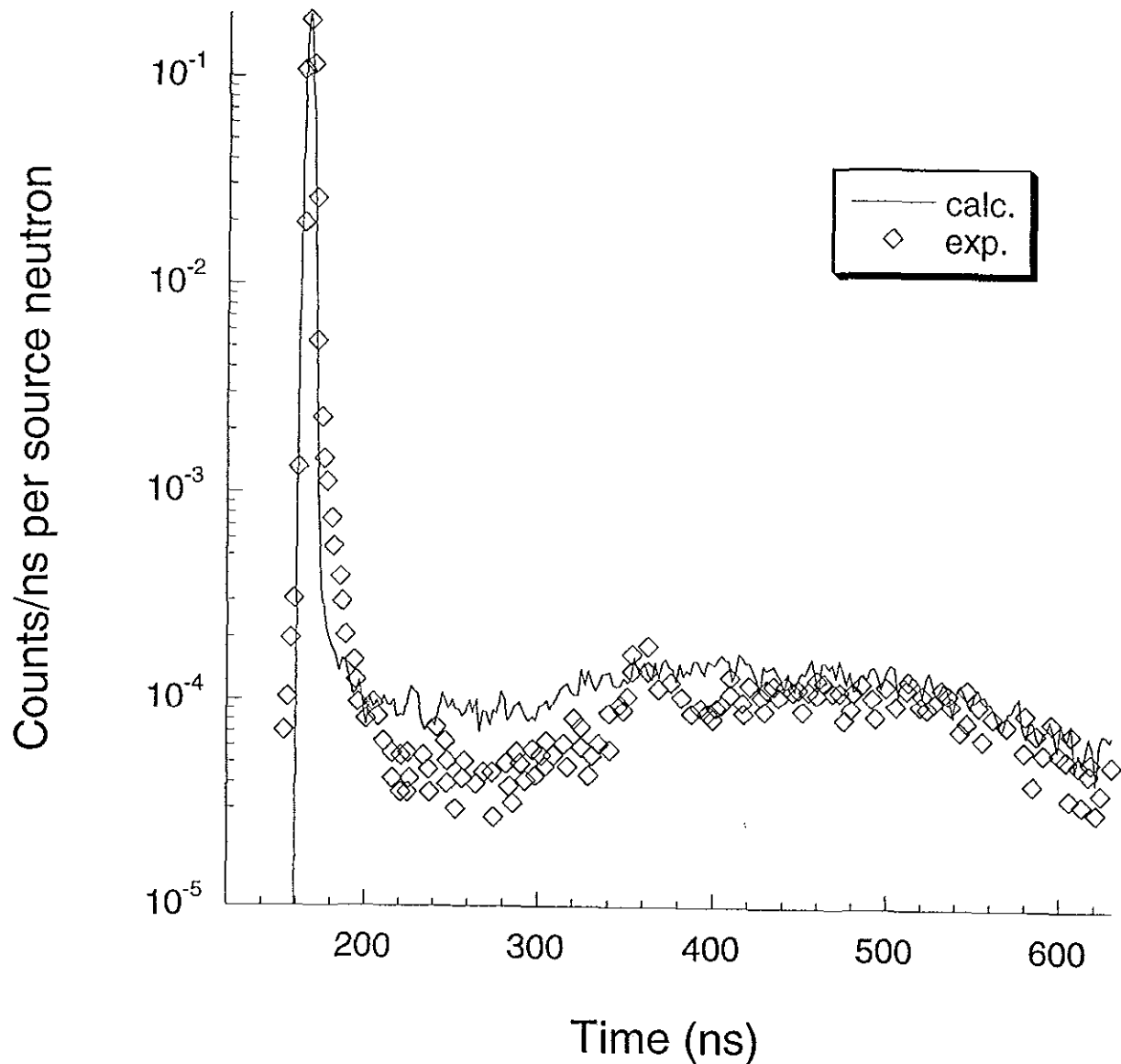


Fig. 11. Comparison between calculated and experimental neutron background spectra using the stilbene scintillator at a bias of ~ 0.8 MeV—experimental data from Ref. 13

actual experiment, it is important to evaluate the level of scattering contributions expected from the experiment to determine a plausible parameter value for the filter.

Pulsed-Sphere Calculations

APPENDIX B contains a series of plots showing the results of the TART calculations represented by a solid line and experimental data represented by symbols for the experiments in the *disp93in* file. A parameter of 0.1 was set in PSEdit to filter out neutrons in all the calculations, counting only the neutrons which arrive at the collimator with a velocity vector making an angle of at least 84° to the reference normal. This value was chosen because it reproduced quite well scattering pattern from the collimator and air for the Ta sphere in the TART run using the collector-surface cylindrical collimator. The low-energy neutron measurements from beryllium using the lithium glass detector are not included in APPENDIX B. These measurements were relatively more sensitive to background effects and therefore neutron absorbers (Cd, Au, ⁶LiD) were employed, water was used as a collimator, and helium-filled bags were placed along the path between the sphere and the detector.¹⁰ These experimental parameters were not documented in detail and thus cannot be modeled.

As in the case of the background spectra, some of the experimental peaks exhibit a shoulder that is not reproduced by the calculations. However, this does not happen for all the pulsed-sphere calculations; actually, some show very good agreement in the peak region. It was mentioned that in some of the old TART input files there is a convolution function included in the neutron source description that has the shape of a Gaussian plus a negative exponential. This convolution function should improve the agreement between calculations and the skewed peaks, and its use could be justified as due to the time distribution of the deuterium beam pulse. L. Hansen recalled that the convolution function was generated using the measured background spectrum for each experi-

ment. Unfortunately, we do not have those spectra to be able to model a function and the differences observed between the data and the calculations do not seem to show a systematic trend to justify the use of a general skewed convolution function.

The target assembly modeled in TART is an extremely simplified representation of the actual apparatus used in the experiment. It accounts for the mass near the pulsed sphere, and can contribute significantly to the neutron spectrum depending on how the mass of the sphere compares to that of the target assembly (~500 g). To illustrate this point, we conducted a TART calculation of the 1.0 mean-free-path Ta sphere (~2300 g) with the target assembly removed. The neutron spectrum is shown in Fig. 12 along with those corresponding to the regular calculation and experiment. In this case, we can see that there is a significant contribution to the spectrum from the target assembly.

Overall, the agreement between the simulation and the experimental data is generally good. In conclusion, the comparison between the calculated and experimental spectra supports the accuracy of the setup modeled here.

ACKNOWLEDGEMENTS

We wish to thank Roger White who provided the conceptual groundwork and overall support necessary to make this project possible. Also we thank him for his insightful discussions and suggestions on the final versions of this report. We gratefully acknowledge John Anderson, Rudy Bauer, Luisa Hansen, Bob Howerton, Ernie Plechaty and Bert Pohl for providing their valuable expertise on the various aspects of the pulsed-sphere experiments. Finally, we would like to thank Dermott Cullen for his assistance with the TART code and Dave Resler for his support with computer related questions.

Ta 1.0 mean free path

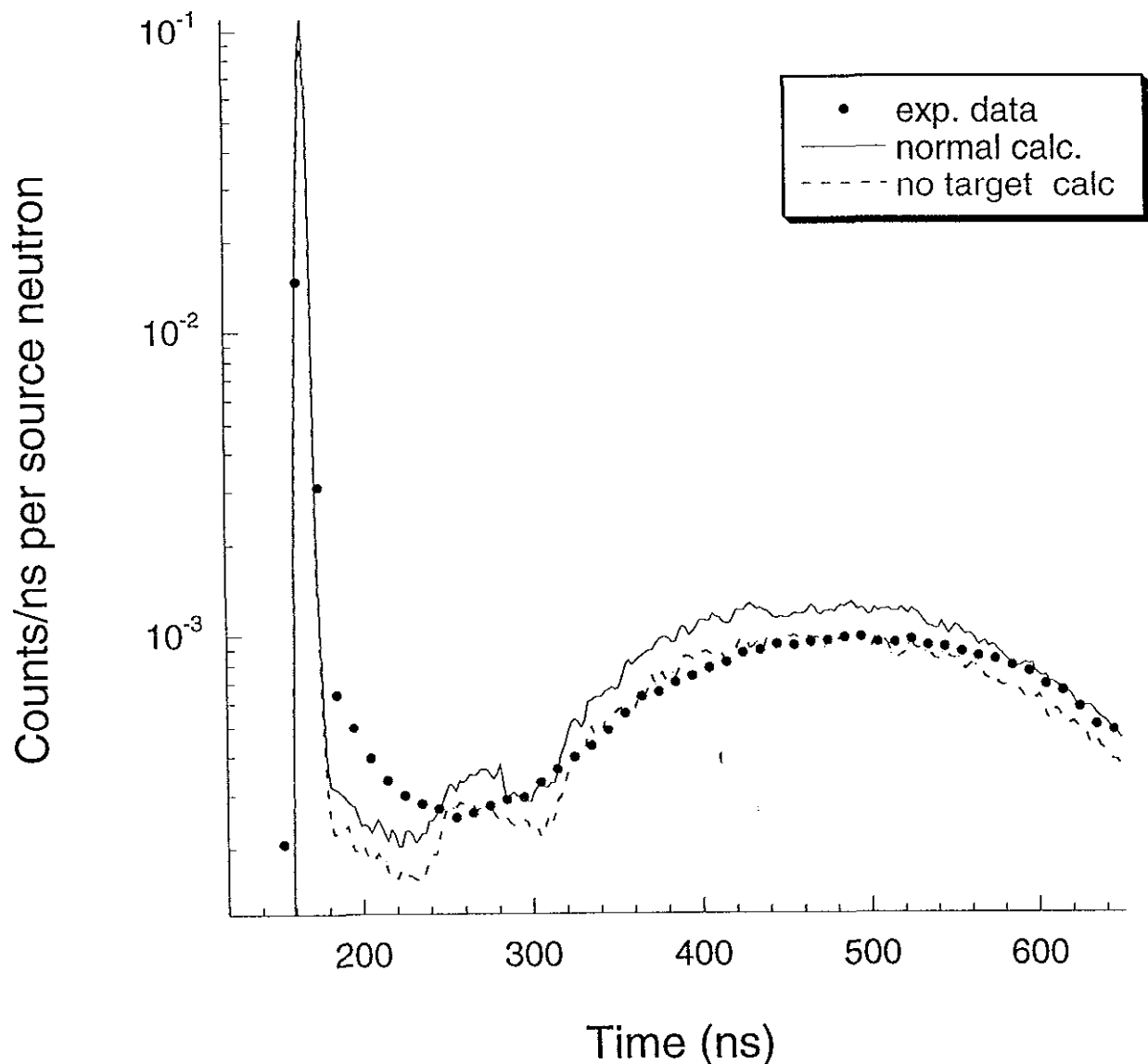


Fig 12 Comparison between calculations with and without target assembly, and experimental data for the 1.0 mean-free-path Ta pulsed sphere

REFERENCES

1. C. Wong, J D Anderson, P. Brown, L F. Hansen, J L Kammerdiener, C M. Logan, and B. A. Pohl, *Livermore Pulsed Sphere Program, Program Summary Through July 1971*, Lawrence Livermore National Laboratory, Report UCRL-51144, Rev. 2, 1972.
2. L. F. Hansen, T. T. Komoto, B. A. Pohl, and C. Wong, *Summary of Measurements and Calculations of Neutron and Gamma-Ray Emission Spectra from Spheres Pulsed with 14-MeV Neutrons*, Lawrence Livermore National Laboratory, Report UCID-19604, 1982
3. L F Hansen, E Goldberg, R J Howerton, T T Komoto, and B A Pohl, *Updated Summary of Measurements and Calculations of Neutron and Gamma-Ray Emission Spectra from Spheres Pulsed with 14-MeV Neutrons*, Lawrence Livermore National Laboratory, Report UCID-19604, Rev 1, 1989
4. D E Cullen, A L Edwards, and E F Plechaty, *TART A Coupled Neutron-Photon Monte Carlo Transport Code*, Lawrence Livermore National Laboratory, Report UCRL-MA-121319, 1995, software version 97.5, 1997
5. J F Ziegler, *TRIM version 96: The Stopping and Range of Ions in Matter*, IBM-Research, 28-0, Yorktown, New York 10598, web site: www.research.ibm.com/ionbeams/, 1997.
6. On-line Data Services $^3\text{H}(\text{d},\text{n})^4\text{H}$ ENDF/B-VI, National Nuclear Data Center, Brookhaven National Laboratory, Upton, New York 11973, telnet. 130.199.112.132, 1997
7. P. Marmier and E Sheldon, *Physics of Nuclei and Particles*, Academic Press, New York, Vol. 1 Appendix C, 1969
8. S J. Bame and J E Petry, *Phys Rev*, **107**, 1616 (1957).
9. G. SA Sidhu, W E. Farley, L F Hansen, T Komoto, B Pohl, and C. Wong, *Nucl Sci Eng* , **66**, 428 (1978)
10. C Wong, E F. Plechaty, R W Bauer, R C Haight, L F Hansen, R J. Howerton, T.T. Komoto, J D. Lee, S T Perkins and B A Pohl, *Measurements and Calculations of the Leakage Multiplication from Hollow Beryllium Spheres*, Lawrence Livermore National Laboratory, Report UCRL-91774, 1985
11. G. W. Hedstrom, *The PSEEDIT Code for the Analysis of the LLNL Pulsed-Sphere Experiments*, Report PD-209, Nuclear Data Group, Lawrence Livermore National Laboratory, 1998.
12. E Goldberg, L F Hansen, T. T Komoto, B A Pohl, R J Howerton, R. E. Dye, E. F. Plechaty, and W E Warren, *Nucl. Sci Eng.*, **105**, 319 (1990).
- 13 L. F Hansen, H. M. Blann, R. J Howerton, T T. Komoto, and B. Pohl, *Nucl. Sci. Eng.*, **92**, 382 (1986)

APPENDIX A^{*}

^{*} References are listed at the end of the appendix

0131804171

H₂O 1 1 mean-free-path
detector 2 NE213 bias ~1.6 MeV
path 731 520 cm
radius 11.1000 cm

TART input file name **h2o11**

The sphere was modeled using the diagram on page 241 of Ref [1]

0131808177

H₂O 1 9 mean-free-path
detector -1 Stilbene bias ~0.8 MeV
path 879 480 cm
radius 19.2600 cm

TART input file name **h2o19**

The sphere was modeled using the diagram on page 247 of Ref [1]

0300602176

⁶Li 0.5 mean-free-path
detector 2 NE213 bias ~1.6 MeV
path 746 340 cm
radius 8.91200 cm

TART input file name: **li605**

The sphere was modeled using the diagram on page 41 of Ref [1].

The masses quoted in the diagram do not agree with those calculated by TART using the volume and density. The density of ⁶Li (0.451 g/cm³) was taken from an earlier input file, the density of the stainless steel is given in other figures of Ref [1] as 7.9 g/cm³. For the lithium the mass variation is a few percent but for the steel casing the mass variation is about 50%. The radii were adjusted in the TART input file to match the masses quoted in the diagram

0300604180

⁶Li 1 1 mean-free-path
detector -1 Stilbene bias: ~0.8 MeV
path 878.000 cm
radius 16.5200 cm

TART input file name **li611**

The sphere was modeled using the diagram on page 51 of Ref [1]

The masses quoted in the diagram do not agree with those calculated by TART using the volume and density. The density of ⁶Li (0.451 g/cm³) was taken from an earlier input file, the density of the stainless steel is given in other figures of Ref [1] as 7.9 g/cm³. For the lithium the mass variation is a few percent but for the steel casing the mass variation is about 50%. The radii were adjusted in the TART input file to match the masses quoted in the diagram

0300606176

^6Li 1.6 mean-free-path
detector 2 NE213 bias ~1.6 MeV
path 746.340 cm
radius 25.5200 cm

TART input file name. li616

The sphere was modeled using the diagram on page 57 of Ref [1]

The masses quoted in the diagram do not agree with those calculated by TART using the volume and density. The density of ^6Li (0.451 g/cm^3) was taken from an earlier input file; the density of the stainless steel is given in other figures of Ref [1] as 7.9 g/cm^3 . For the lithium the mass variation is a few percent but for the steel casing the mass variation is about 50%. The radii were adjusted in the TART input file to match the masses quoted in the diagram

0300702176

^7Li 0.5 mean-free-path
detector 2 NE213 bias ~1.6 MeV
path 746.340 cm
radius 8.91200 cm

TART input file name li705

The sphere was modeled using the diagram on page 63 of Ref [1]

The masses quoted in the diagram do not agree with those calculated by TART using the volume and density. The density of ^7Li (0.515 g/cm^3) was taken from an earlier input file, the density of the stainless steel is given in other figures of Ref [1] as 7.9 g/cm^3 . For the lithium the mass variation is a few percent but for the steel casing the mass variation is about 50%. The radii were adjusted in the TART input to match the masses quoted in the diagram

0300704180

^7Li 1.1 mean-free-path
detector -1 Stilbene bias ~0.8 MeV
path 878.000 cm
radius 16.5200 cm

TART input file name li711

The sphere was modeled using the diagram on page 73 of Ref. [1].

The masses quoted in the diagram do not agree with those calculated by TART using the volume and density. The density of ^7Li (0.515 g/cm^3) was taken from an earlier input file; the density of the stainless steel is given in other figures of Ref [1] as 7.9 g/cm^3 . For the lithium the mass variation is a few percent but for the steel casing the mass variation is about 50%. The radii were adjusted in the TART input to match the masses quoted in the diagram

0300706176

^7Li 1 6 mean-free-path
detector 2 NE213 bias ~1.6 MeV
path 746 340 cm
radius 25 5200 cm

TART input file name: li716

The sphere was modeled using the diagram on page 79 of Ref [1].

The masses quoted in the diagram do not agree with those calculated by TART using the volume and density. The density of ^7Li (0.515 g/cm^3) was taken from an earlier input file, the density of the stainless steel is given in other figures of Ref [1] as 7.9 g/cm^3 . For the lithium the mass variation is a few percent but for the steel casing the mass variation is about 50%. The radii were adjusted in the TART input to match the masses quoted in the diagram

0301004178

^7Li 1 0 mean-free-path
detector 1 NE213 bias ~0.8 MeV
path 945 540 cm
radius 8 97000 cm

TART input file name: lid10

The sphere was modeled using the diagram on page 41 of Ref [1]. This is not the actual diagram for this sphere. However, it was adopted because the radius quoted in the header agrees with that of the corresponding ^6Li sphere. The density of the material LiD (0.7 g/cm^3) was taken from an earlier input file. The density of the steel casing was 7.9 g/cm^3 .

0301008180

^7Li 1 9 mean-free-path
detector -1 Stilbene bias ~0.8 MeV
path 878 000 cm
radius 16 5200 cm

TART input file name: lid19

The sphere was modeled using the diagram on page 51 of Ref [1]. This is not the actual diagram for this sphere. However, it was adopted because the radius quoted in the header agrees with that of the corresponding ^6Li sphere. The density of the material LiD (0.7 g/cm^3) was taken from an earlier input file. The density of the steel casing was 7.9 g/cm^3 .

0301012178

LiD 3.0 mean-free-path
detector 1 NE213 bias ~0.8 MeV
path 731.520 cm
radius 25.5200 cm

TART input file name **lid30**

The sphere was modeled using the diagram on page 57 of Ref. [1]. This is not the actual diagram for this sphere. However, it was adopted because the radius quoted in the header agrees with that of the corresponding ^6Li sphere. The density of the material LiD (0.7 g/cm^3) was taken from an earlier input file. The density of the steel casing was 7.9 g/cm^3 .

0400903180

^9Be 0.8 mean-free-path
detector -1 Stilbene bias ~0.8 MeV
path 878.000 cm
radius 12.5800 cm

TART input file name **be08**

The sphere was modeled using the diagram on page 85 of Ref. [1]. This is a hollow sphere with internal radius of 8.00 cm

0400903183

^9Be 0.8 mean-free-path
detector -1 Stilbene bias ~0.8 MeV
path 728.000 cm
radius 12.5800 cm

TART input file name **be08_83**

The sphere was modeled using the diagram on page 85 of Ref. [1]. This is a hollow sphere with an internal radius of 8.00 cm. The original flight path in the header (722.000 cm) did not agree with the flight path quoted in Ref. [2] (728 cm) for the same experiment. The flight path in the header was changed to 728 cm

0400910183

^9Be 2.5 mean-free-path
detector -1 Stilbene bias ~0.8 MeV
path 728.000 cm
radius 21.8400 cm

TART input file name **be25**

The sphere model was taken from an earlier input file. This is a hollow sphere with an internal radius of 8.00 cm. The original flight path in the header (722.000 cm) did not agree with the flight path quoted in Ref. [2] (728 cm) for the same experiment. The flight path in the header was changed to 728 cm

0400914183

⁹Be 3 5 mean-free-path
detector -1 Stilbene bias ~0.8 MeV
path 728 000 cm
radius 27 9400 cm

TART input file name. **be35**

The sphere model was taken from an earlier input file. This is a hollow sphere with an internal radius of 8.00 cm. The original flight path in the header (722 000 cm) did not agree with the flight path quoted in Ref [2] (728 cm) for the same experiment. The flight path in the header was changed to 728 cm. There is one beryllium shell missing in the backward direction according to an earlier input file and Ref[2]

0400923183

⁹Be 0.8 mean-free-path
detector 0 Stilbene bias ~3.0 MeV
path 728 000 cm
radius 12 5800 cm

TART input file name **be08_83**

The sphere was modeled using the diagram on page 85 of Ref [1]. This is a hollow sphere with an internal radius of 8.00 cm. The original flight path in the header (722 000 cm) did not agree with the flight path quoted in Ref [2] (728 cm) for the same experiment. The flight path in the header was changed to 728 cm.

0400930183

⁹Be 2 5 mean-free-path
detector 0 Stilbene bias ~3.0 MeV
path 728 000 cm
radius 21.8400 cm

TART input file name **be25**

The sphere model was taken from an earlier input file. This is a hollow sphere with an internal radius of 8.00 cm. The original flight path in the header (722 000 cm) did not agree with the flight path quoted in Ref. [2] (728 cm) for the same experiment. The flight path in the header was changed to 728 cm

0400934183

⁹Be 3 5 mean-free-path
detector 0 Stilbene bias ~3 0 MeV
path 728 000 cm
radius 27.9400 cm

TART input file name **be35**

The sphere diagram was taken from an earlier input file. This is a hollow sphere with an internal radius of 8 00 cm. There is one beryllium shell missing in the backward direction according to an earlier input file and Ref[2]. The original flight path in the header (722 000 cm) did not agree with the flight path quoted in Ref [2] (728 cm) for the same experiment. The flight path in the header was changed to 728 cm

0400943183

⁹Be 0 8 mean-free-path
detector 4 NE213 bias ~3 0 MeV
path 728 000 cm
radius 12.5800 cm

TART input file name **be08_83**

The sphere was modeled using the diagram on page 85 of Ref [1]. This is a hollow sphere with an internal radius of 8 00 cm. The original flight path in the header (722.000 cm) did not agree with the flight path quoted in Ref [2] (728 cm) for the same experiment. The flight path in the header was changed to 728 cm

0400950183

⁹Be 2 5 mean-free-path
detector 4 NE213 bias ~3 0 MeV
path 728 000 cm
radius 21 8400 cm

TART input file name **be25**

The sphere model was taken from an earlier input file. This is a hollow sphere with an internal radius of 8 00 cm. There is one beryllium shell missing in the backward direction according to an earlier input file and Ref[2]. The original flight path in the header (722 000 cm) did not agree with the flight path quoted in Ref. [2] (728 cm) for the same experiment. The flight path in the header was changed to 728 cm

0400954183

⁹Be 3 5 mean-free-path
detector 4 NE213 bias ~3 0 MeV
path 728.000 cm
radius 27.9400 cm

TART input file name **be35**

The sphere model was taken from an earlier input file. This is a hollow sphere with an internal radius of 8.00 cm. There is one beryllium shell missing in the backward direction according to earlier input file and Ref[2]. The original flight path in the header (722 000 cm) did not agree with the flight path quoted in Ref. [2] (728 cm) for the same experiment. The flight path in the header was changed to 728 cm.

0400963183

⁹Be 0 8 mean-free-path
detector 1 NE213 bias ~0 8 MeV
path 728 000 cm
radius 12 5800 cm

TART input file name **be08_83**

The sphere was modeled using the diagram on page 85 of Ref [1]. This is a hollow sphere with an internal radius of 8.00 cm. The flight path in the header (722.000 cm) does not agree with the flight path quoted in Ref [2] (728 cm) for the same experiment. The header flight path was used in the input file.

0400970183

⁹Be 2 5 mean-free-path
detector 1 NE213 bias ~0 8 MeV
path 728 000 cm
radius 21.8400 cm

TART input file name **be25**

The sphere model was taken from an earlier input file. This is a hollow sphere with an internal radius of 8 00 cm. There is one beryllium shell missing in the backward direction according to an earlier input file and Ref[2]. The flight path in the header (722 000 cm) does not agree with the flight path quoted in Ref. [2] (728 cm) for the same experiment. The header flight path was used in the input file.

0400974183

⁹Be 3.5 mean-free-path
detector 1 NE213 bias ~0.8 MeV
path 728 000 cm
radius 27.9400 cm

TART input file name **be35**

The sphere model was taken from an earlier input file. This is a hollow sphere with an internal radius of 8.00 cm. There is one beryllium shell missing in the backward direction according to earlier input file and Ref[2]. The flight path in the header (722 000 cm) does not agree with the flight path quoted in Ref [2] (728 cm) for the same experiment. The header flight path was used in the input file

0601202171

C 0.5 mean-free-path
detector 2 NE213 bias ~1.6 MeV
path 766 000 cm
radius 4 18700 cm

TART input file name **c05**

The sphere was modeled using the diagram on page 91 of Ref [1]. The density was defined at 1.8660 g/cm³ to match the mass of carbon quoted in the diagram. The density is within the expected range for amorphous carbon (1.8-2.1 g/cm³)

0601205171

C 1.3 mean-free-path
detector 2 NE213 bias ~1.6 MeV
path 766.000 cm
radius 10 1600 cm

TART input file name **c13**

The sphere was modeled using the diagram on page 101 of Ref. [1]. The density was defined at 1.7642 g/cm³ to match the mass of carbon quoted in the diagram. The density is within the expected range for amorphous carbon (1.8-2.1 g/cm³).

0601212171

C 2.9 mean-free-path
detector 2 NE213 bias ~1.6 MeV
path 766 000 cm
radius 20.9600 cm

TART input file name **c29**

The sphere was modeled using the diagram on page 111 of Ref [1]. The density was defined at 1.8527 g/cm³ to match the mass of carbon quoted in the diagram. The density is within the expected range for amorphous carbon (1.8-2.1 g/cm³)

0631403180

CH₂ 0 8 mean-free-path
detector -1 Stilbene bias ~0.8 MeV
path 878.000 cm
radius 16.5000 cm

TART input file name **ch208**

The sphere was modeled using the diagram on page 269 of Ref [1]. However, the diameter of the outer conical aperture (6.97 cm) seems mistaken after looking at the larger combined sphere on page 275. Because the conical angle of the large sphere is about 4 deg, in agreement with other sphere diagrams, the corresponding diameter (5.72 cm) was adopted instead

0631405183

CH₂ 1 8 mean-free-path
detector -1 Stilbene bias ~0.8 MeV
path 728.000 cm
radius 25.5000 cm

TART input file name **ch218**

The sphere was modeled using the diagram on page 275 of Ref [1]. The header flight path was changed from 722 to 728 cm

0631425183

CH₂ 1 8 mean-free-path
detector 0 Stilbene bias ~3.0 MeV
path 728.000 cm
radius 25.5000 cm

TART input file name **ch218**

The sphere was modeled using the diagram on page 275 of Ref [1]. The header flight path was changed from 722 to 728 cm

0631445183

CH₂ 1 8 mean-free-path
detector 4 NE213 bias ~3.0 MeV
path 728.000 cm
radius 25.5000 cm

TART input file name **ch218**

The sphere was modeled using the diagram on page 275 of Ref [1]. The header flight path was changed from 722 to 728 cm

0631465183

CH₂ 1 8 mean-free-path
detector 1 NE213 bias. ~0.8 MeV
path 728.000 cm
radius 25.5000 cm

TART input file name. **ch218**

The sphere was modeled using the diagram on page 275 of Ref. [1]. The header flight path was changed from 722 to 728 cm.

0635004180

CF₂ 1 8 mean-free-path
detector -1 Stilbene bias ~0.8 MeV
path 878.000 cm
radius 16.5000 cm

TART input file name **cf218**

The sphere was modeled using the diagram on page 293 of Ref. [1]

0701402175

N 0 6 mean-free-path
detector 2 NE213 bias ~1.6 MeV
path 782.300 cm
radius 10.5800 cm

TART input file name **n06**

The sphere was modeled using the diagram on page 133 of Ref [1]. This diagram actually corresponds to an oxygen sphere but the stainless steel container should be the same according to the dimensions presented in Fig 1 of Ref [3]

0701404175

N 1 1 mean-free-path
detector 2 NE213 bias: ~1.6 MeV
path 782.300 cm
radius 19.0500 cm

TART input file name **n11**

The sphere was modeled using the diagram on page 121 of Ref [1].

0701431175

N 7 7 mean-free-path
detector 2 NE213 bias ~1.6 MeV
path 955 040 cm
radius 129 310 cm

TART input file name **n77**

The diagram for this sphere container had to be inferred from data in Refs [3,4]. The composition and density of the Dewar container was taken from an earlier input file. Also the collimator was modified to allow the detector view the whole sphere

0731428175

Air 7.0 mean-free-path
detector 2 NE213 bias ~1.6 MeV
path 953 770 cm
radius 999 990 cm

TART input file name **air70**

The Dewar container was the same one used for liquid nitrogen 7 7 mfp (0701431175). The density of the liquid air (0.8935 g/cm^3) was taken from Ref [5] and its composition was taken from Ref [6]. Also the collimator was modified to allow the detector view the whole sphere

0801603176

O 0.7 mean-free-path
detector 2 NE213 bias ~1.6 MeV
path 782 300 cm
radius 10 5800 cm

TART input file name **o07**

The sphere was modeled using the diagram on page 133 of Ref. [1]

2600004171

Fe 0.9 mean-free-path
detector 2 NE213 bias ~1.6 MeV
path 766 000 cm
radius 4 46000 cm

TART input file name. **fe09**

The sphere was modeled using the diagram on page 201 of Ref. [1].

2600012171

Fe 3 0 mean-free-path
detector 2 NE213 bias ~1.6 MeV
path 766 000 cm
radius 13 4100 cm

TART input file name **fe30**

The sphere was modeled using the diagram on page 211 of Ref [1]

2600019171

Fe 4 8 mean-free-path
detector 2 NE213 bias ~1.6 MeV
path 766 000 cm
radius 22 3000 cm

TART input file name **fe48**

The sphere was modeled using the diagram on page 221 of Ref [1]

2900004178

Cu 1 0 mean-free-path
detector 1 NE213 bias ~0.8 MeV
path 945.540 cm
radius 4 00000 cm

TART input file name **cu10**

The sphere was modeled using information from Refs [7,8]

2900012178

Cu 3 0 mean-free-path
detector 1 NE213 bias ~0.8 MeV
path 945.540 cm
radius 12 0000 cm

TART input file name **cu30**

The sphere was modeled by changing the radius of the 1 mfp sphere. The conical aperture was slightly modified so that the mass of copper matched the value shown in Ref [8]

2900020178

Cu 5.0 mean-free-path
detector 1 NE213 bias ~0.8 MeV
path 731.520 cm
radius 20.0000 cm

TART input file name: **cu50**

The sphere was modeled by changing the radius of the 1 mfp sphere. The conical aperture was slightly modified so that the mass of copper matched the value shown in Ref [8].

4109304178 nb-1 0

Nb 1.0 mean-free-path
detector 1 NE213 bias ~0.8 MeV
path 945.540 cm
radius 4.00000 cm

TART input file name **nb10**

The sphere model is the same one used for the 1 mfp Cu sphere. In this way, the mass of niobium agrees with that shown in Ref [8].

4109312178

Nb 3.0 mean-free-path
detector 1 NE213 bias ~0.8 MeV
path 945.540 cm
radius 14.6100 cm

TART input file name **nb30**

The diagram for this sphere was based on the 1 mfp Cu sphere. The conical aperture was slightly modified so that the mass of niobium matched the value shown in Ref [8].

5000004178

Sn 1.0 mean-free-path
detector 1 NE213 bias:~0.8 MeV
path 945.450 cm
radius 5.97300 cm

TART input file name **sn10**

There is no other information about this sphere other than the header. The diagram of the Cu 1.0 mfp sphere was adopted

6716504181

Ho 1 0 mean-free-path
detector -1 Stilbene bias: ~0.8 MeV
path 878 000 cm
radius 4 60400 cm

TART input file name: ho10

The model for this sphere was based on the Fe 0.9 mfp sphere. The weight of this sphere quoted in Ref [9] is 3.54 kg and cannot be matched with any reasonable geometrical variation that would include a conical hole to accommodate the target assembly. It appears that either the radius or the weight is in error. The model sphere weight is 3.36 kg.

7318104180

Ta 1 0 mean-free-path
detector -1 Stilbene bias: ~0.8 MeV
path 878 000 cm
radius 3 40000 cm

TART input file name: ta10

The sphere was modeled using data from Ref [7] and the conical aperture was slightly adjusted to match the mass quoted in Ref [9].

7318112178

Ta 3 0 mean-free-path
detector 1 NE213 bias ~0.8 MeV
path 945.540 cm
radius 10 2000 cm

TART input file name: ta30_78

The sphere model was based on the Ta 1 mfp sphere and the conical aperture was slightly adjusted to match the mass quoted in Ref [9].

7318112180

Ta 3 0 mean-free-path
detector -1 Stilbene bias: ~0.8 MeV
path 878.000 cm
radius 10.2000 cm

TART input file name: ta30

The sphere model was based on the Ta 1 mfp sphere and the conical aperture was slightly adjusted to match the mass quoted in Ref [9].

7400004175

W 1.0 mean-free-path
detector 2 NE213 bias ~1.6 MeV
path 801.400 cm
radius 10.3600 cm

TART input file: w10

The description for this sphere was prepared from blueprints provided by L F. Hansen

7400004186

W 1.0 mean-free-path
detector 1 NE213 bias ~0.8 MeV
path 849.300 cm
radius 10.3600 cm

TART input file: w10_86

The description for this sphere was obtained from blueprints provided by L F. Hansen. The detector was changed from 2 to 1 in the file *disp93in* because it resulted in a better agreement with the experimental data that, in addition, ranges down to 0.8 MeV

7400008175

W 2.0 mean-free-path
detector 2 NE213 bias ~1.6 MeV
path 801.400 cm
radius 10.3600 cm

TART input file: w20

The description for this sphere was obtained from blueprints provided by L F. Hansen

7400012175

W 3.0 mean-free-path
detector 2 NE213 bias ~1.6 MeV
path 801.400 cm
radius 10.3600 cm

TART input file: w30

The description for this sphere was obtained from blueprints provided by L.F. Hansen

7919708178

Au 2 0 mean-free-path
detector -1 Stilbene bias ~0.8 MeV
path 945.940 cm
radius 6.21900 cm

TART input file au20

The geometrical parameters of the sphere were taken from Ref [7] The conical aperture in the sphere was modified slightly to make the mass agree with that quoted in Ref [9]

7919708180

Au 2 0 mean-free-path
detector -1 Stilbene bias ~0.8 MeV
path 878.000 cm
radius 6.21900 cm

TART input file au20_80

The geometrical parameters of the sphere were taken from Ref [7] The conical aperture in the sphere was modified slightly to make the mass agree with that quoted in Ref [9]

8200004180

Pb 1 0 mean-free-path
detector -1 Stilbene bias ~0.8 MeV
path 878.000 cm
radius 8.97000 cm

TART input file. pb10

The geometrical parameters of the sphere were taken from Ref.[7] The radius quoted in the header under radius appears wrong The conical aperture in the sphere was modified slightly to make the mass agree with that quoted in Ref [9]

9023204178

Th 0.8 mean-free-path
detector 1 NE213 bias ~0.8 MeV
path 945.540 cm
radius 5.75700 cm

TART input file: th23210

The geometrical parameters of the sphere were taken from Ref.[7]. The conical aperture in the sphere was modified slightly to make the mass agree with that quoted in Ref. [8].

9223503176

^{235}U 0.7 mean-free-path
detector 2 NE213 bias ~1.6 MeV
path 945.540 cm
radius 5.93900 cm

TART input file **u23507**

The sphere was modeled using data from Refs [10, 11]

9223506177

^{235}U 1.5 mean-free-path
detector -1 Stilbene bias ~0.8 MeV
path 879 000 cm
radius 5.92500 cm

TART input file **u23515**

The sphere was modeled using data from Ref [11]

9223803178

^{238}U 0.8 mean-free-path
detector 1 NE213 bias ~0.8 MeV
path 945 540 cm
radius 3.63000 cm

TART input file **u23808**

The model for the sphere was prepared using data from Ref. [7]. The sphere composition and density were taken from an earlier input file. The mass of the sphere agrees within 1% with the mass quoted in Ref [8]. However, the composition of the sphere is slightly different (99% U, 1% C and Si) than that used in the old input file (99.4% U and 0.6%C)

9223811176

^{238}U 2.8 mean-free-path
detector 2 NE213 bias. ~1.6 MeV
path 746 340 cm
radius 10.9100 cm

TART input file: **u23828**

The model for the sphere was prepared using data from Ref [7] for the 0.8 mfp sphere and modifying the radius. The sphere composition and density were taken from an earlier input file. The mass of the sphere agrees within 1% with the mass quoted in Ref. [8]. However, the composition of the sphere is slightly different (99% U, 1% C and Si) than that used in the earlier input file (99.4% U and 0.6%C)

9423903176

^{239}Up 0.7 mean-free-path
detector 2 NE213 bias ~1.6 MeV
path 945.540 cm
radius 3.71000 cm

TART file name **pu07**

The model for this sphere was prepared from Fig 2b Ref [10] The Pu composition was taken from an earlier input file and the density defined at 15.79 g/cm³ to match the sphere mass quoted in Table 1 of Ref [11] There is no reference to the actual density of this material and previous input files give different values (15.76 and 15.81 g/cm³)

9423905377

^{239}Pu 1.25 mean-free-path
detector -1 Stilbene bias ~0.8 MeV
path 879.480 cm
radius 5.49600 cm

TART file name: **pu12**

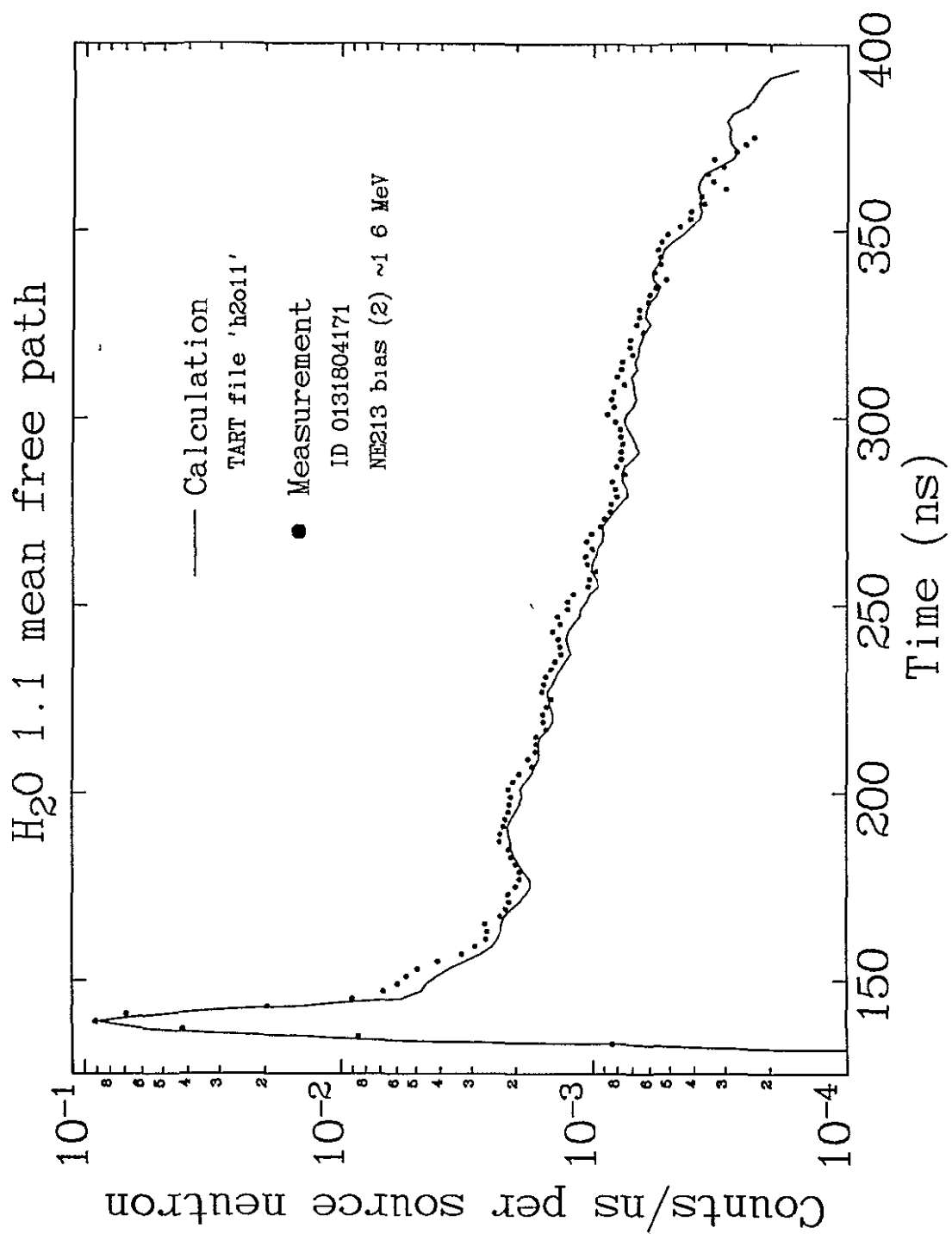
The model for this sphere was prepared from Fig 1 Ref [11] The Pu composition was taken from an earlier input file and the density defined at 16.11 g/cm³ to match the sphere mass quoted in Table 1 of Ref. [11] There is no reference to the actual density of this material and previous input files give different values (15.76 and 15.81 g/cm³)

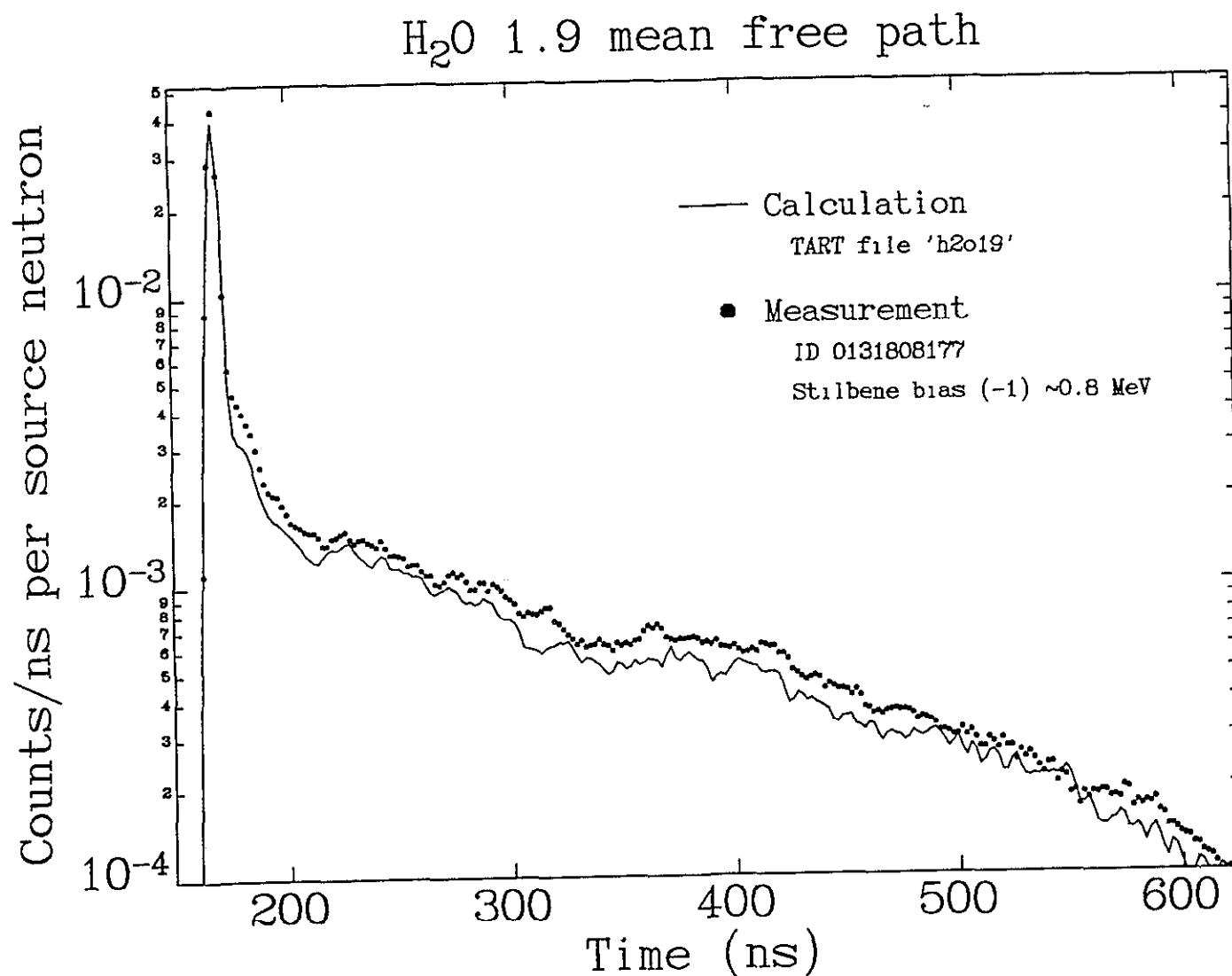
REFERENCES

1. C. Wong, J.D. Anderson, P. Brown, L F Hansen, J L Kammerdiener, C Logan and B Pohl *Livermore Pulsed Sphere Program Summary through July 1971*, UCRL-51144, Rev I and Addendum, Lawrence Livermore National Laboratory, February 10, 1972
2. C. Wong, E.F. Plechaty, R.W. Bauer, R.C. Haight, L F Hansen, R.J. Howerton, T.T. Komoto, J.D. Lee, S.T. Perkins and B. Pohl, *Measurements and Calculations of Leakage Multiplication from Hollow Beryllium Spheres*, UCRL-91774, April 1985.
3. L F. Hansen, T. Komoto, E F. Plechaty, B A. Pohl, G S. Sidhu and C. Wong, Nucl. Sci. Eng., 62, 550 (1977).
4. G S. A. Sidhu, W E. Farley, L F. Hansen, T. Komoto, B. Pohl and C. Wong, Nucl. Sci. Eng., 63, 48 (1977)
5. Lide, D.R , Editor, *CRC Handbook of Chemistry and Physics*, 6-1, 72nd Edition, 1991-1992.
6. G S. A. Sidhu, W E. Farley, L.F. Hansen, T. Komoto, B. Pohl and C. Wong, Nucl. Sci. Eng., 66, 428 (1978)
7. E. Goldberg, L F. Hansen, T T. Komoto, B A. Pohl, R J. Howerton, R E. Dye, E F. Phechaty and W E. Warren, Nucl. Sci. Eng., 105, 319 (1990)

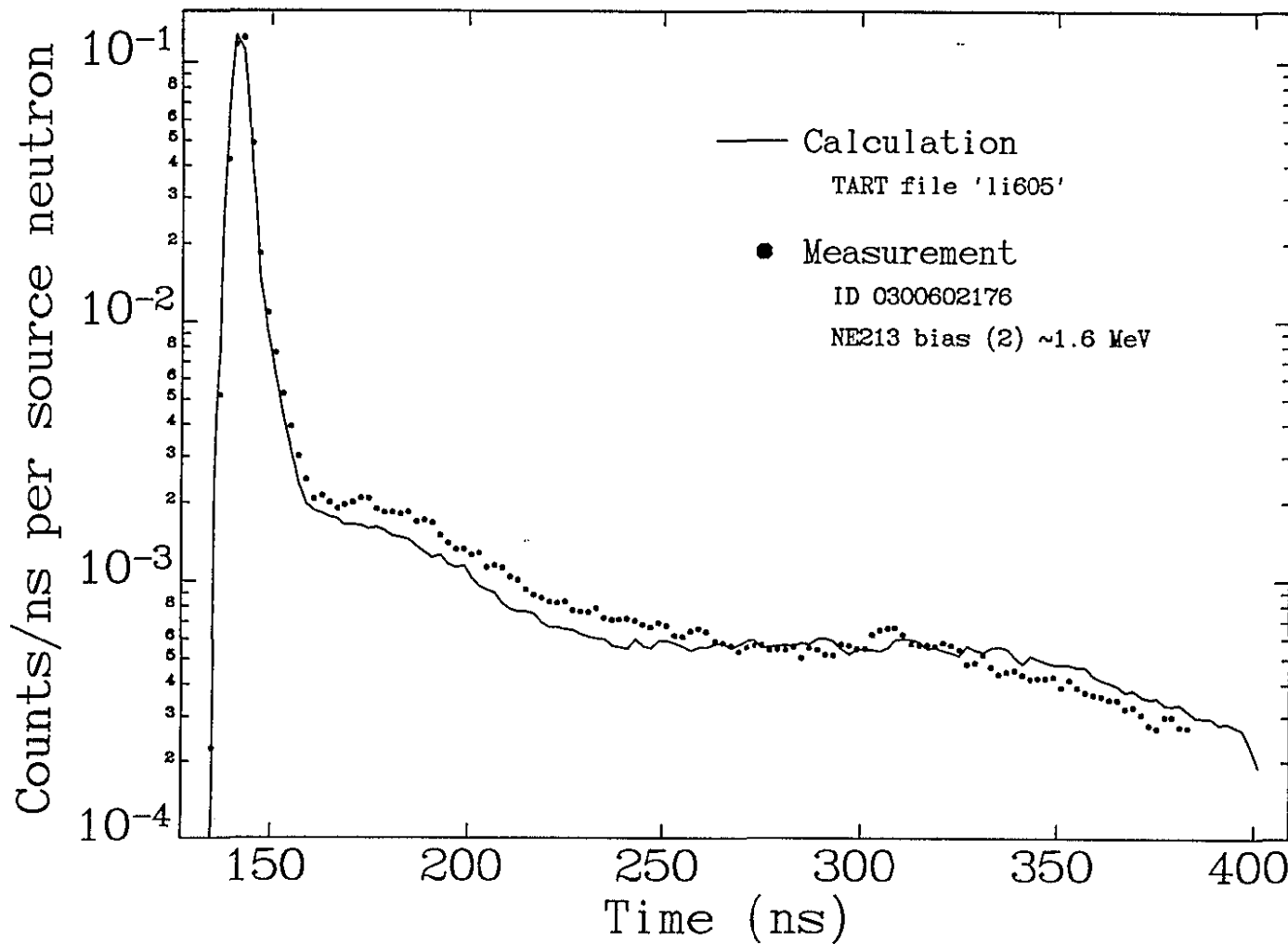
8. L F. Hansen, C Wong, T T Komoto, B A Pohl and R J. Howerton, Nucl Tech., 51, 70 (1980)
- 9 L.F Hansen, H M Blann, R J Howerton, T T Komoto and B Pohl, Nucl Sci Eng , 92, 382 (1986).
10. T.B Gosnell and B A Pohl, *Spectrum Synthesis High-Precision, High-Accuracy Calculation of HPGe Pulse-Height Spectra from Thick Actinide Assemblies*, UCRL-JC-120585, April 1995
- 11 L F Hansen, C Wong, T T Komoto, B A Pohl, E Goldberg, R J Howerton and W Webster, Nucl Sci Eng , 72, 35 (1979)

APPENDIX B

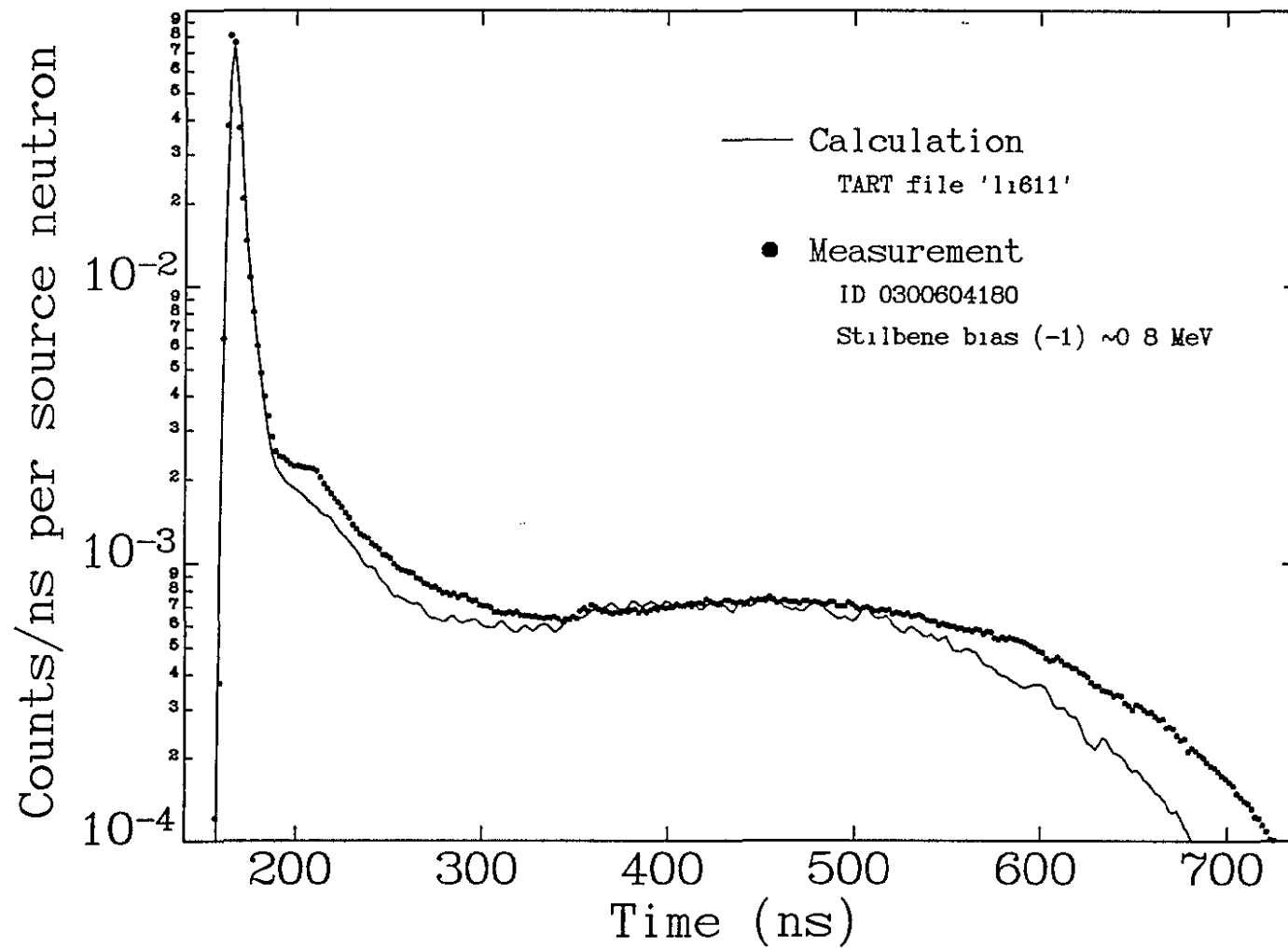




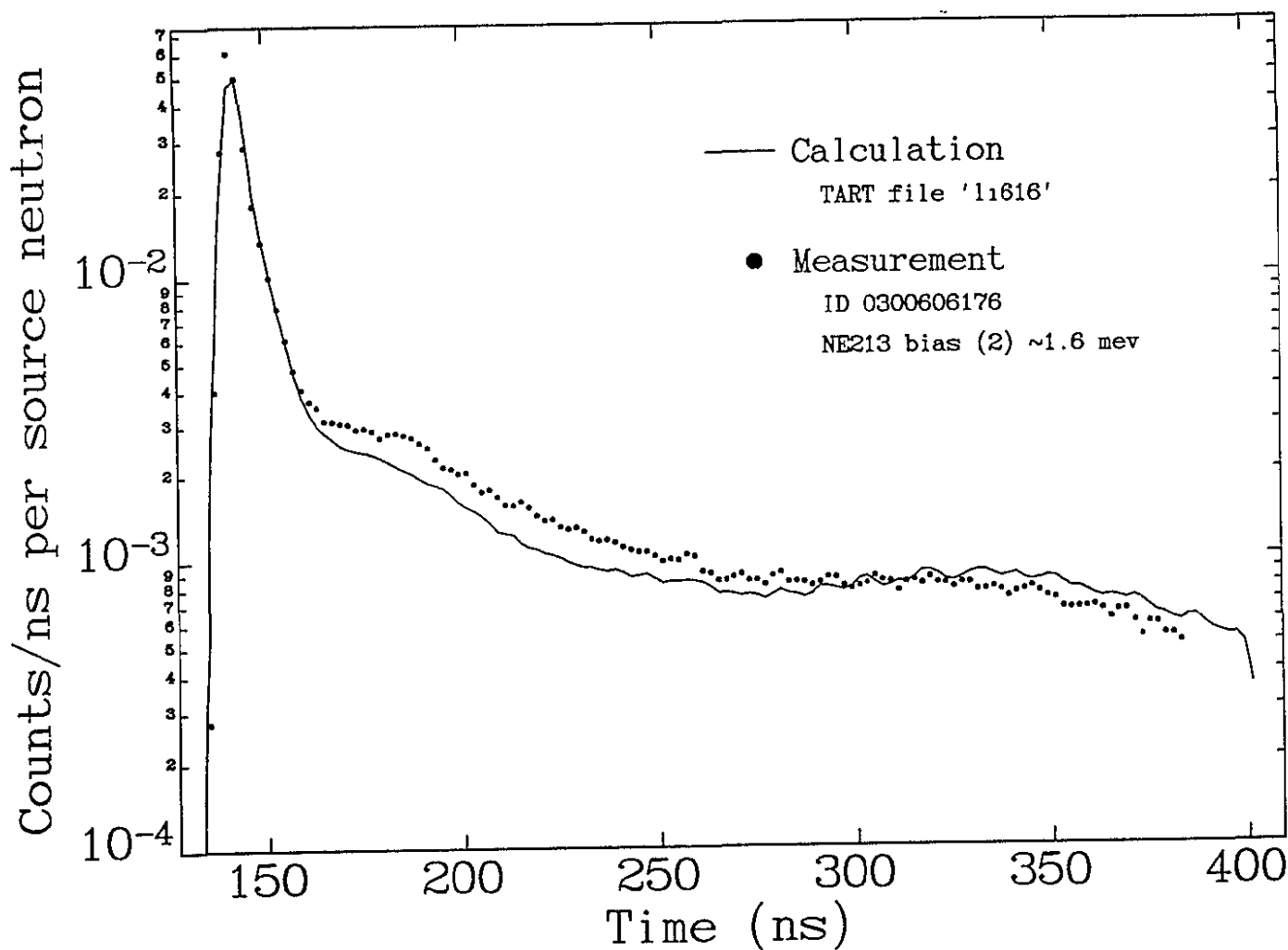
^{6}Li 0.5 mean free path

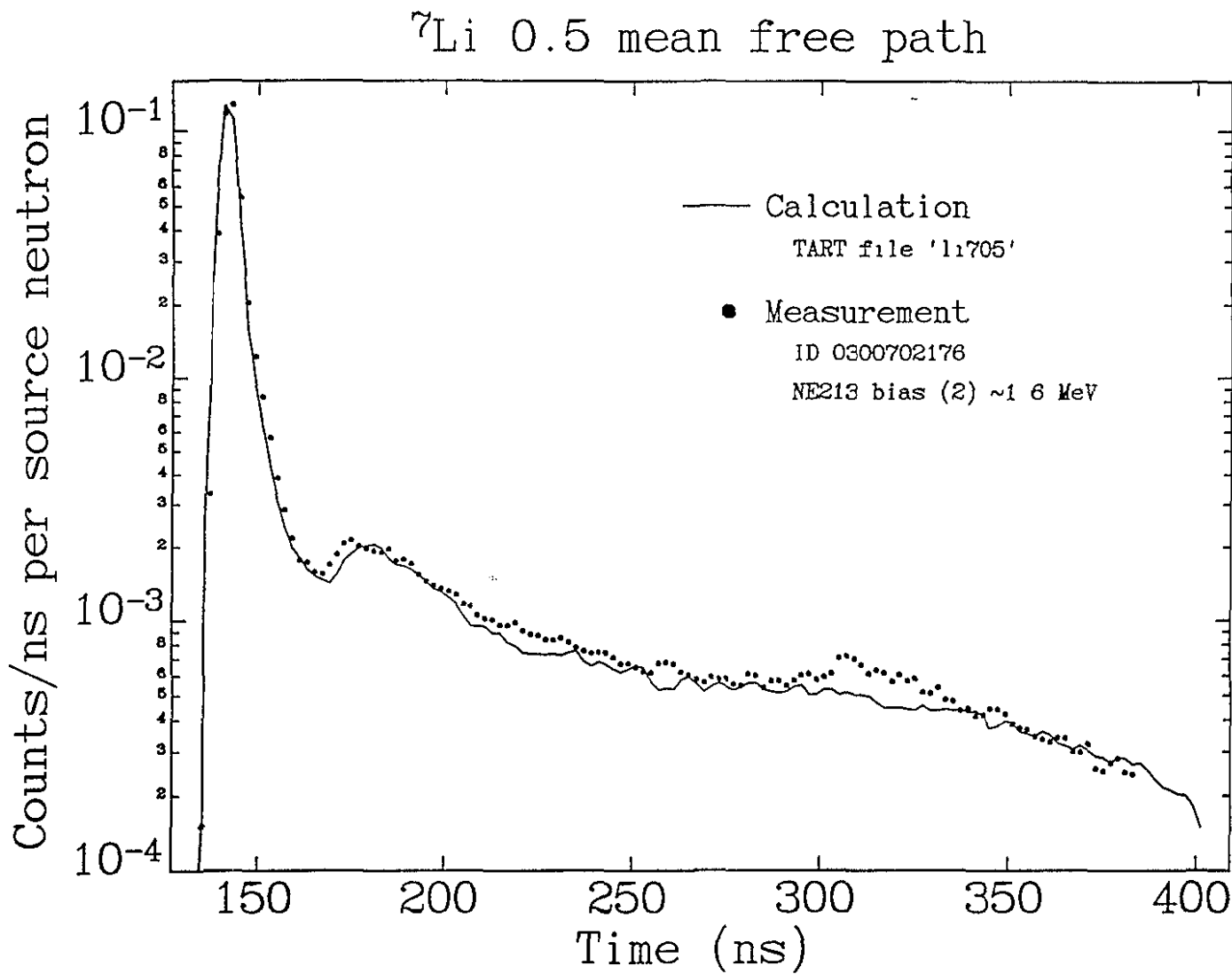


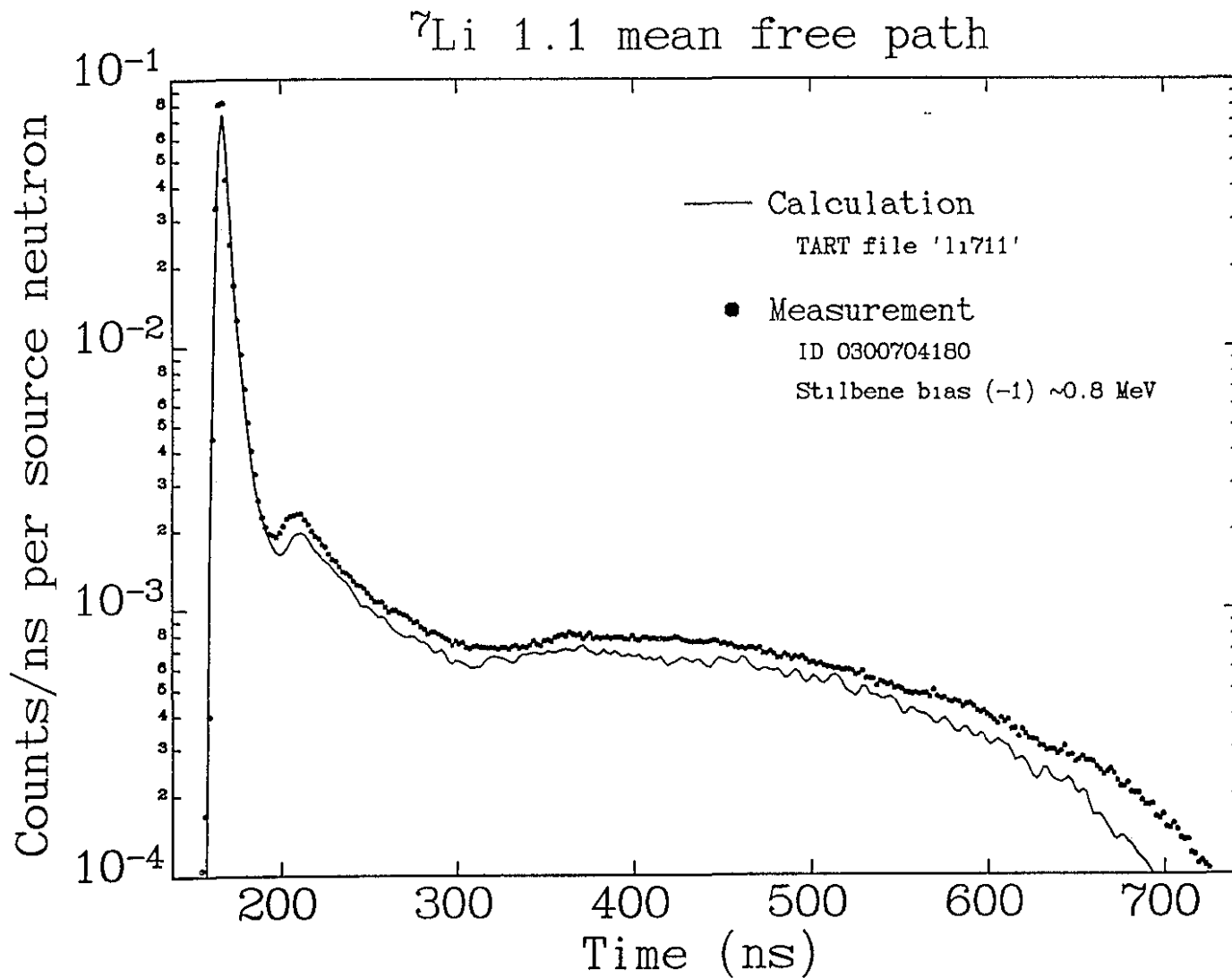
^{6}Li 1.1 mean free path

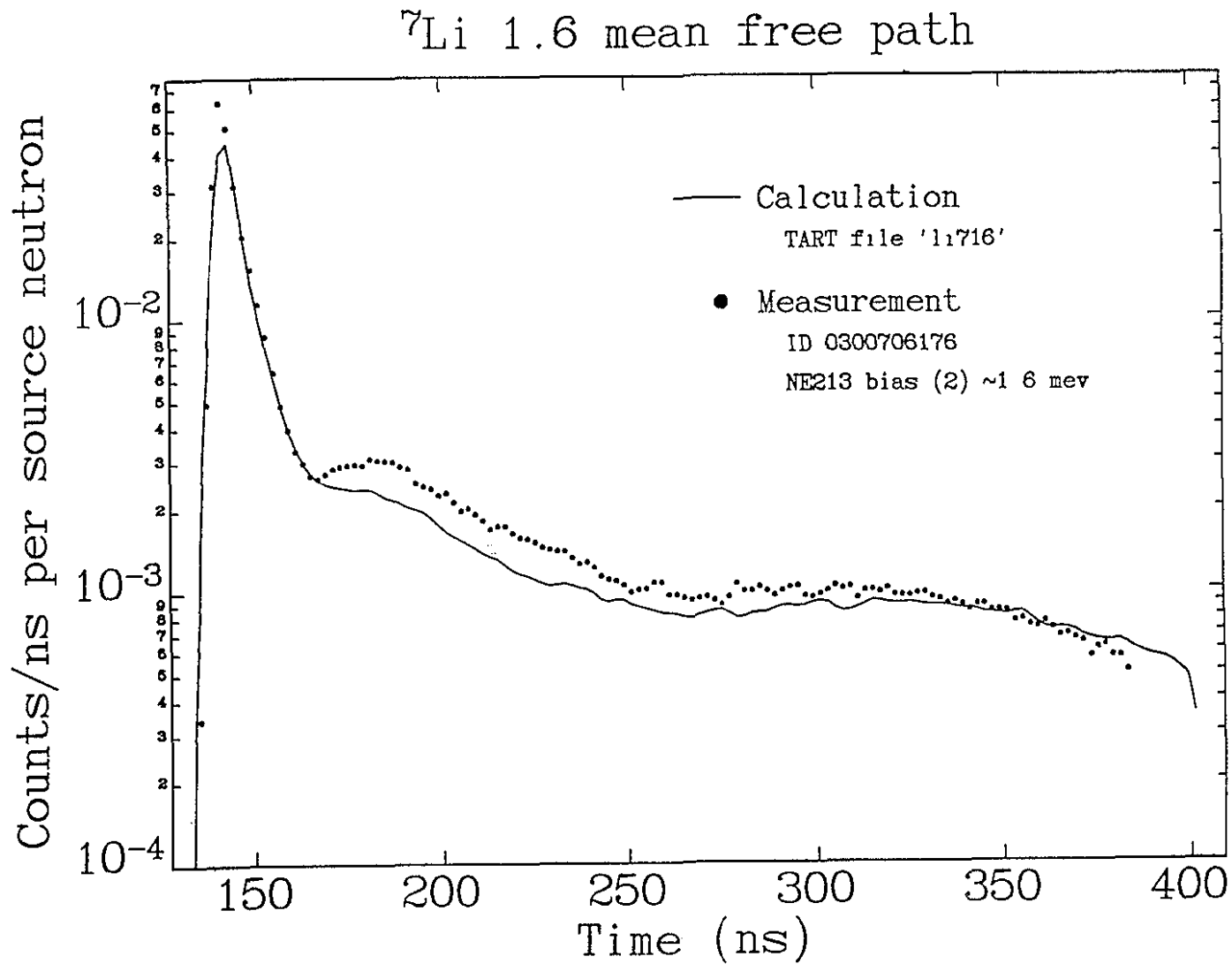


^{6}Li 1.6 mean free path

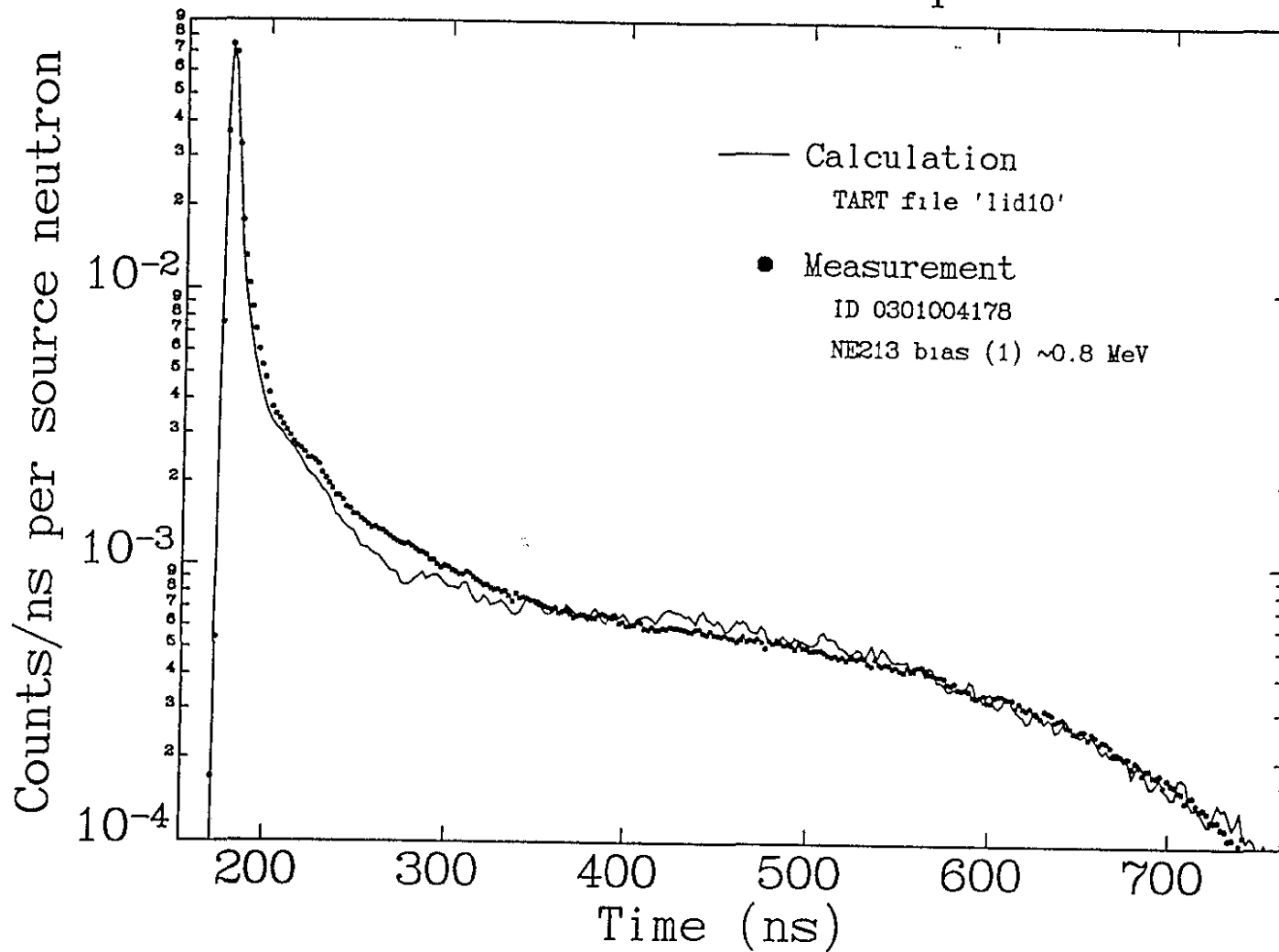




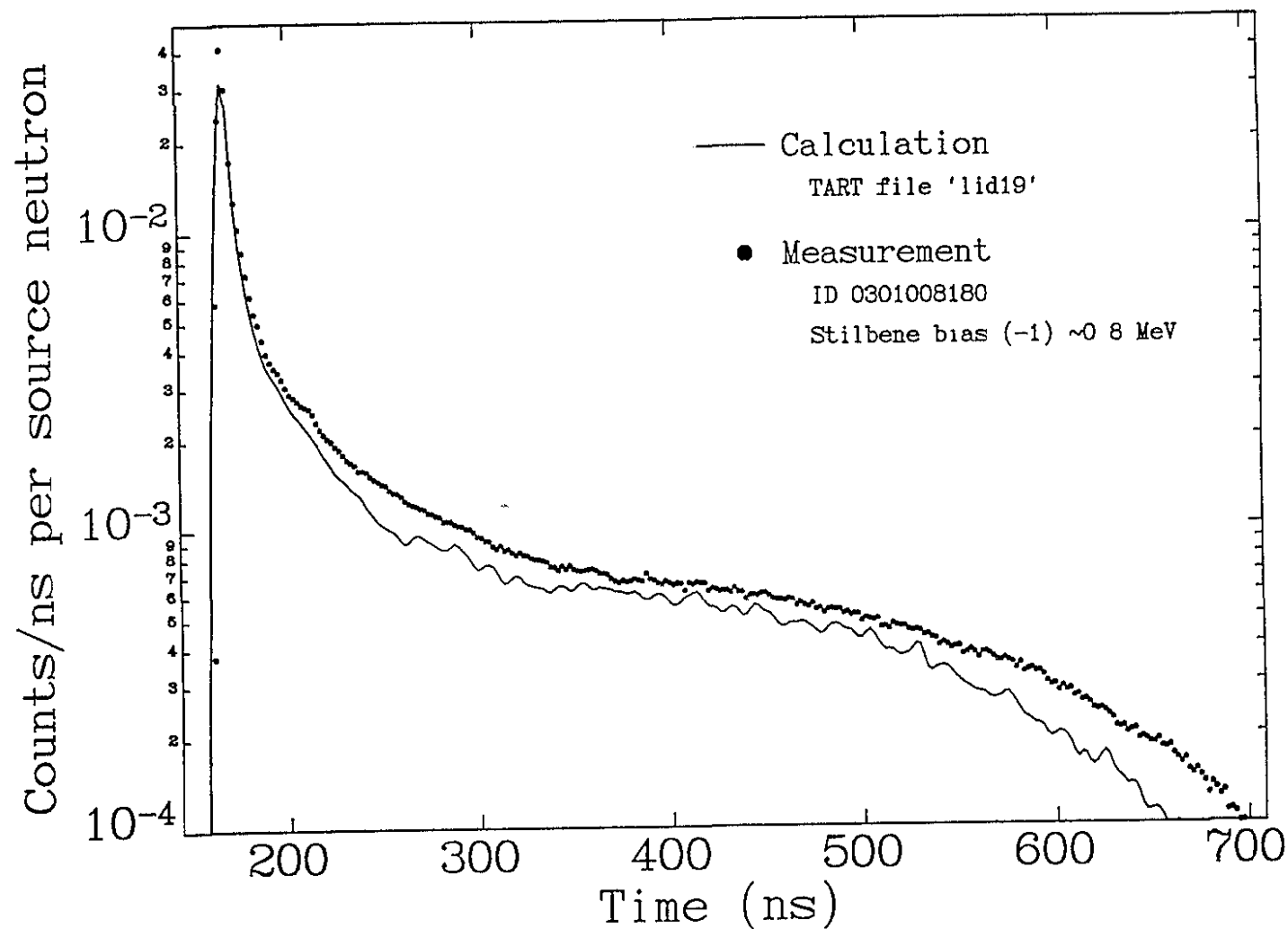


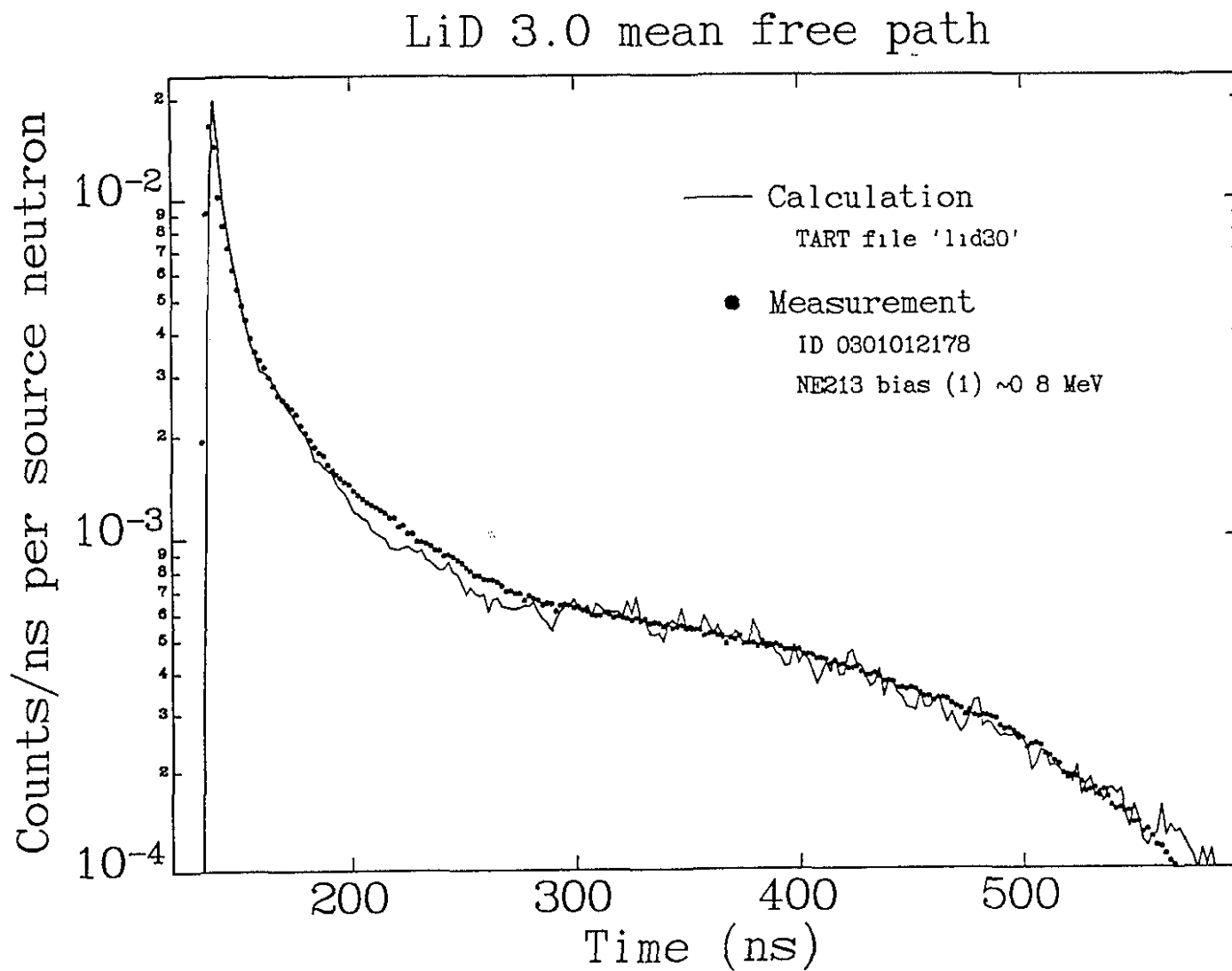


LiD 1.0 mean free path

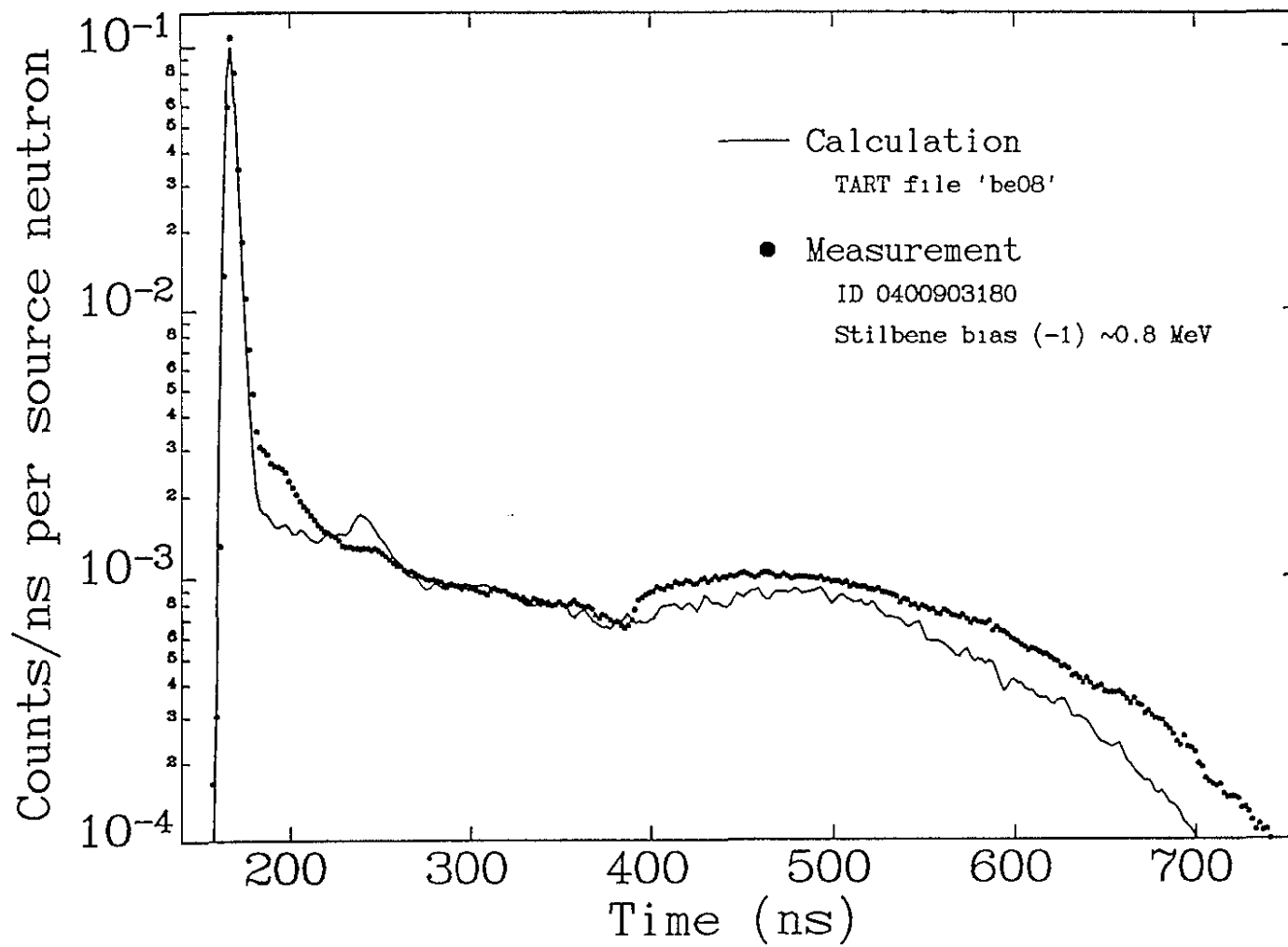


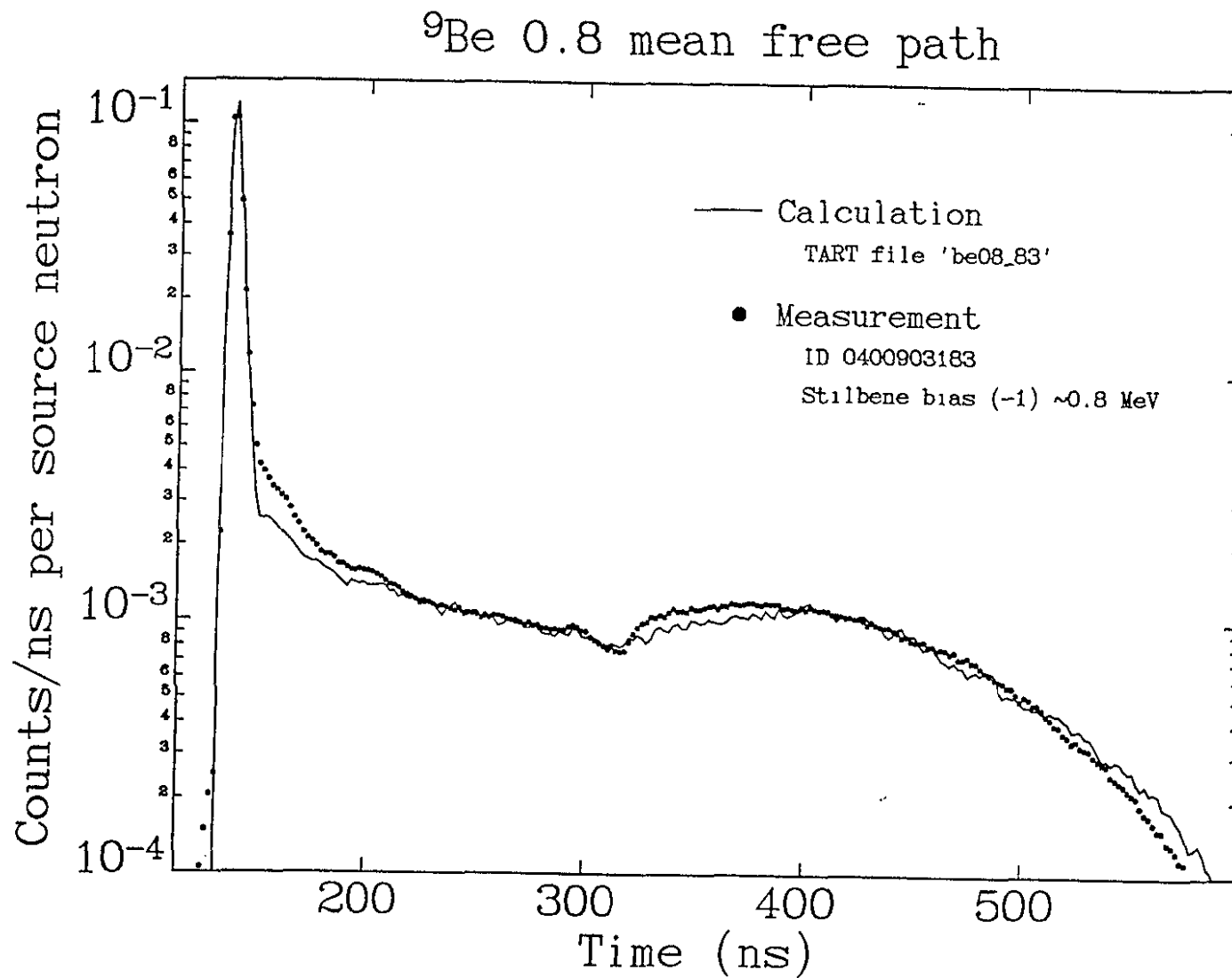
LiD 1.9 mean free path

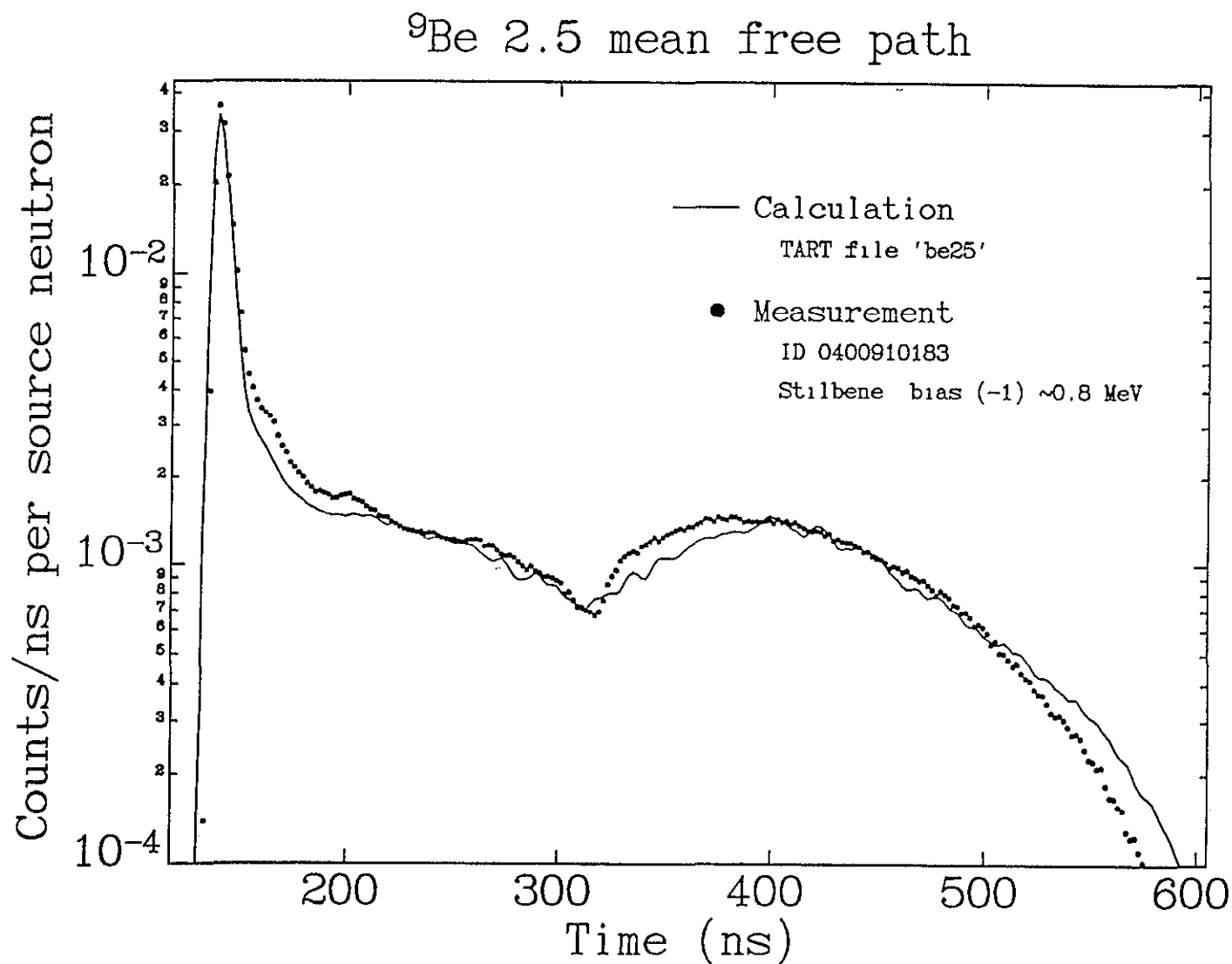




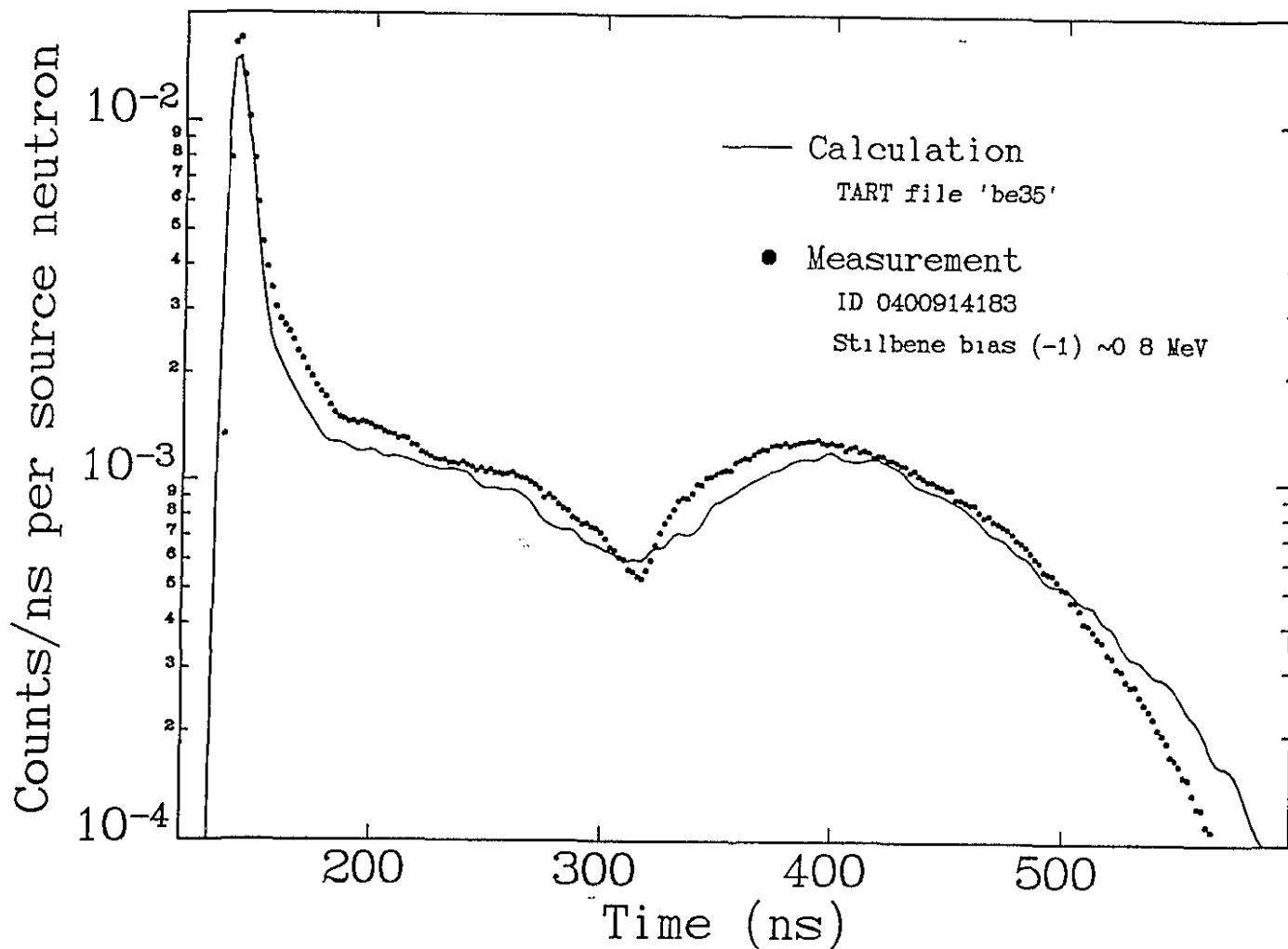
^{9}Be 0.8 mean free path

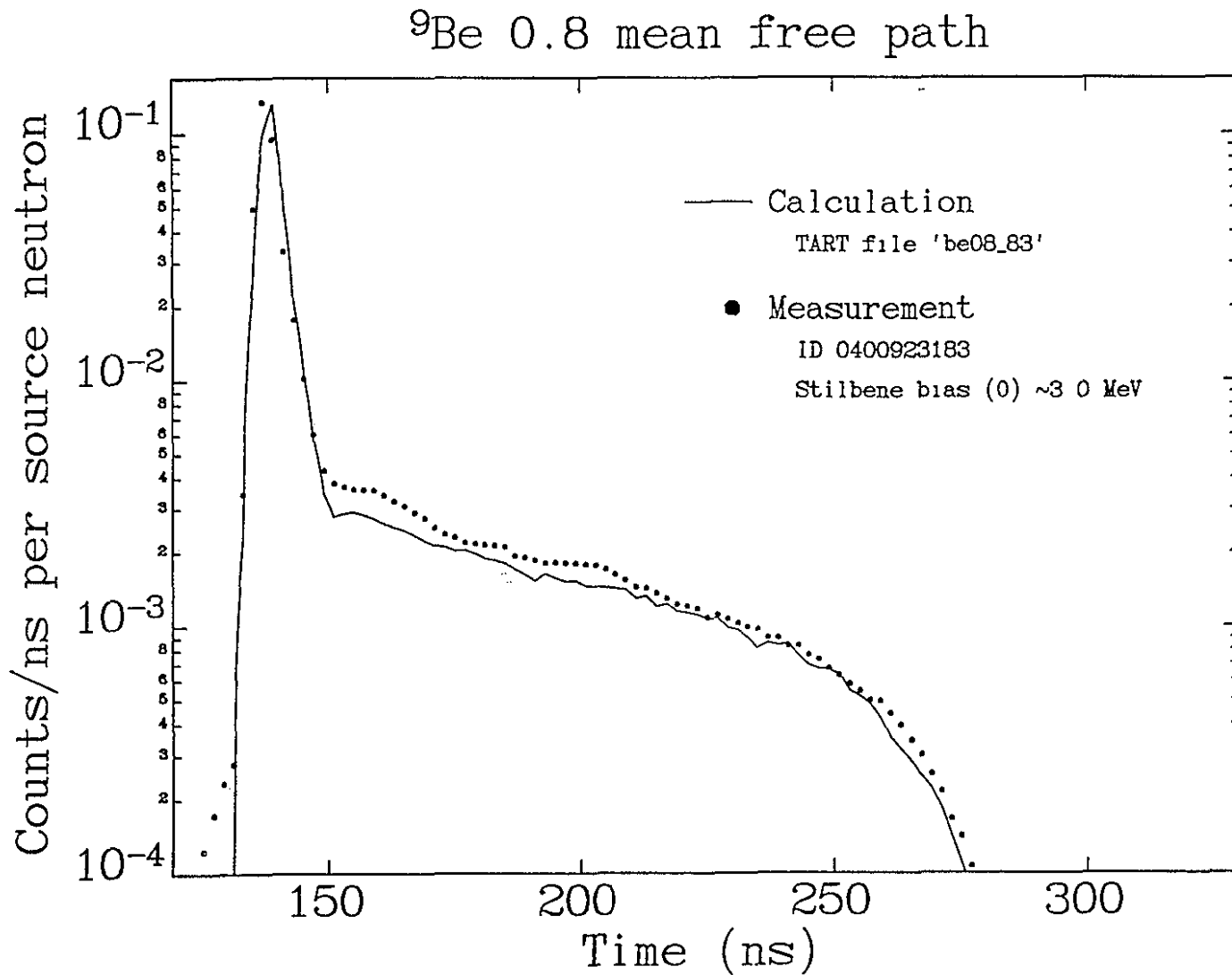


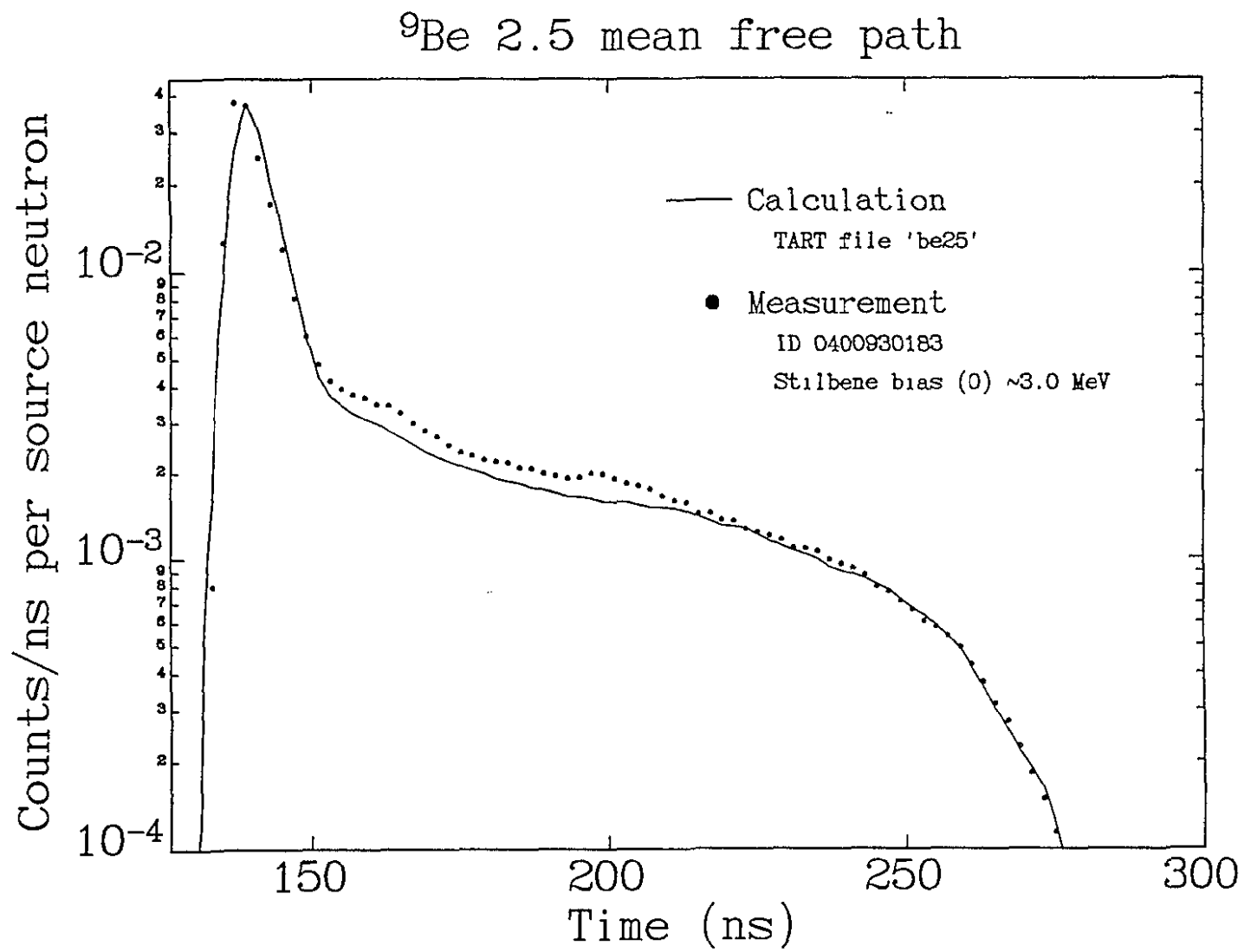




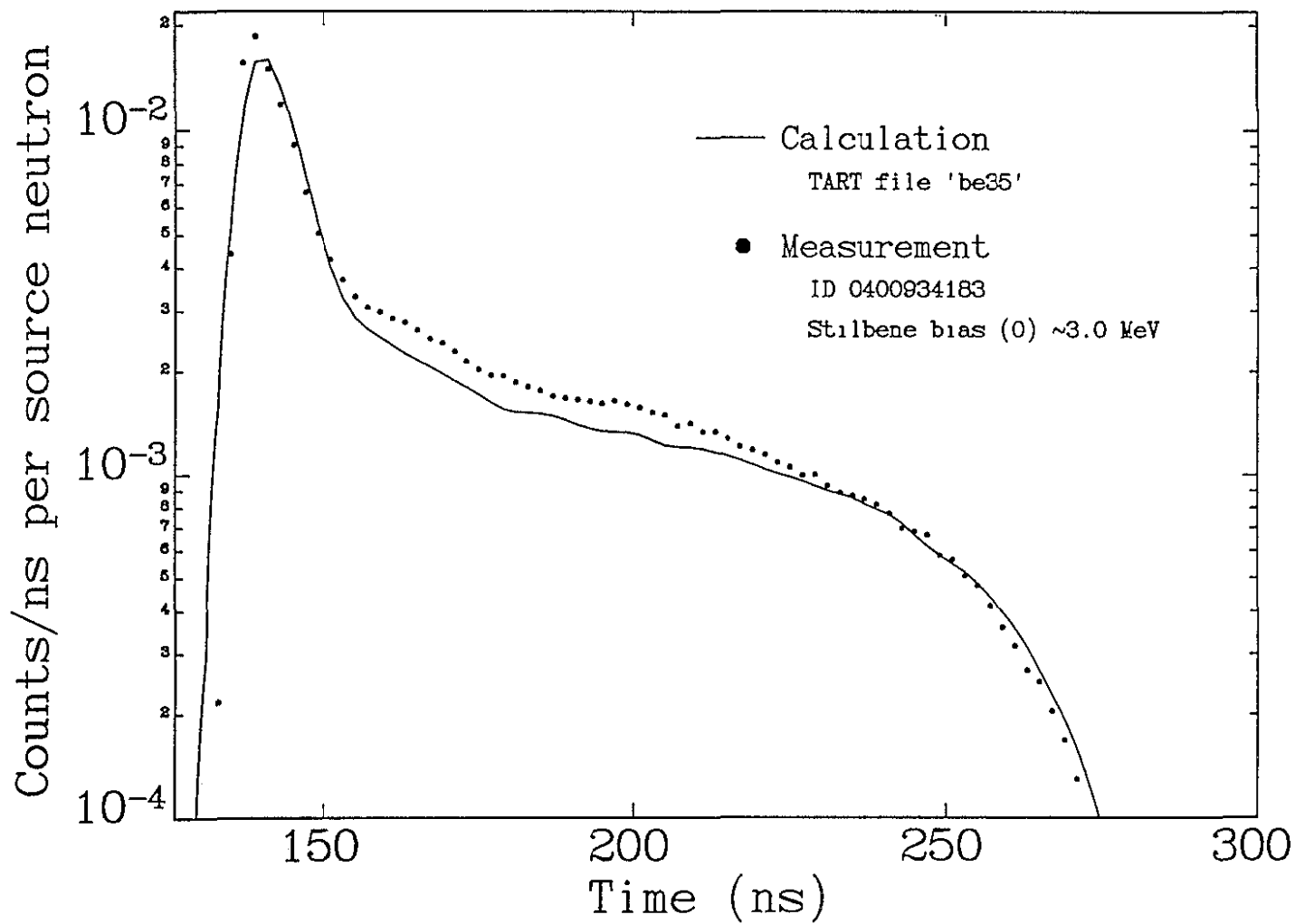
^{9}Be 3.5 mean free path

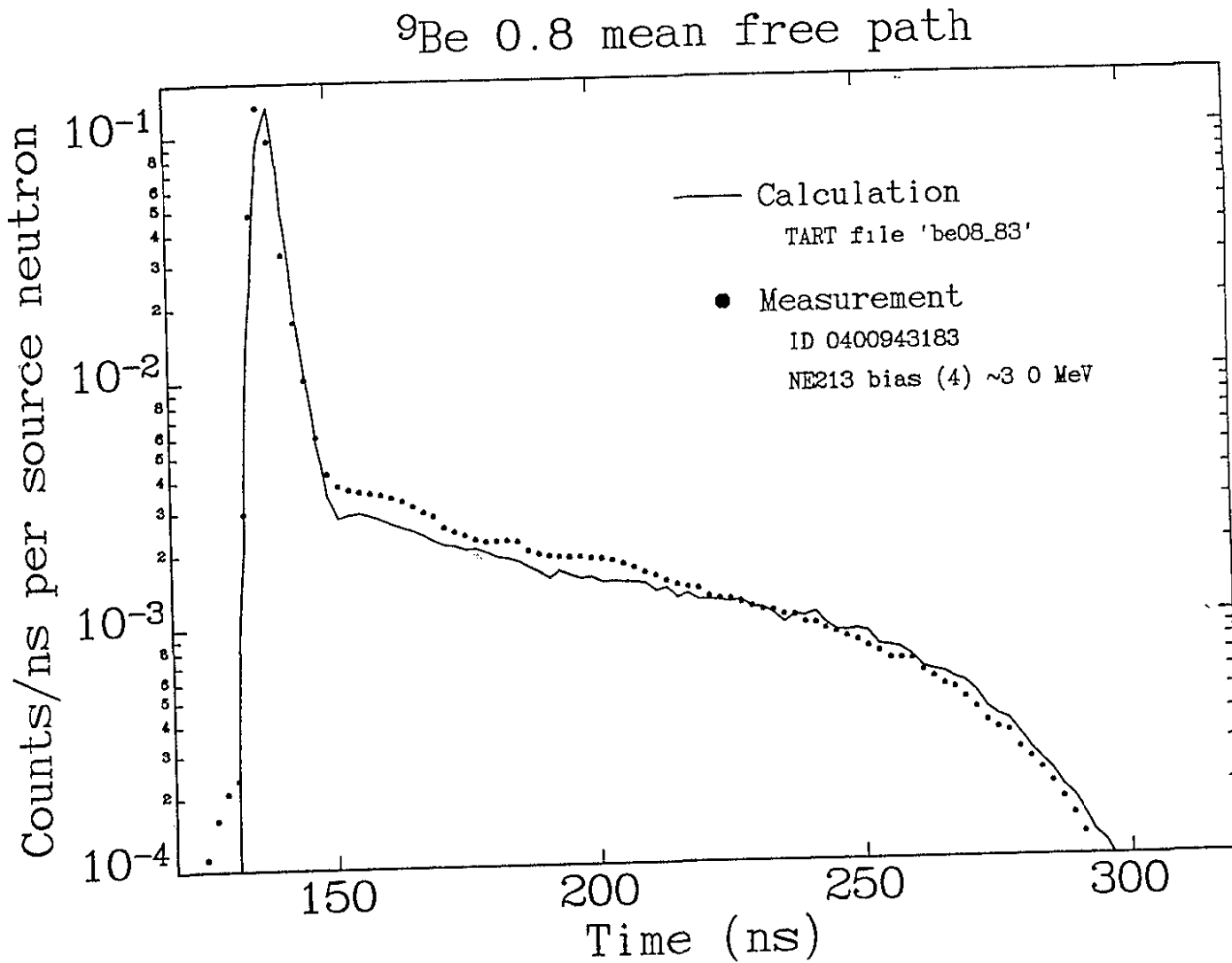




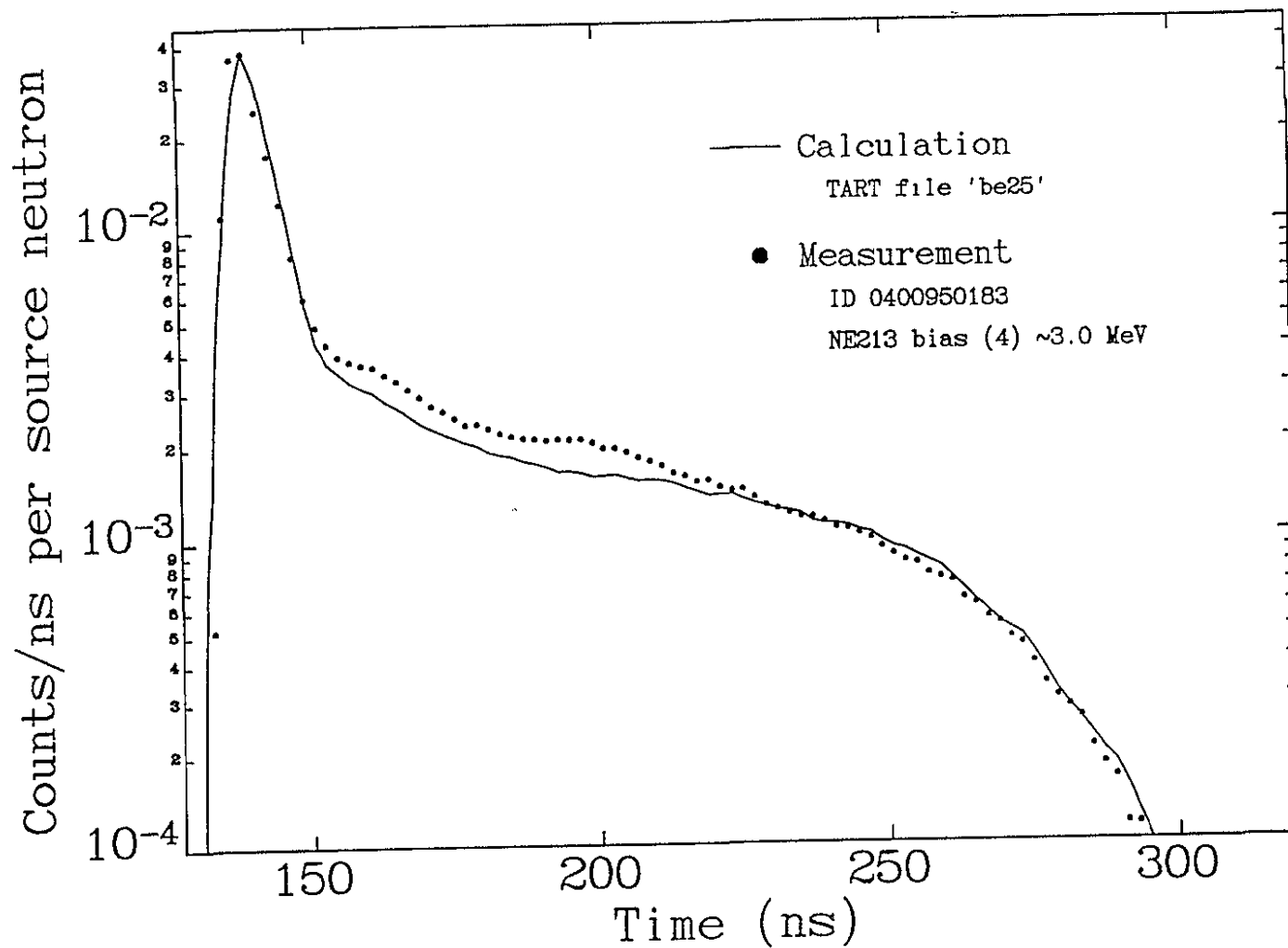


^{9}Be 3.5 mean free path

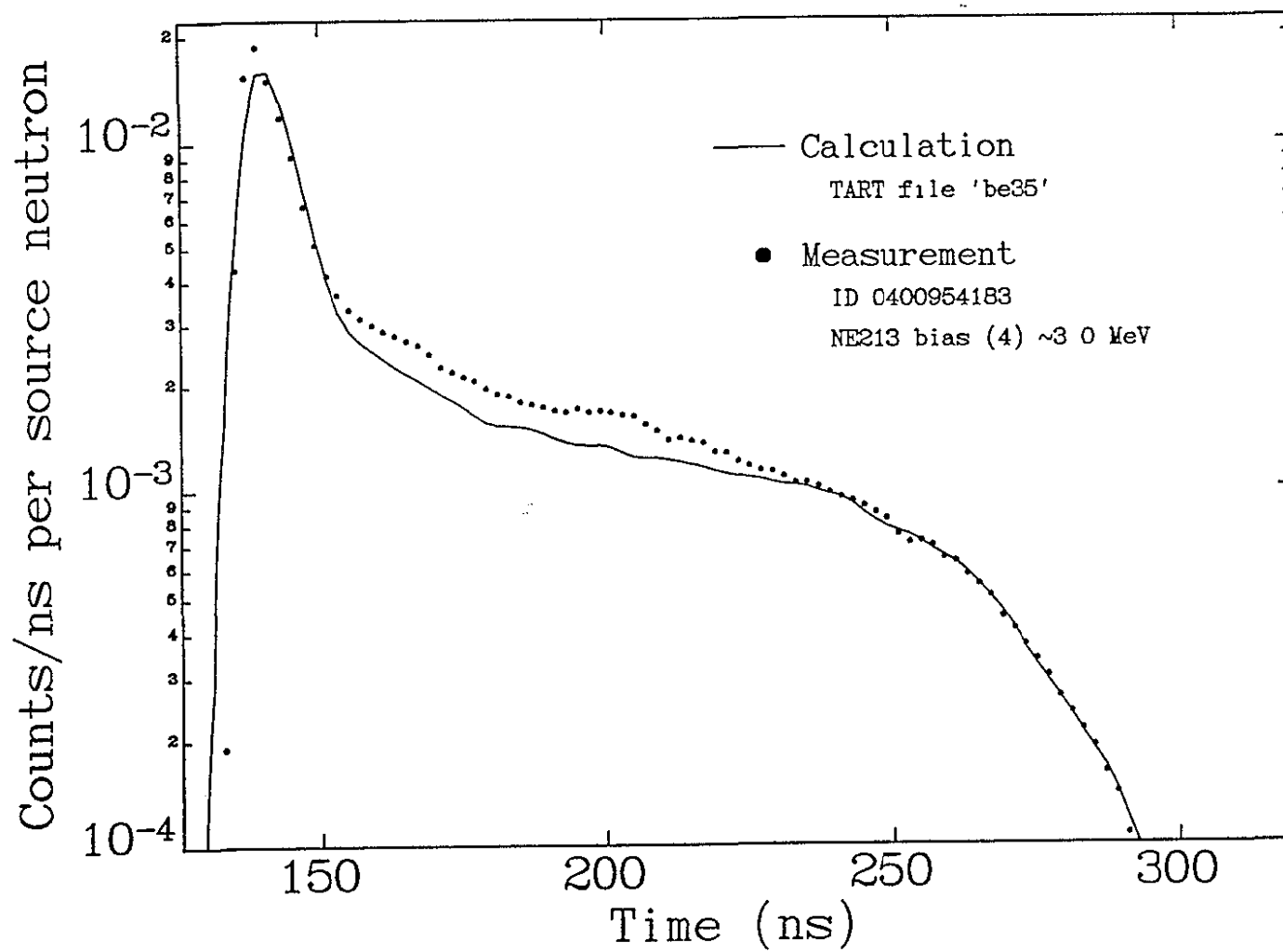


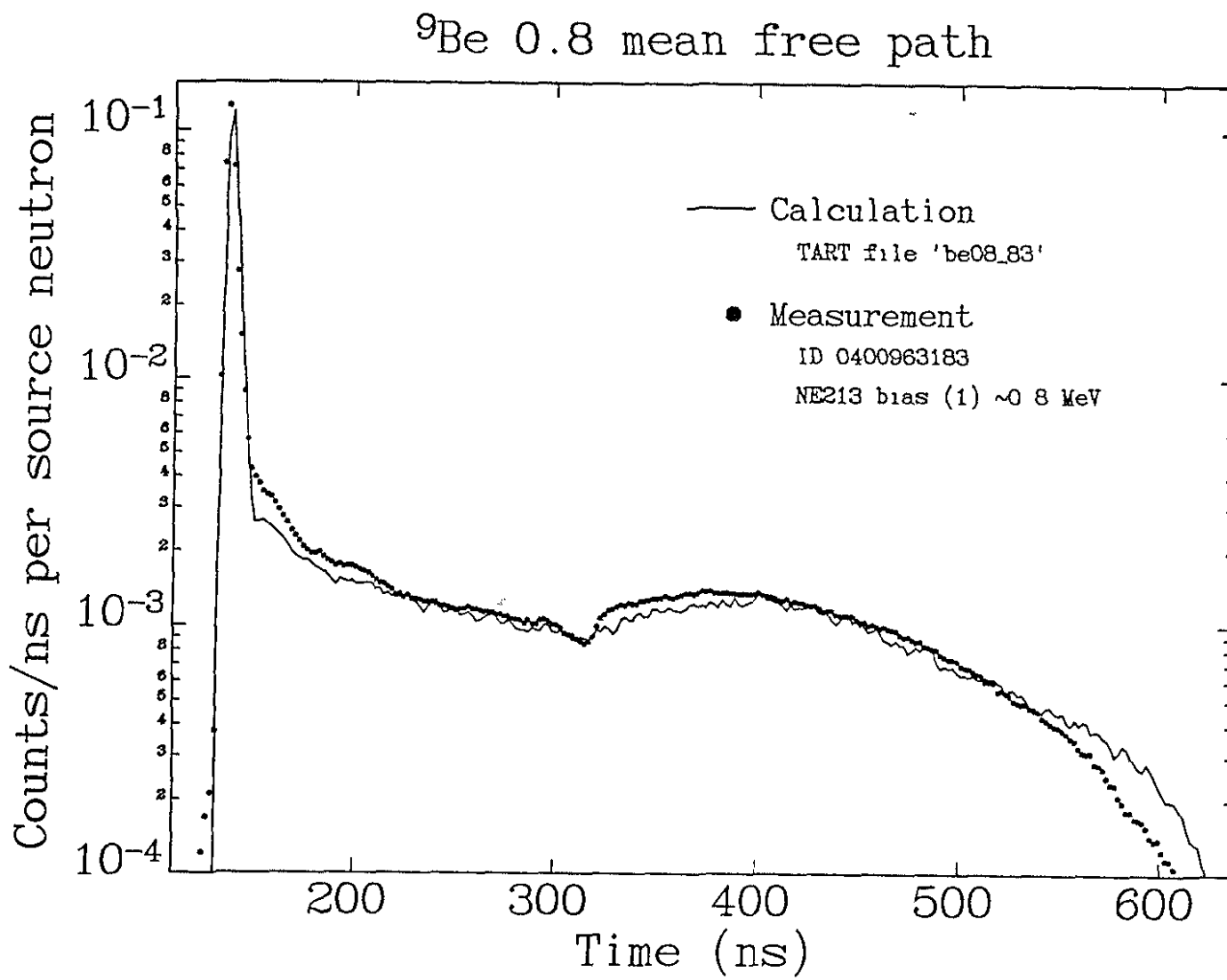


^{9}Be 2.5 mean free path

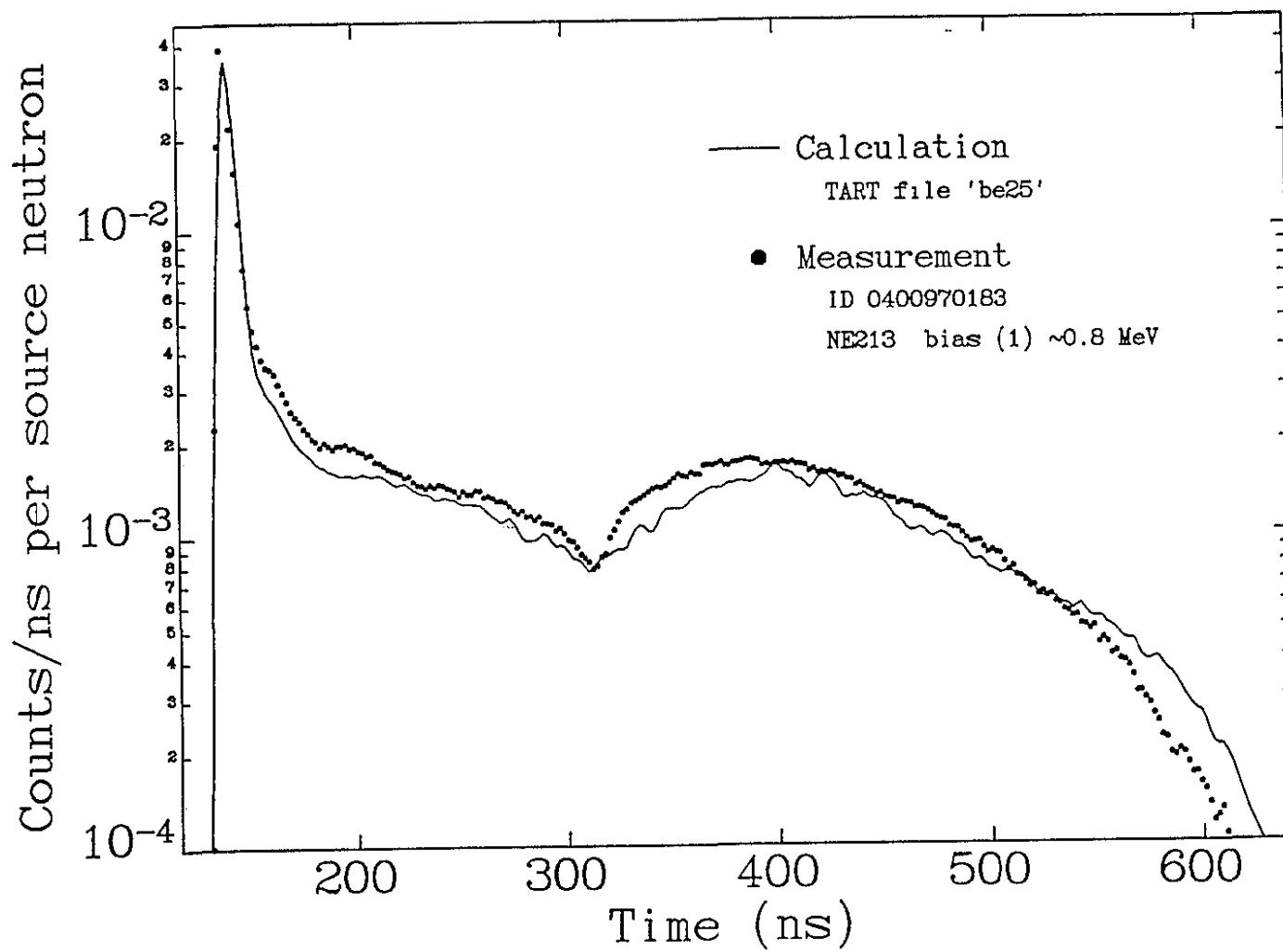


^{9}Be 3.5 mean free path

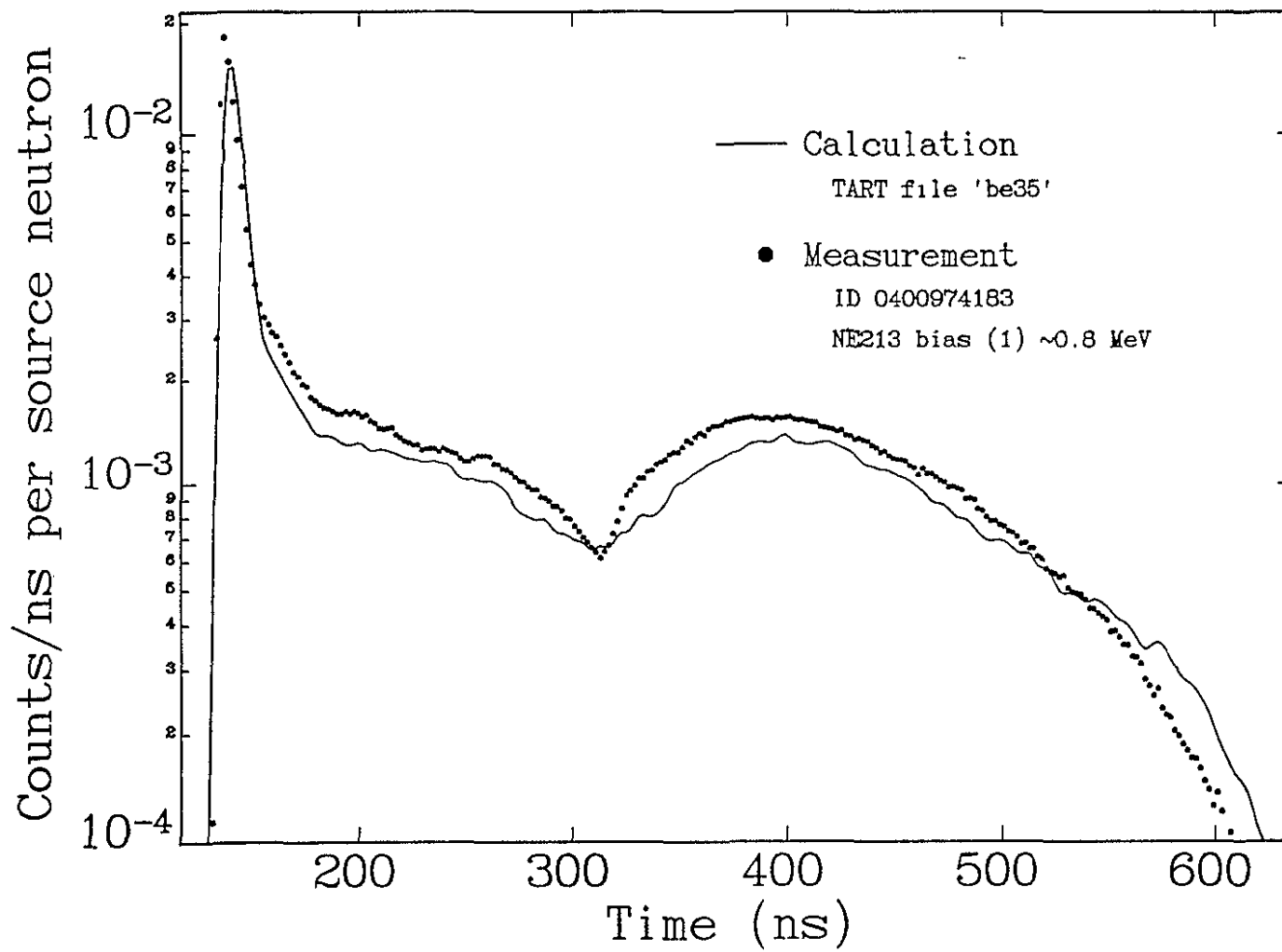




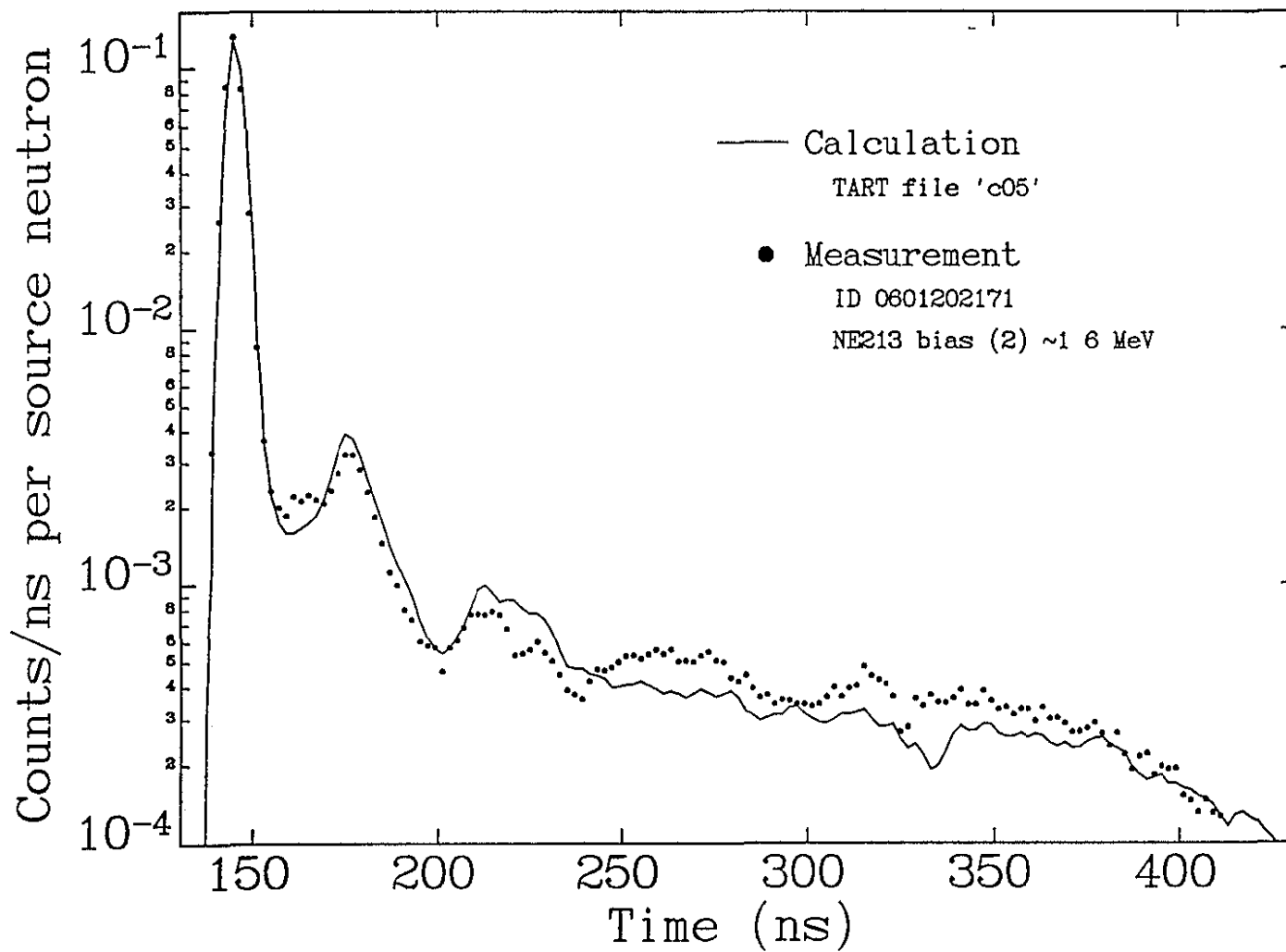
^{9}Be 2.5 mean free path

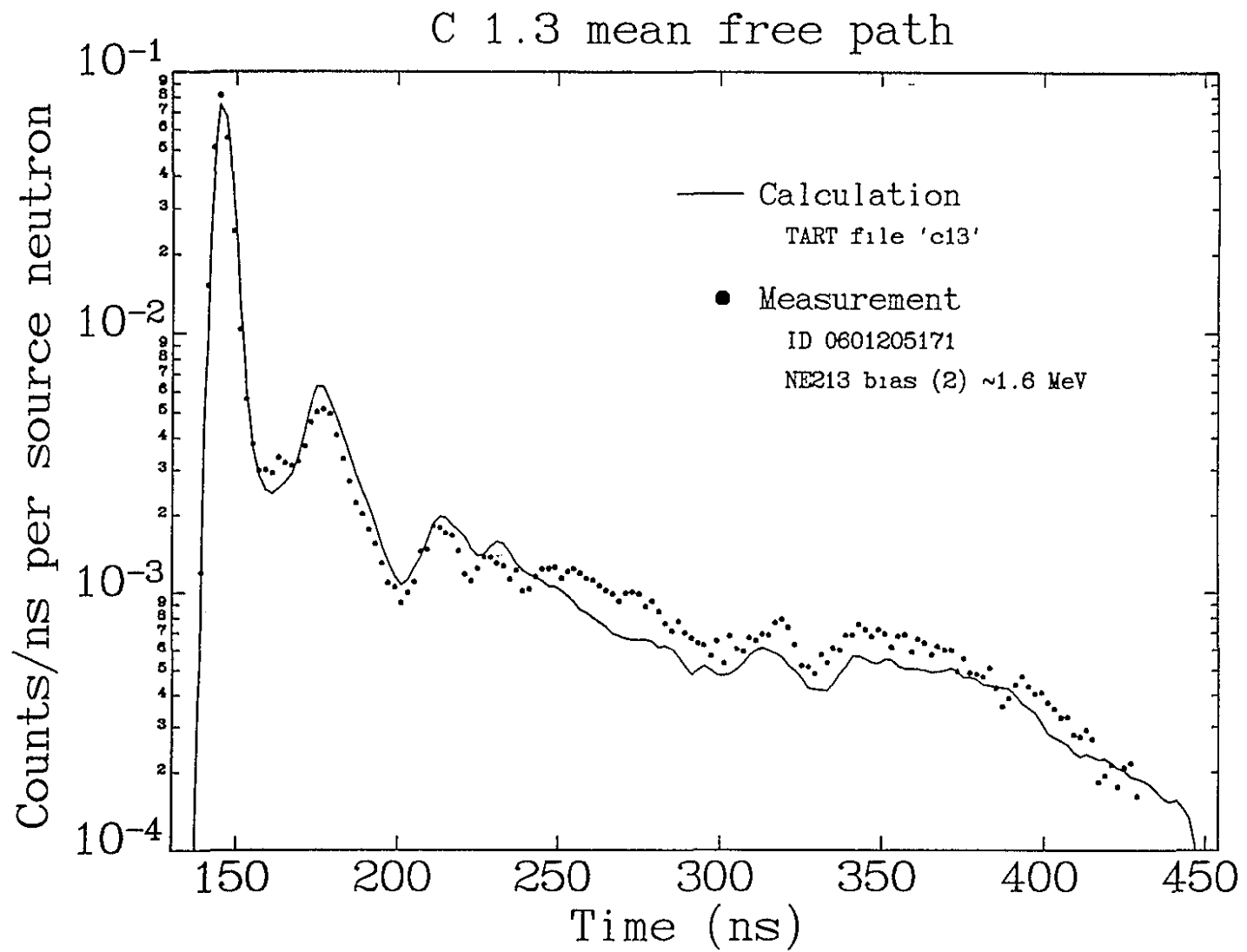


^{9}Be 3.5 mean free path

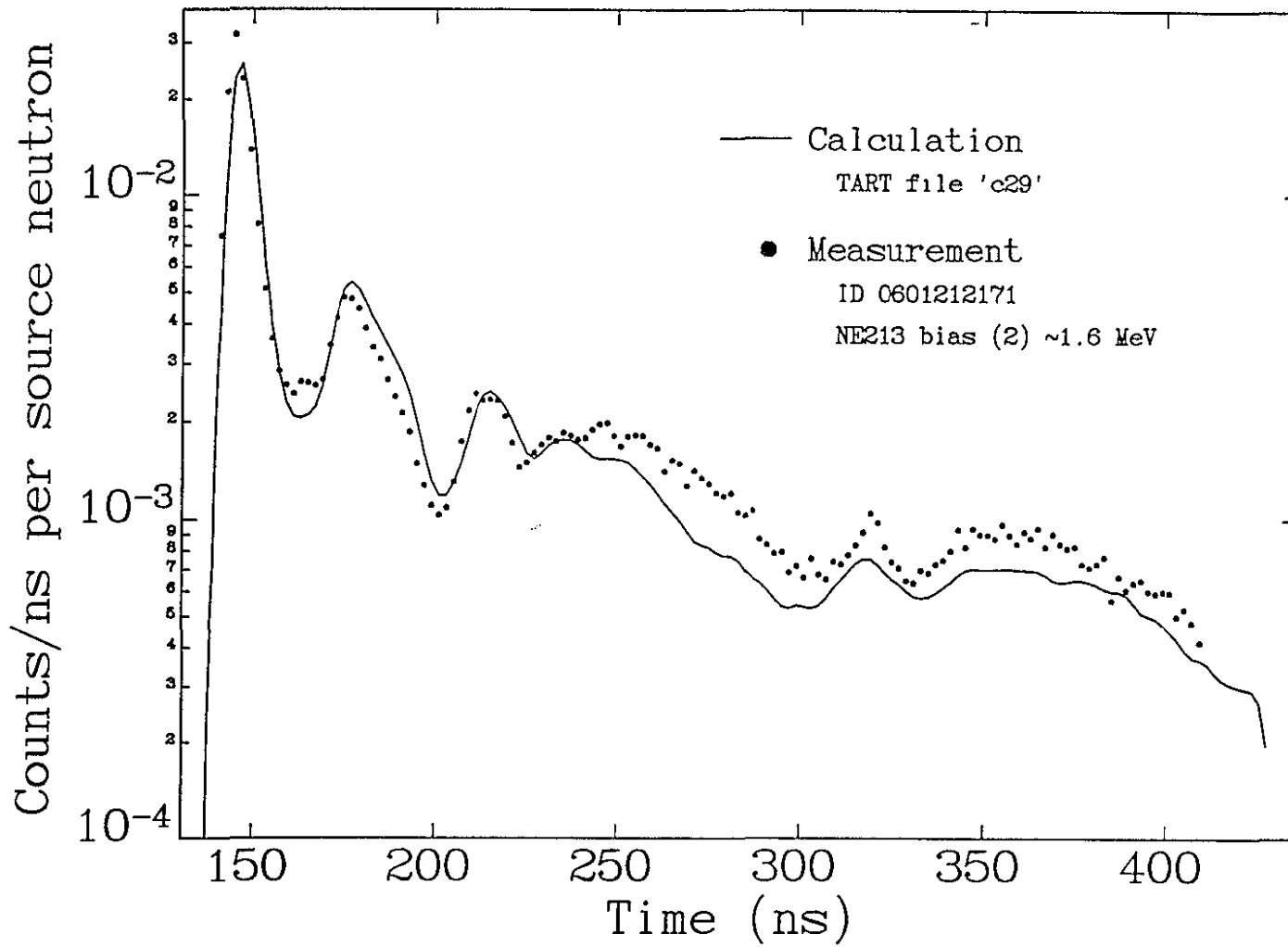


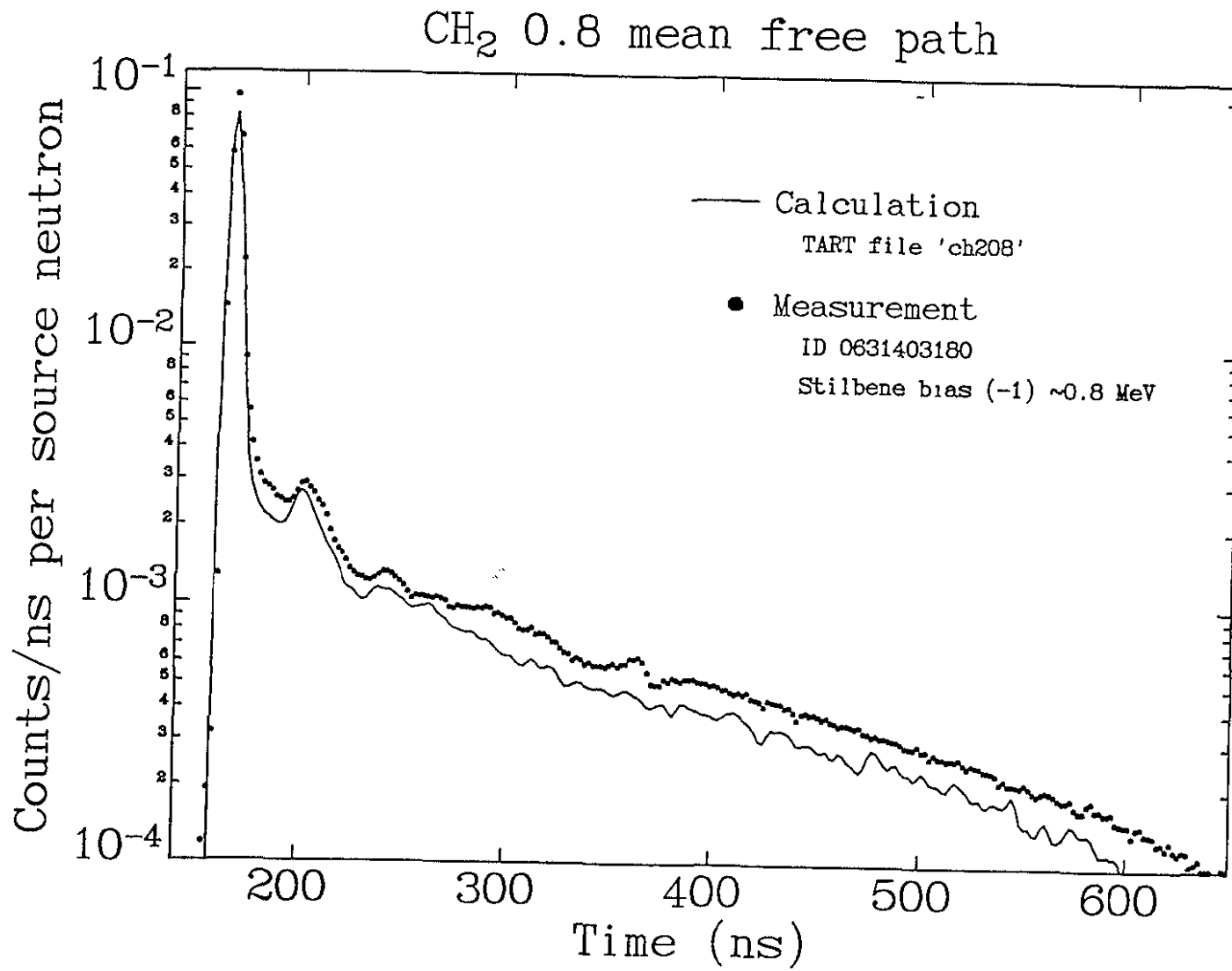
C 0.5 mean free path

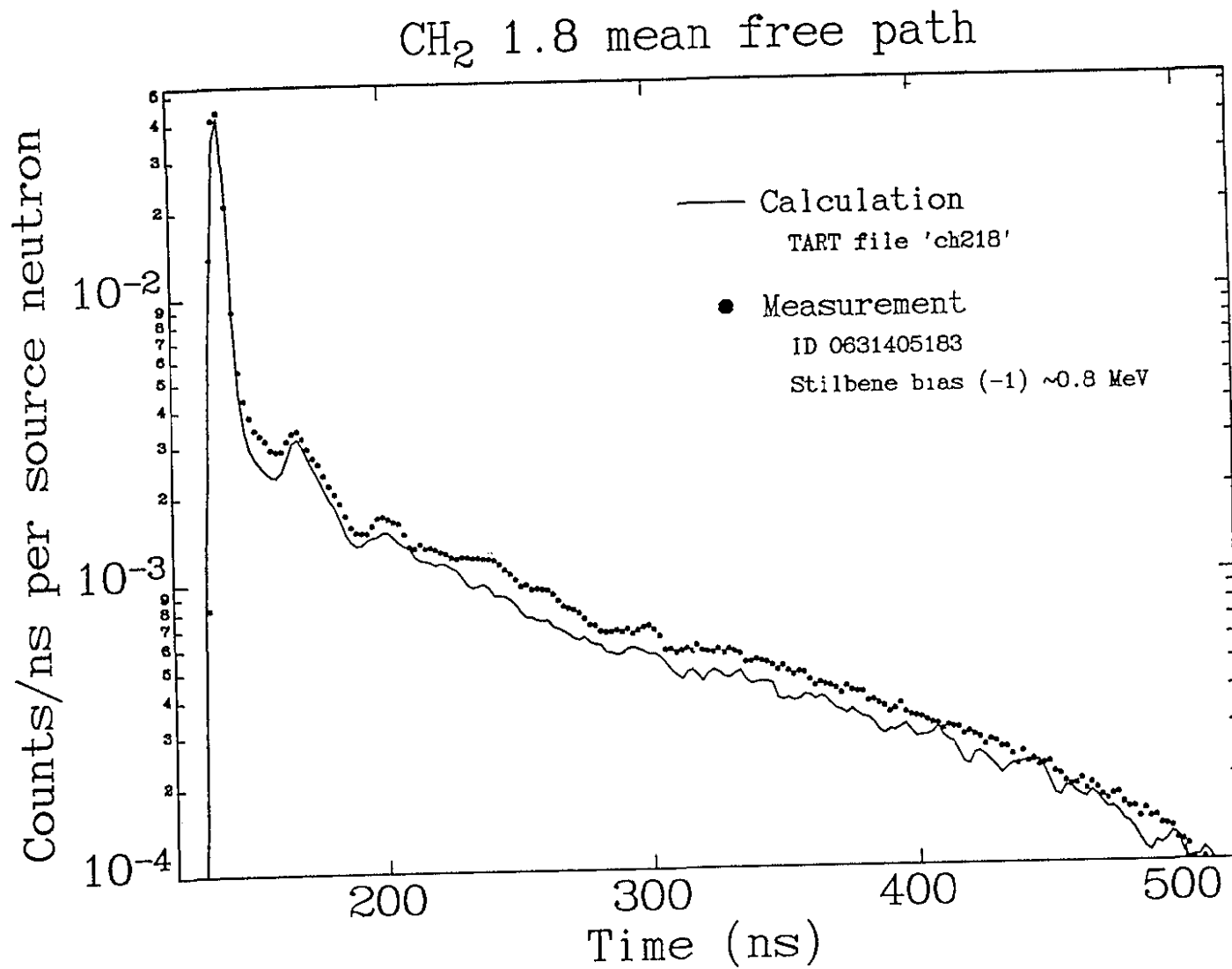


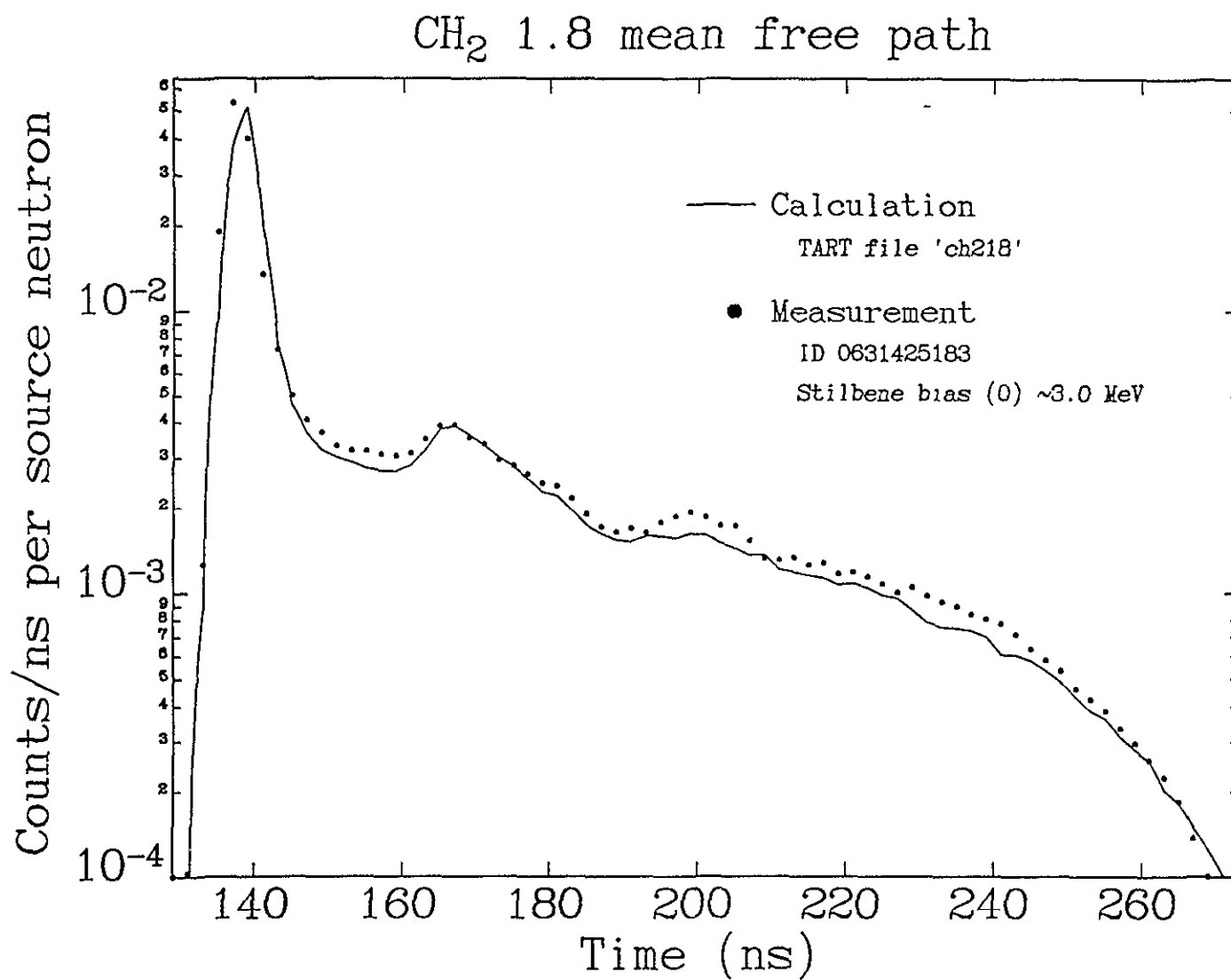


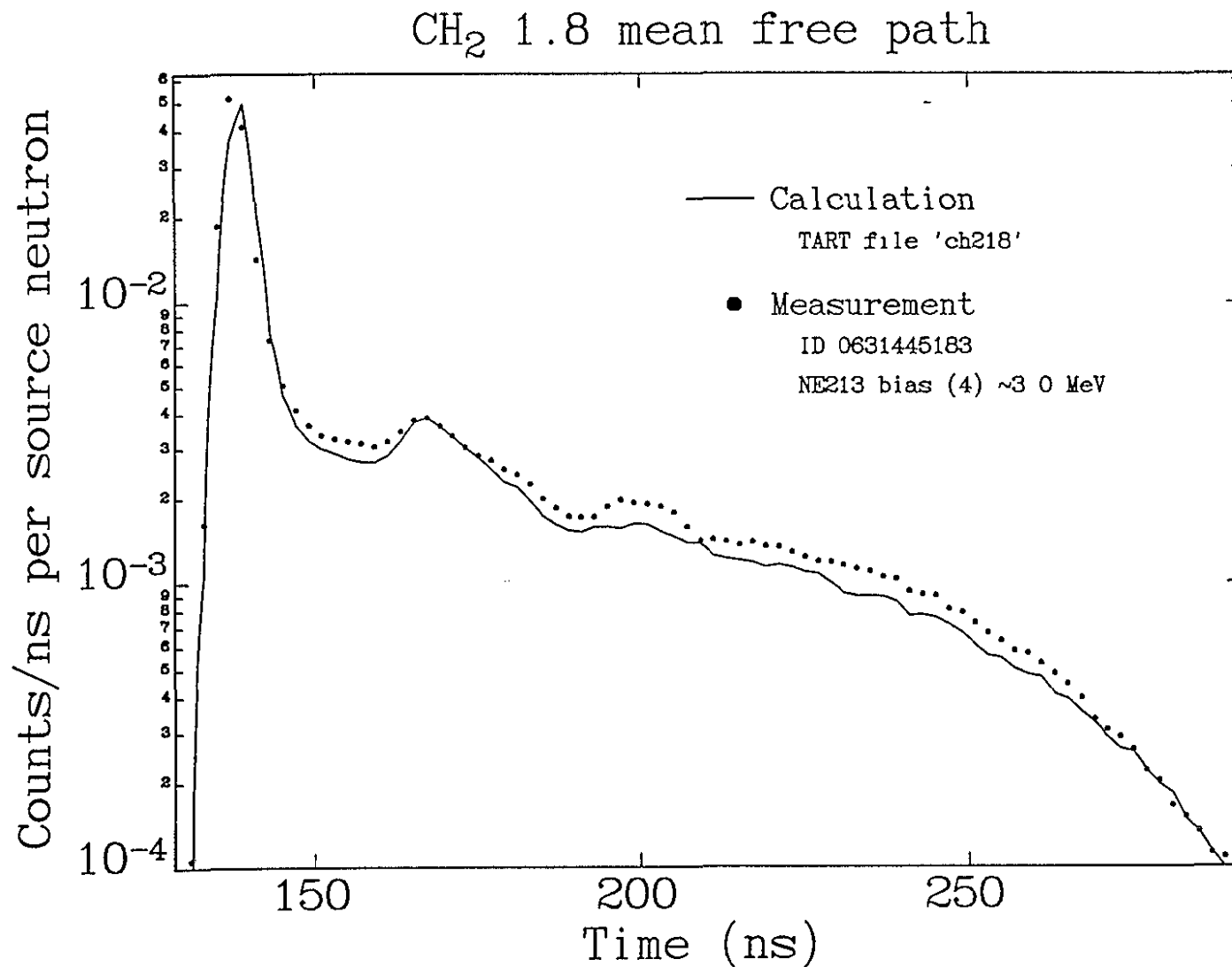
C 2.9 mean free path



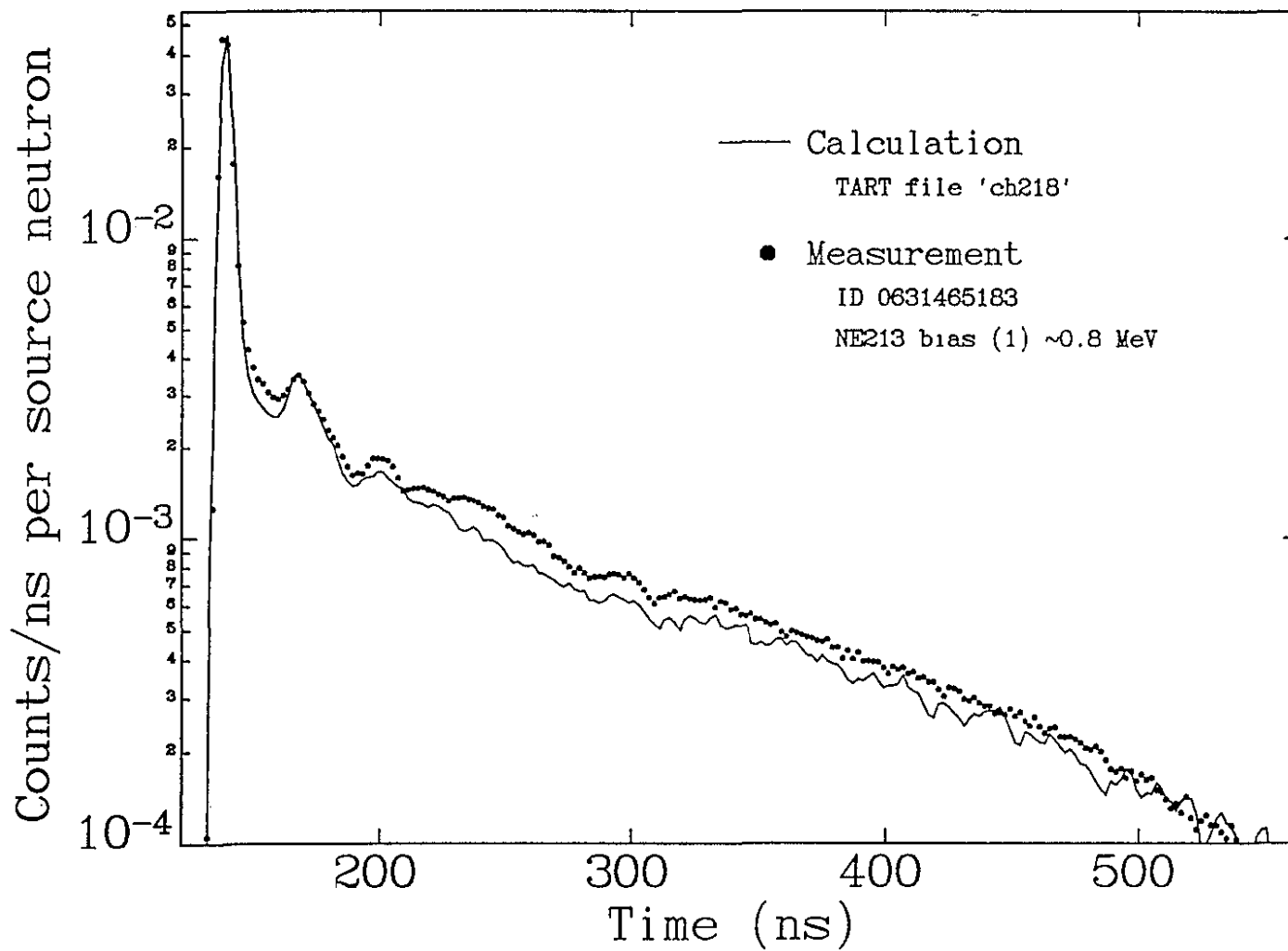


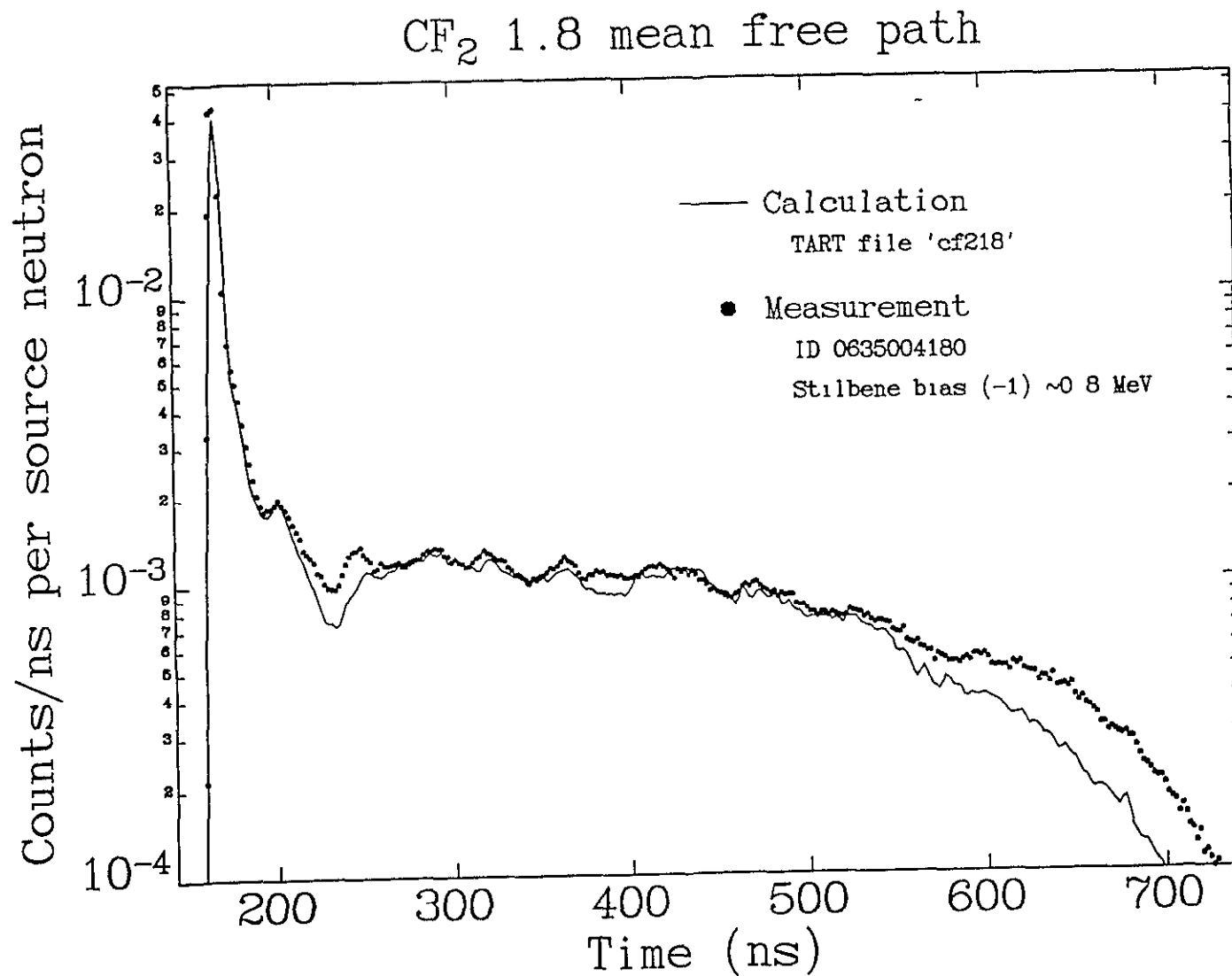




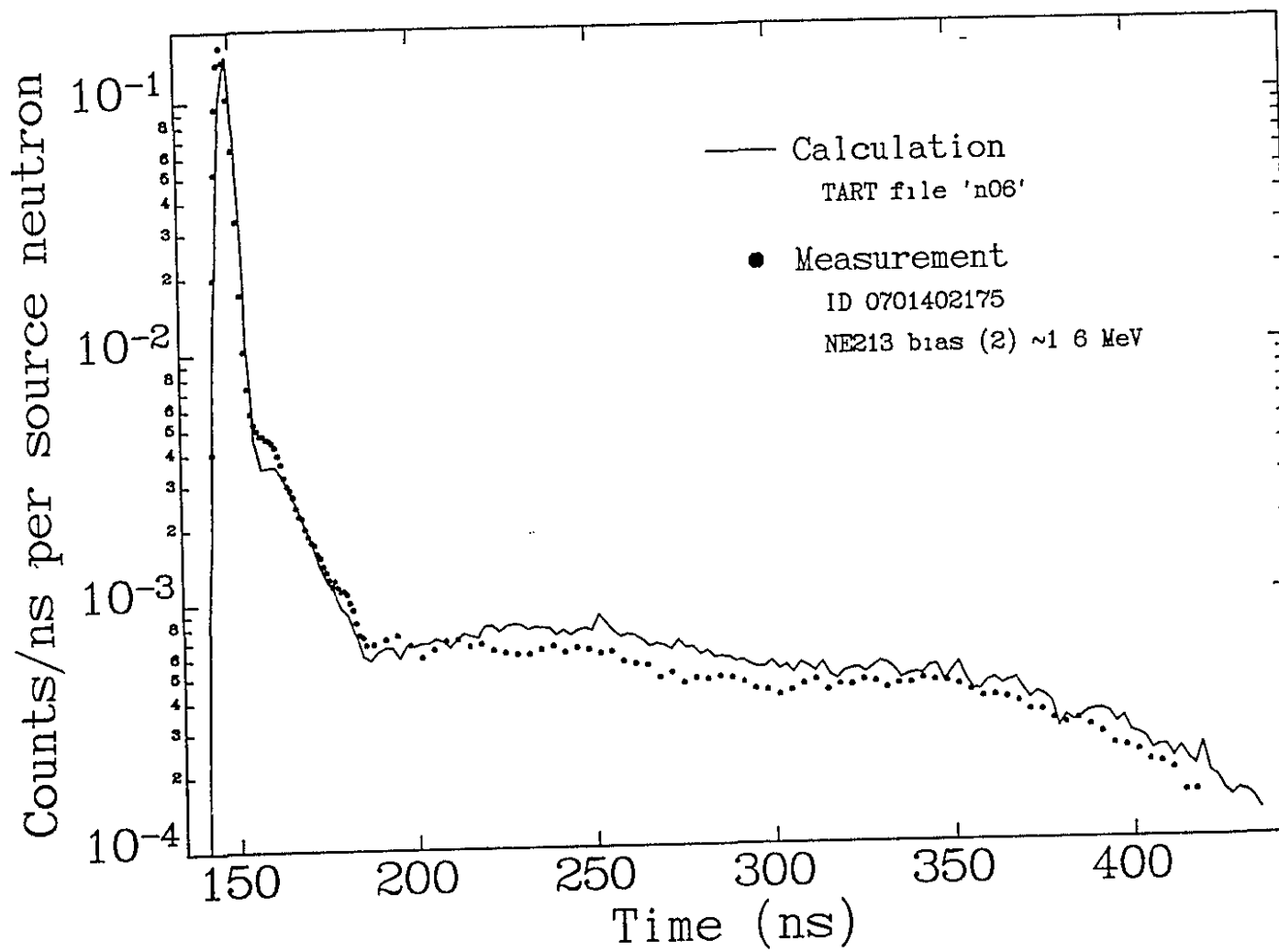


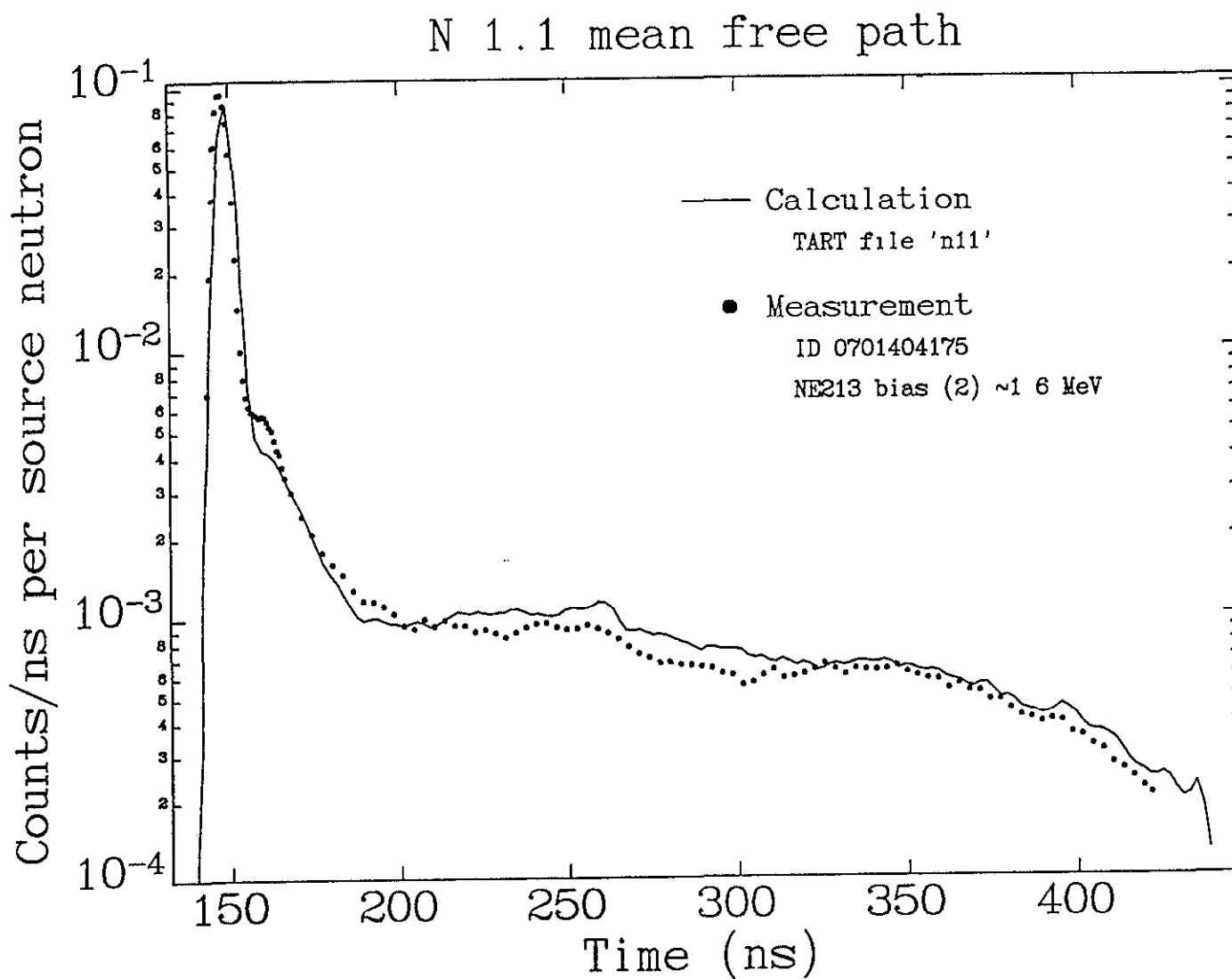
CH₂ 1.8 mean free path

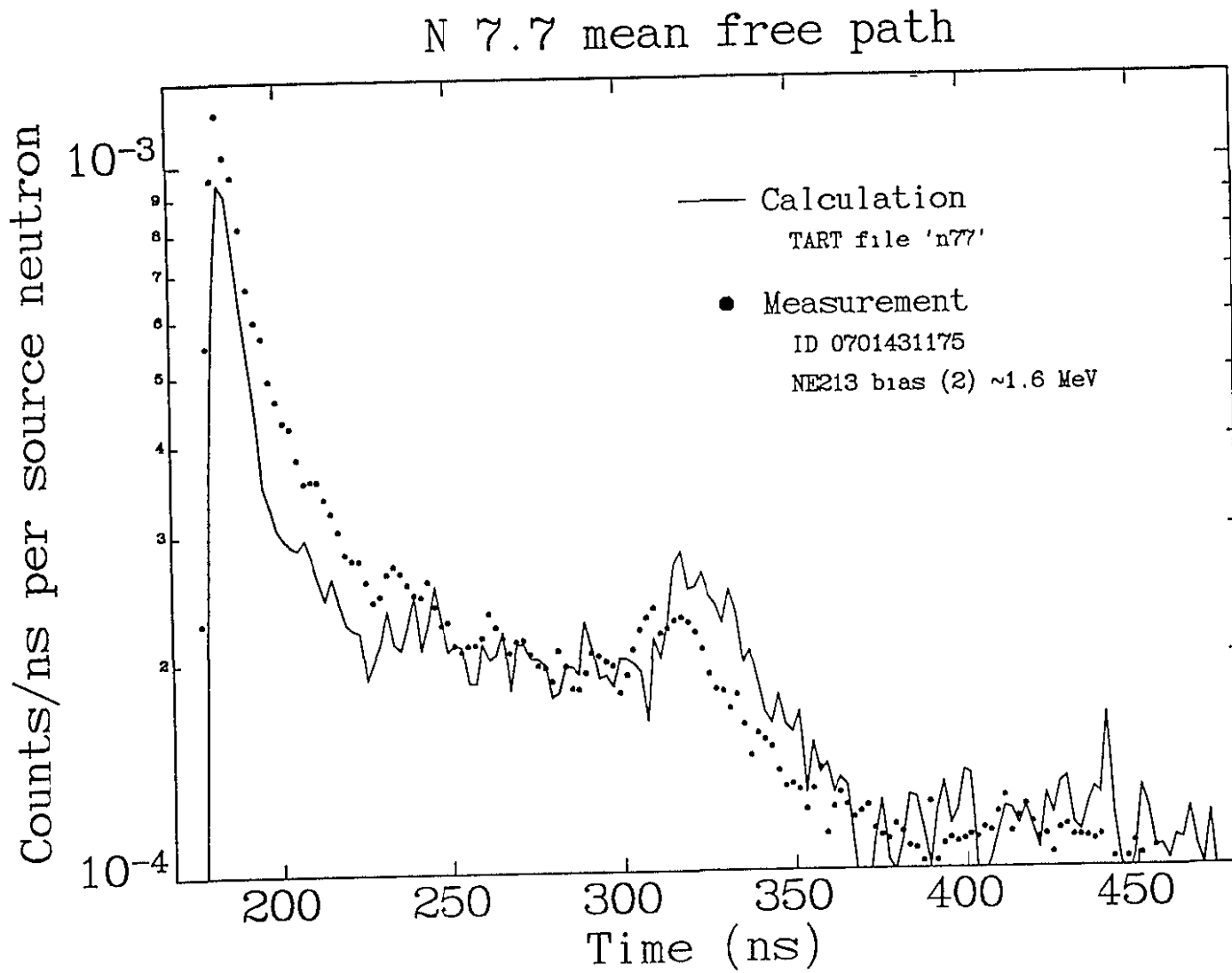




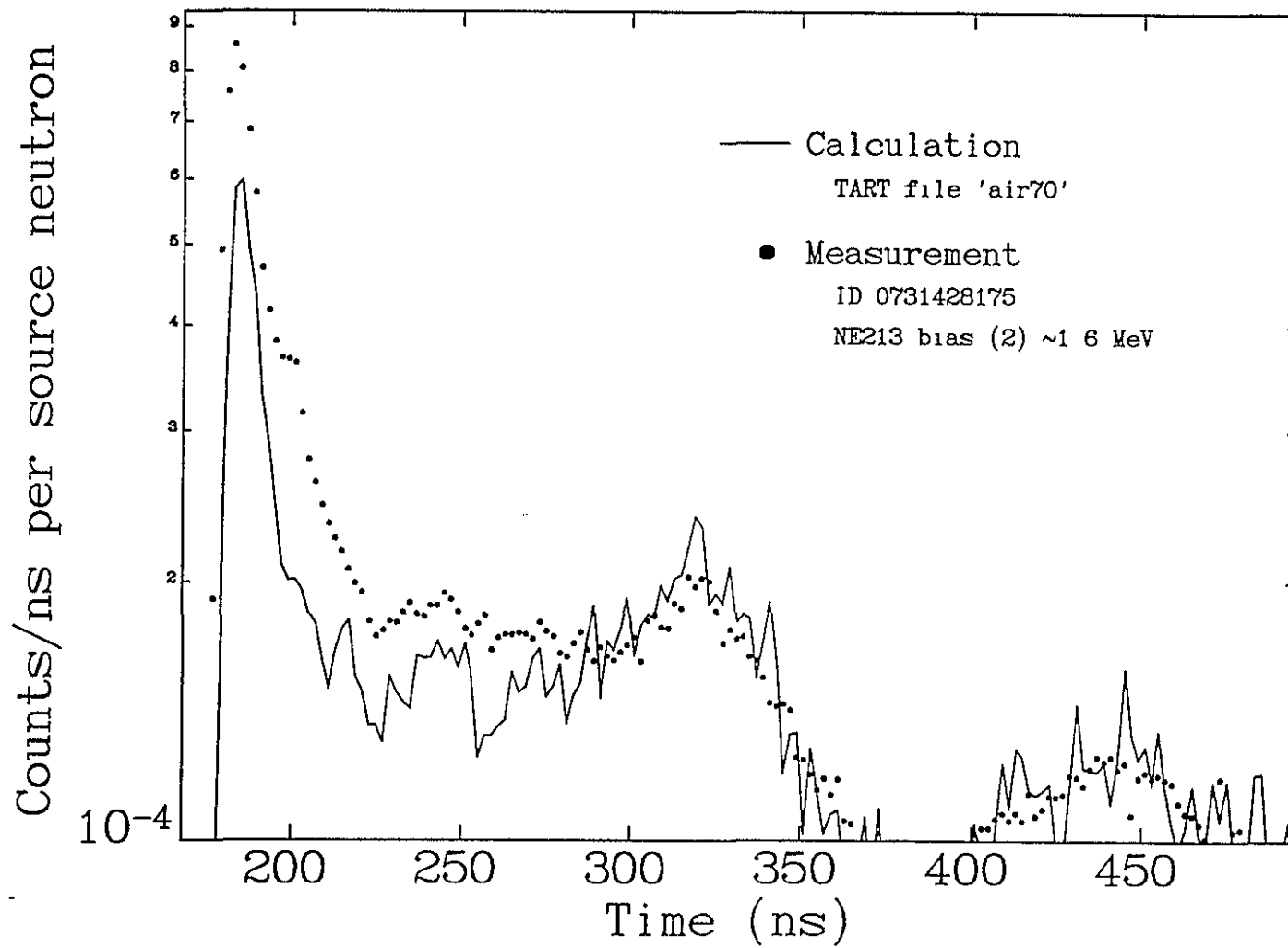
N 0.6 mean free path

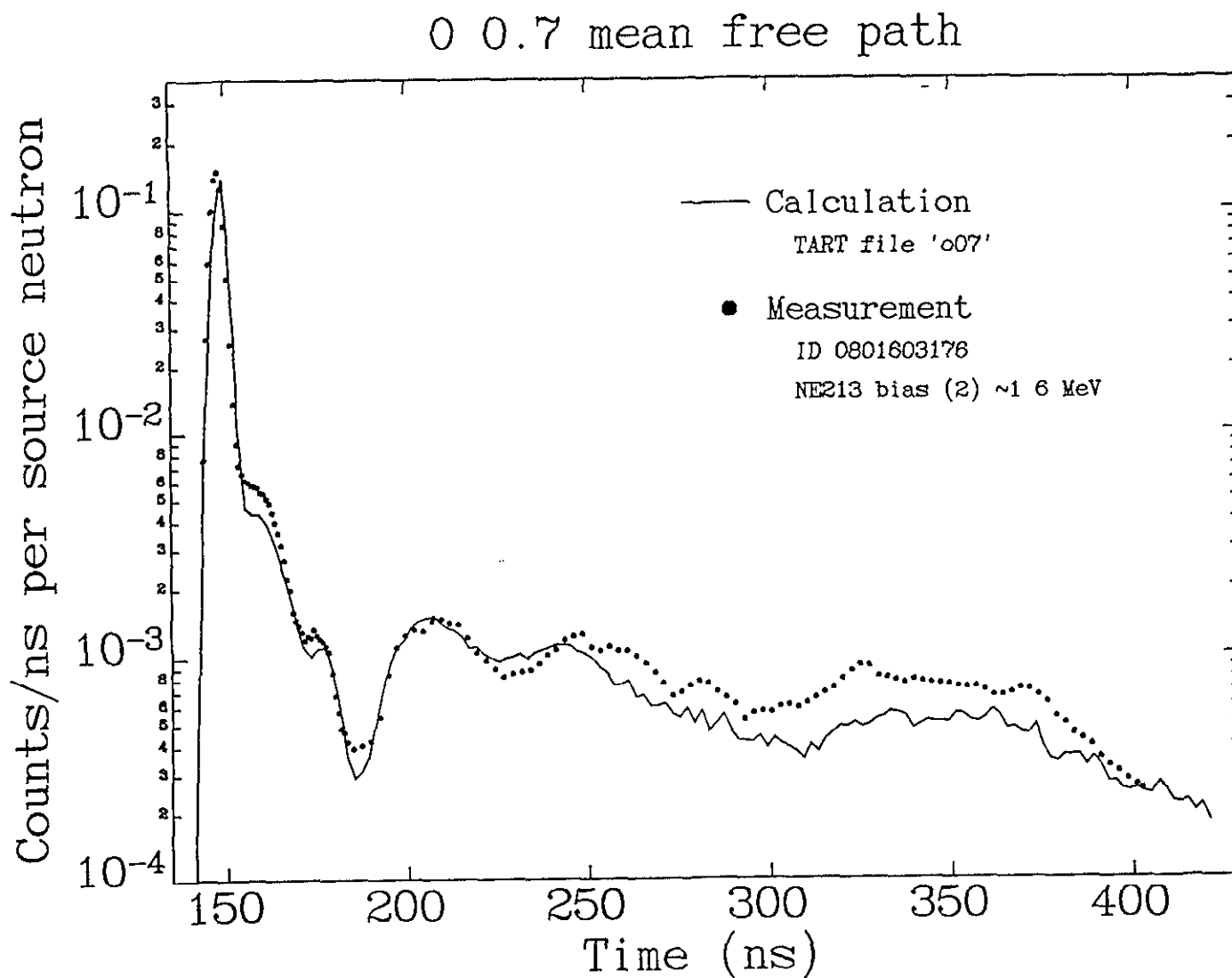


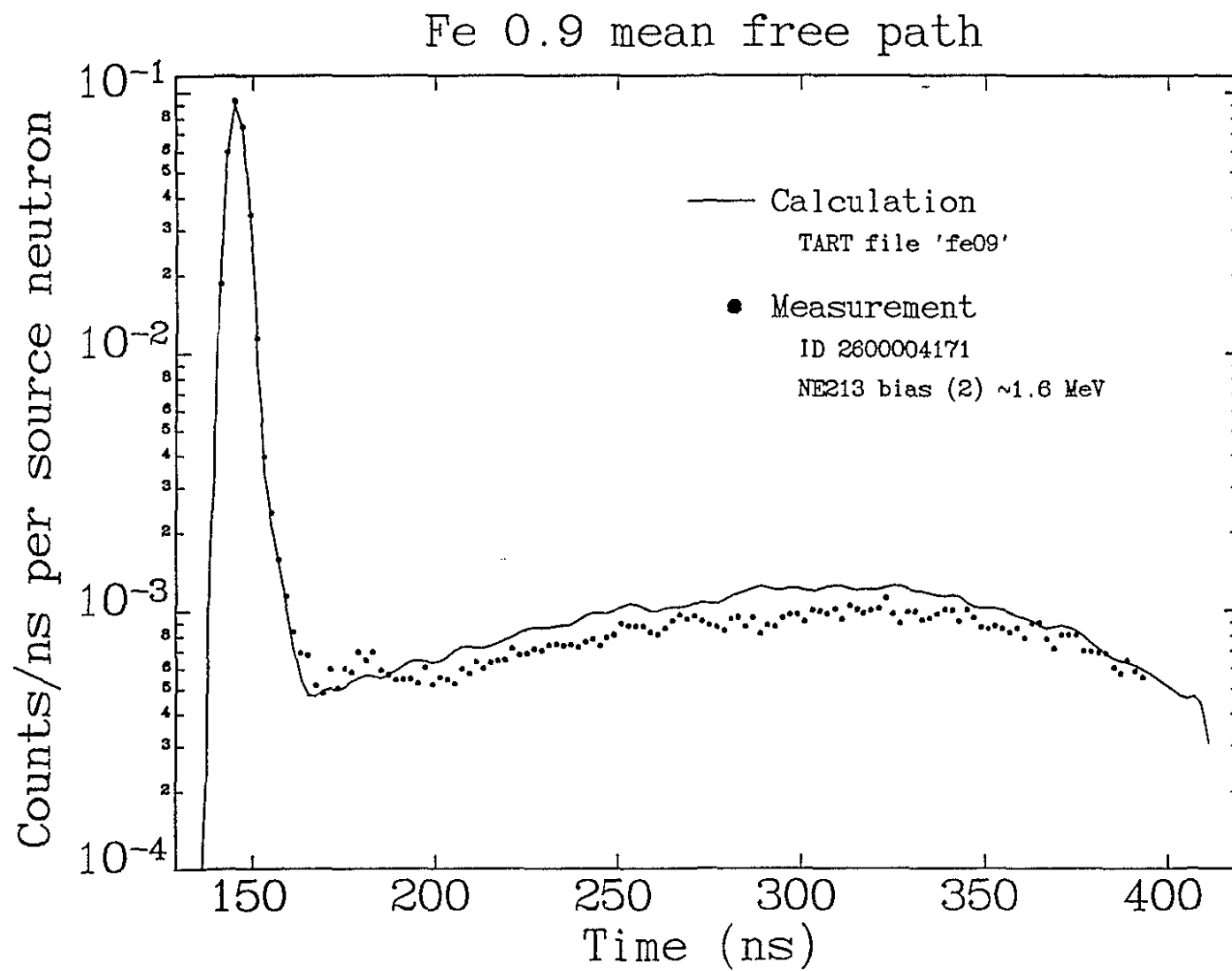




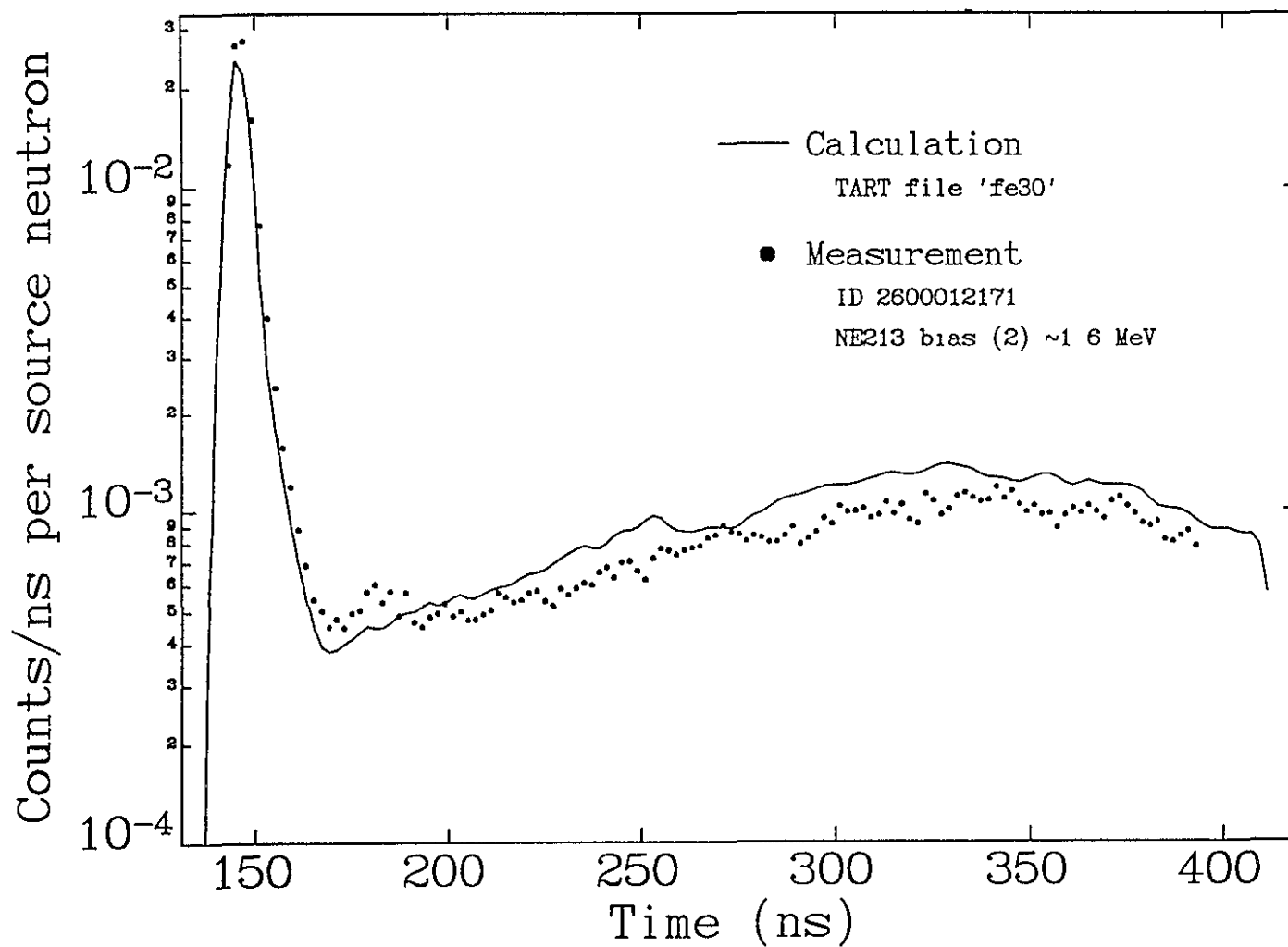
Air 7.0 mean free path

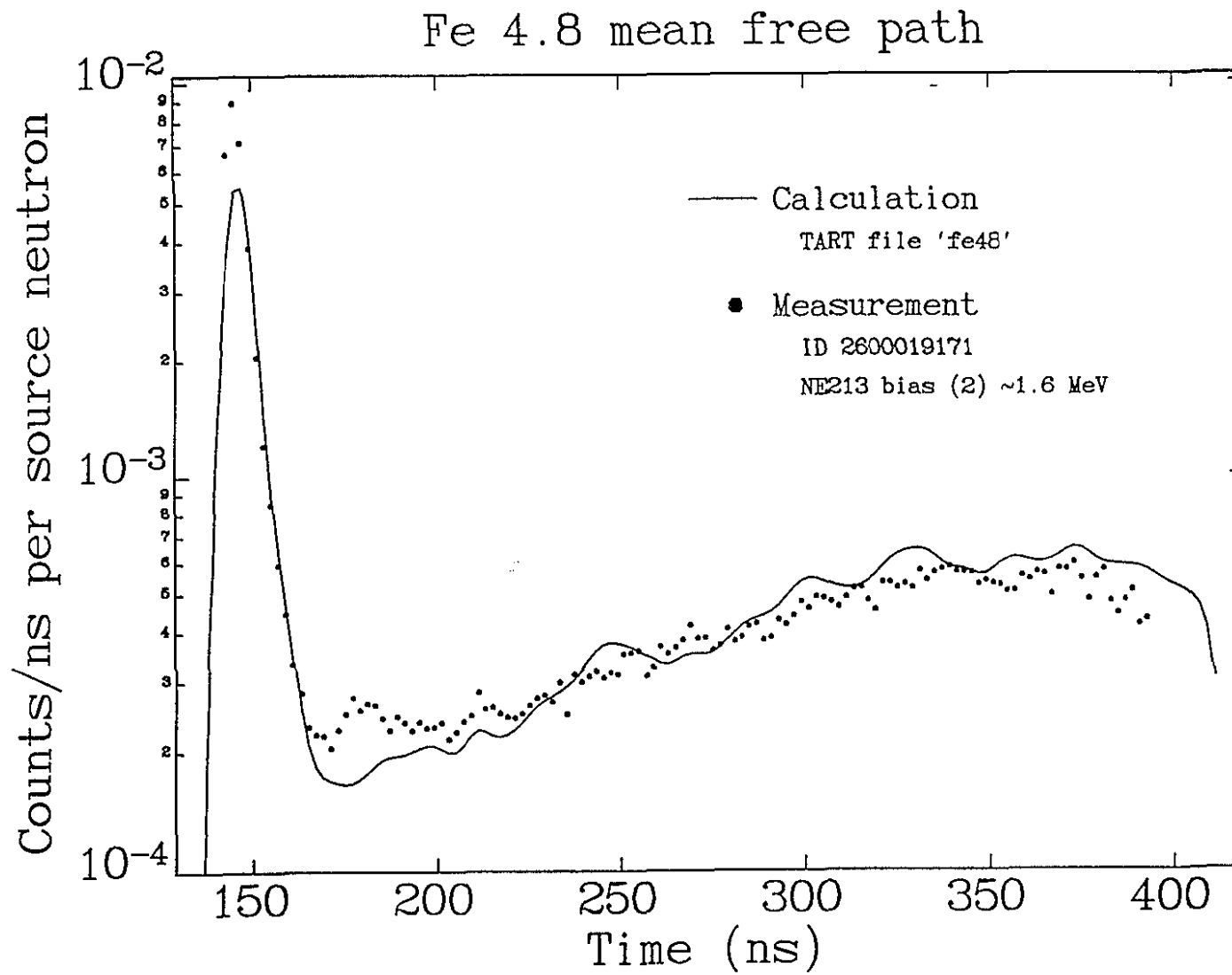


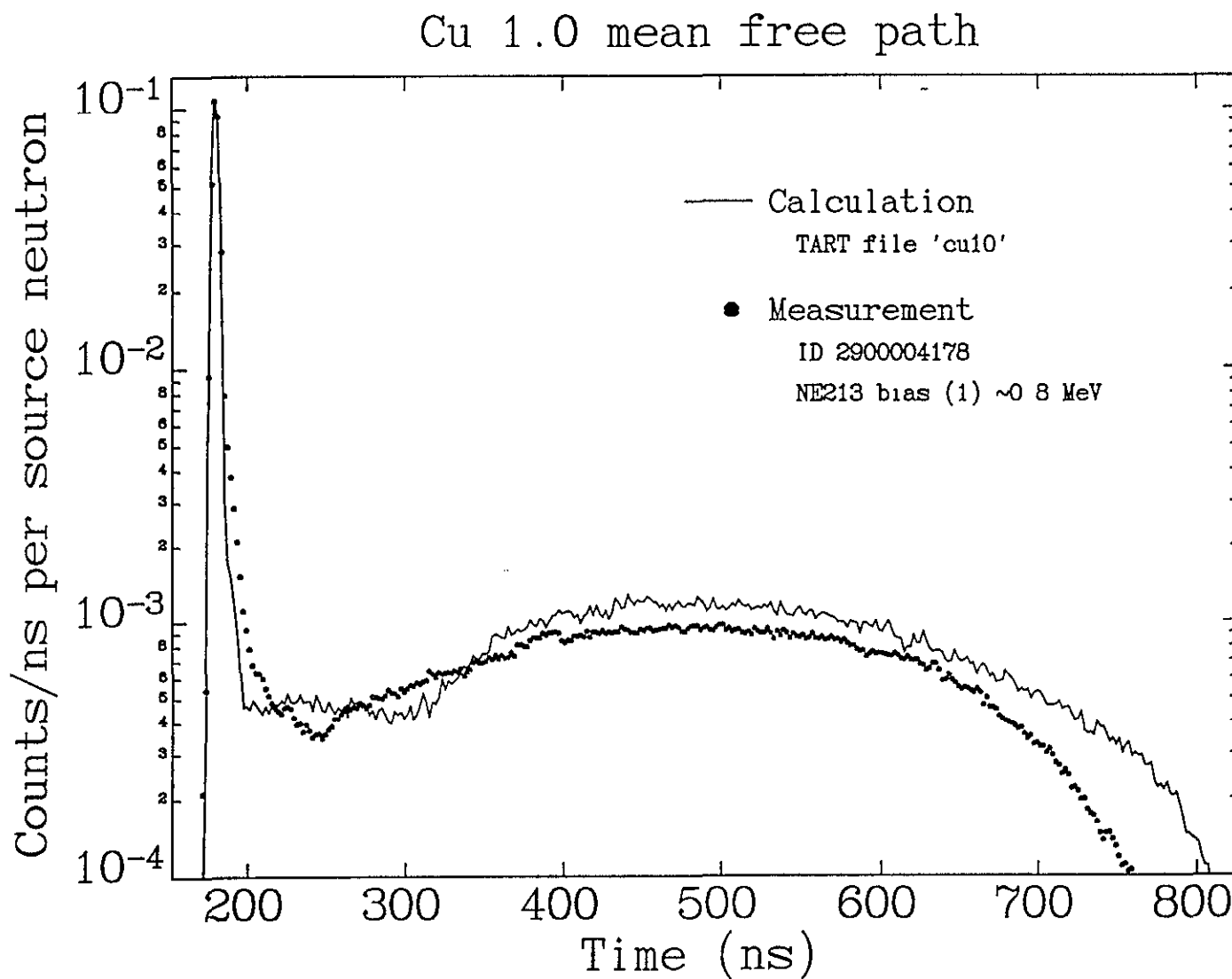




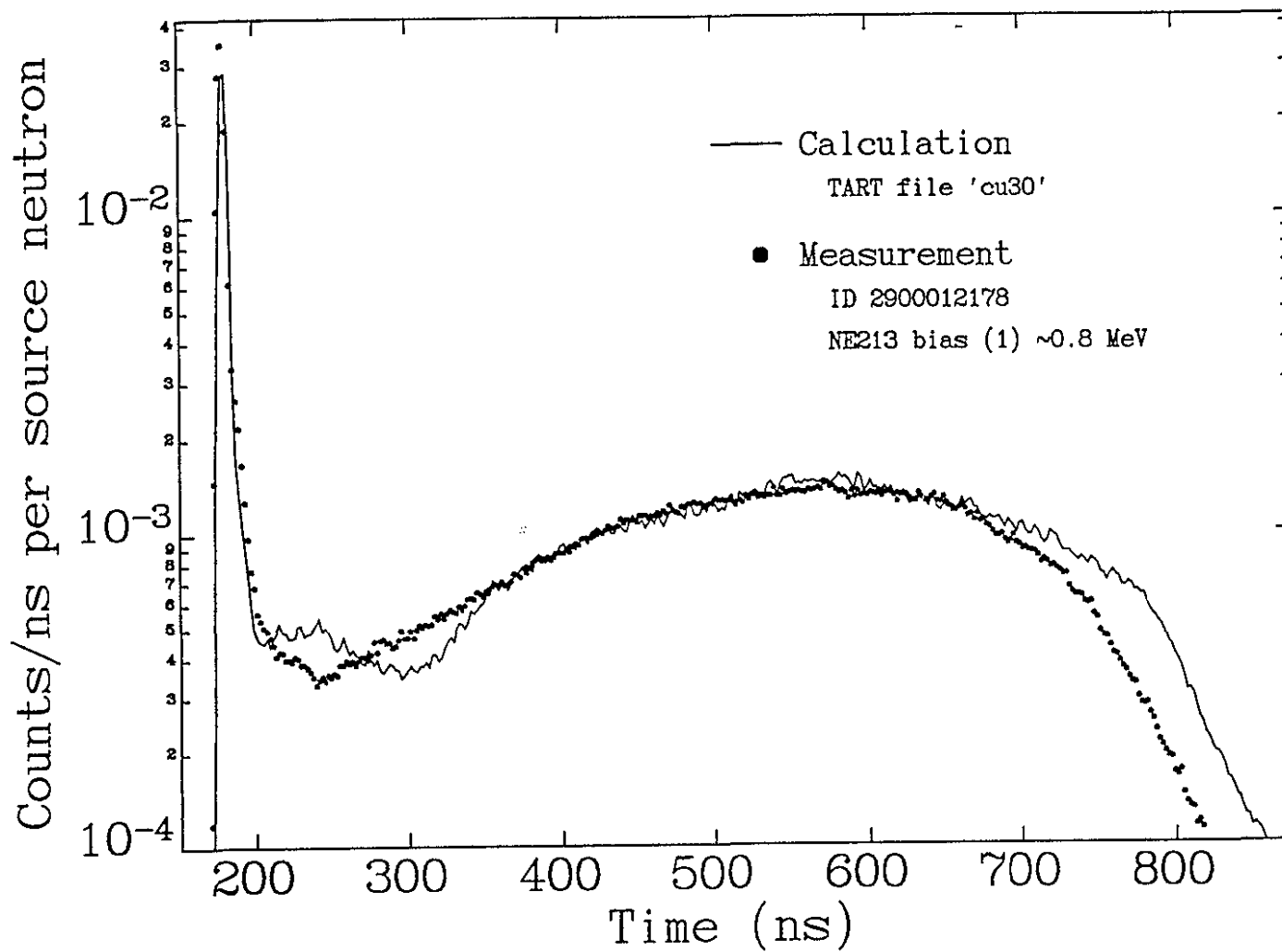
Fe 3.0 mean free path



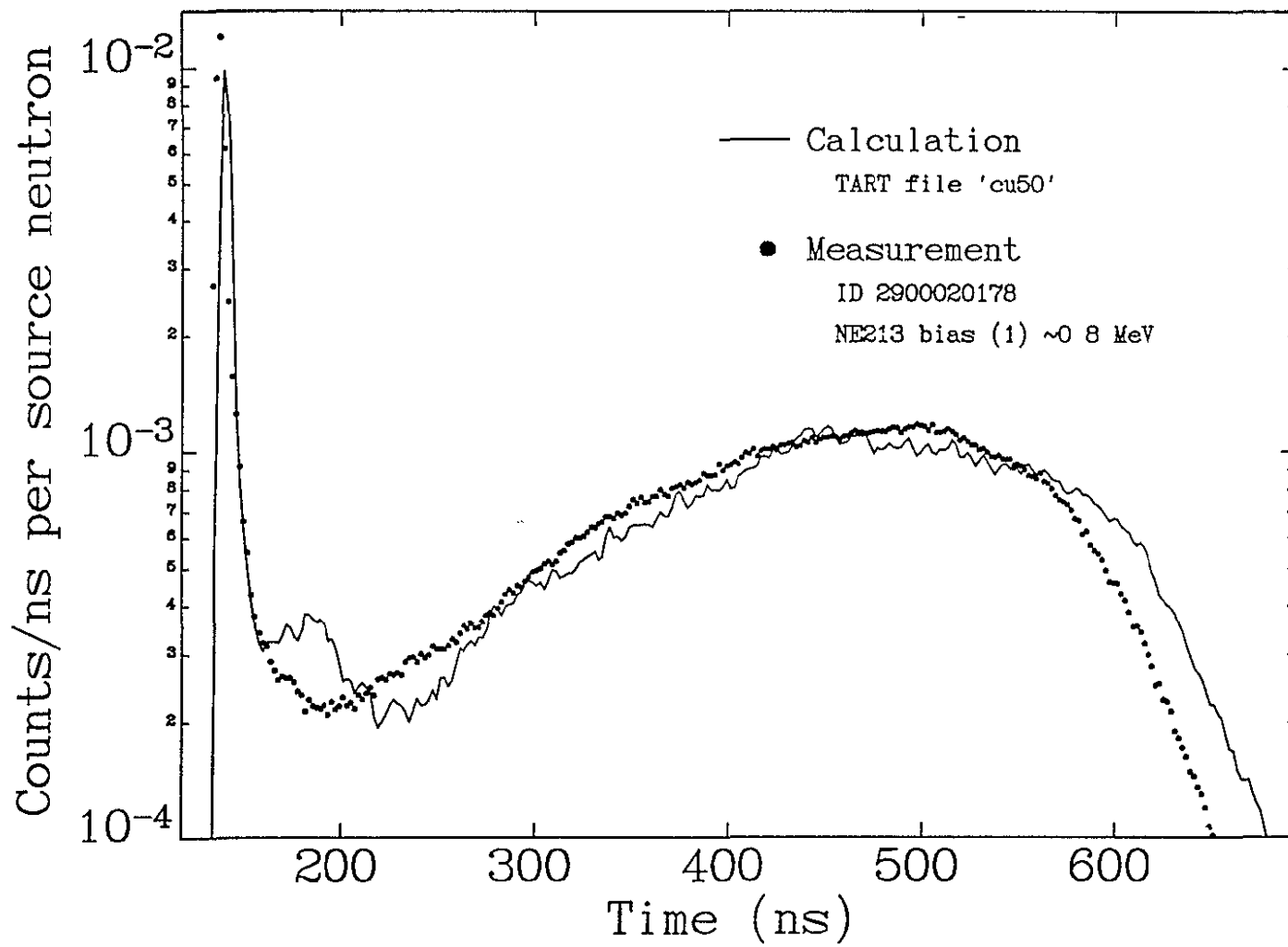


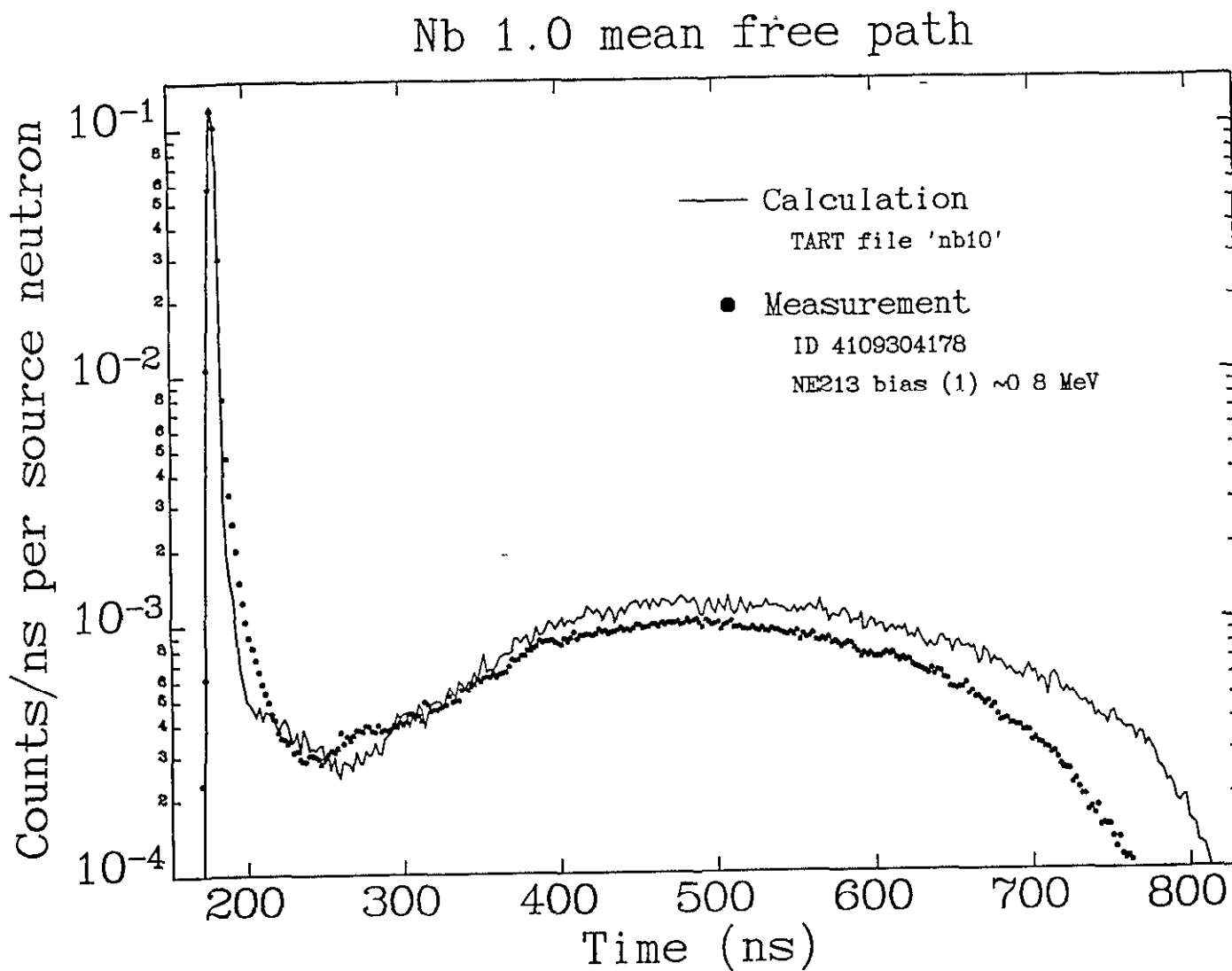


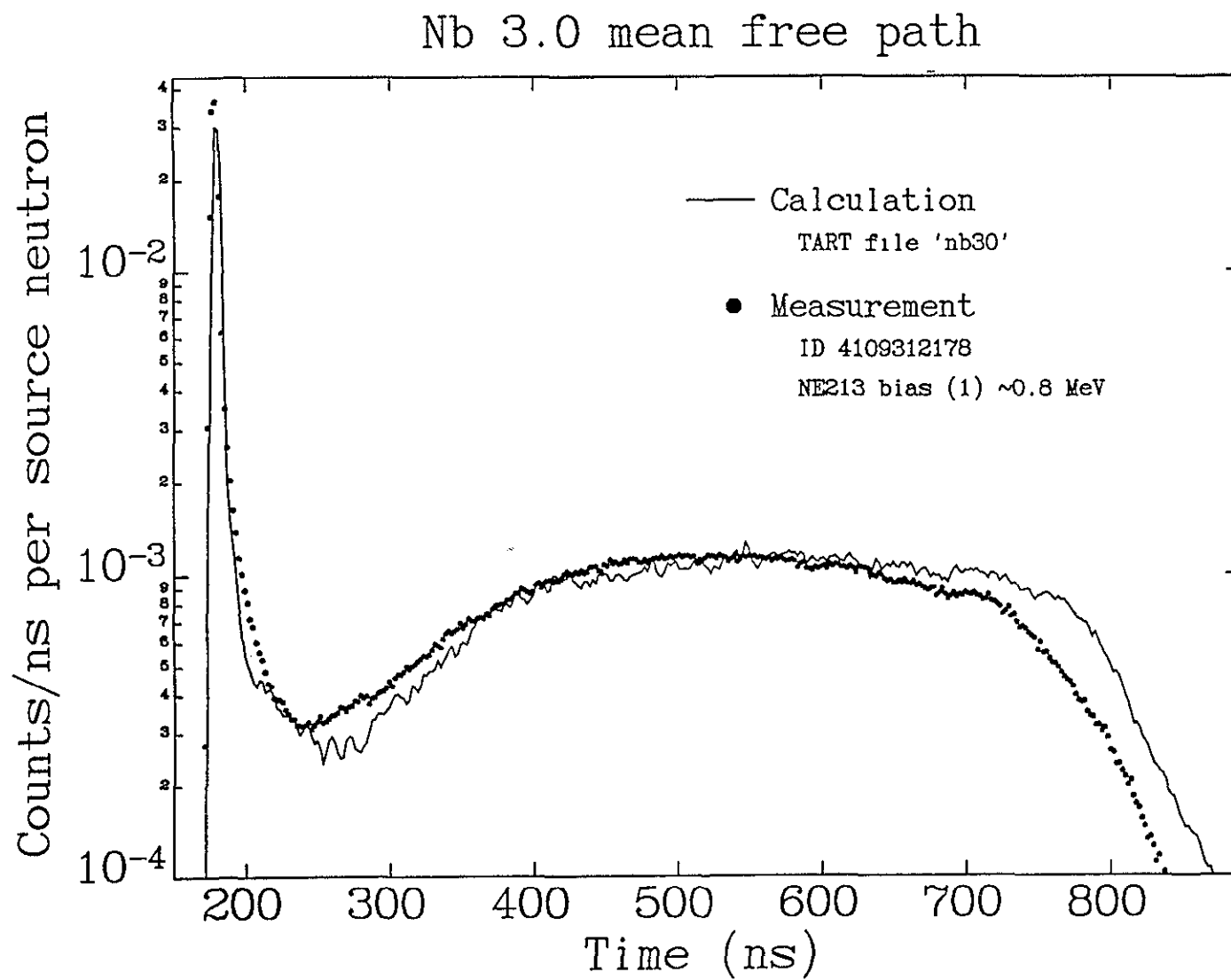
Cu 3.0 mean free path



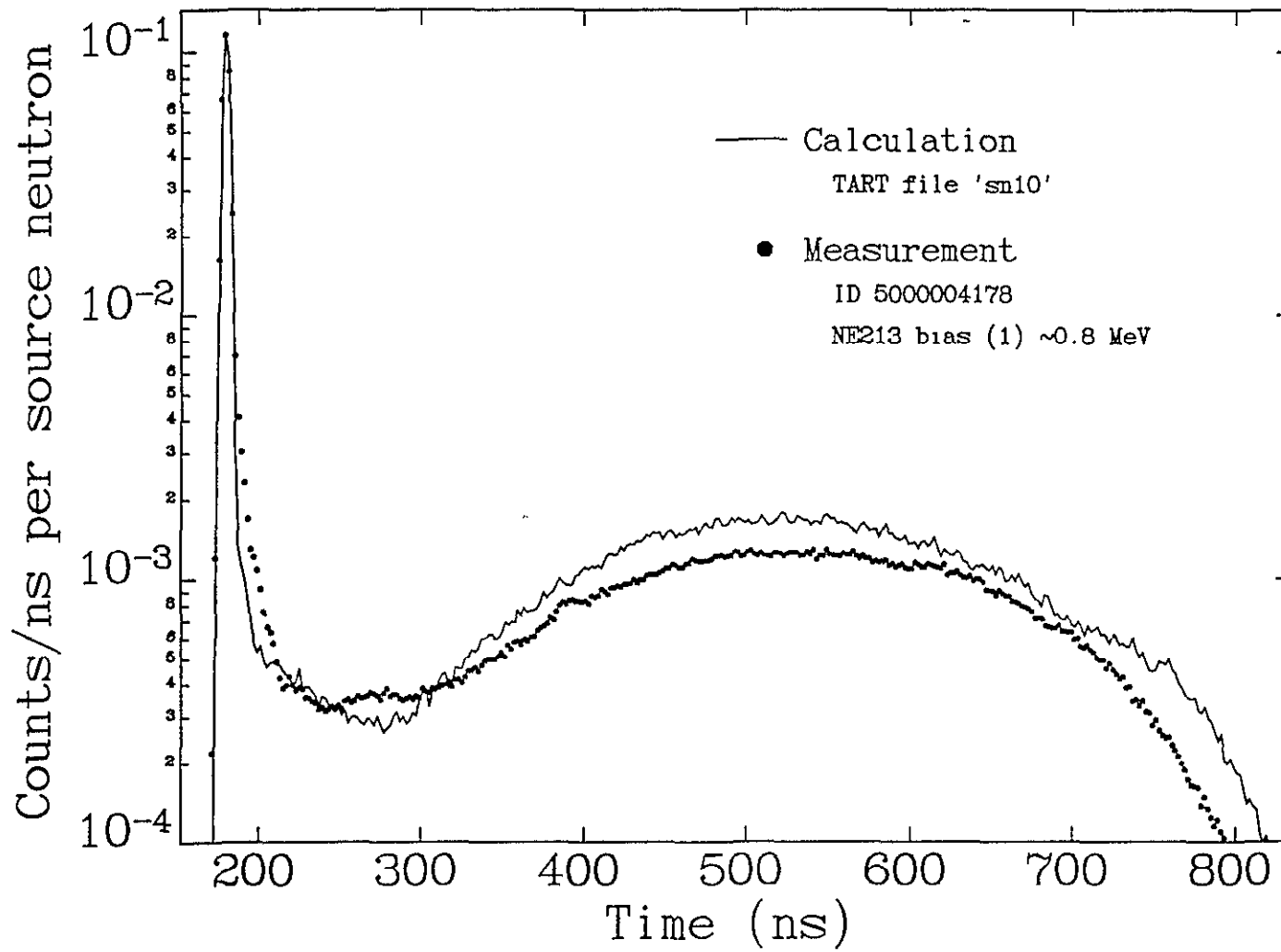
Cu 5.0 mean free path

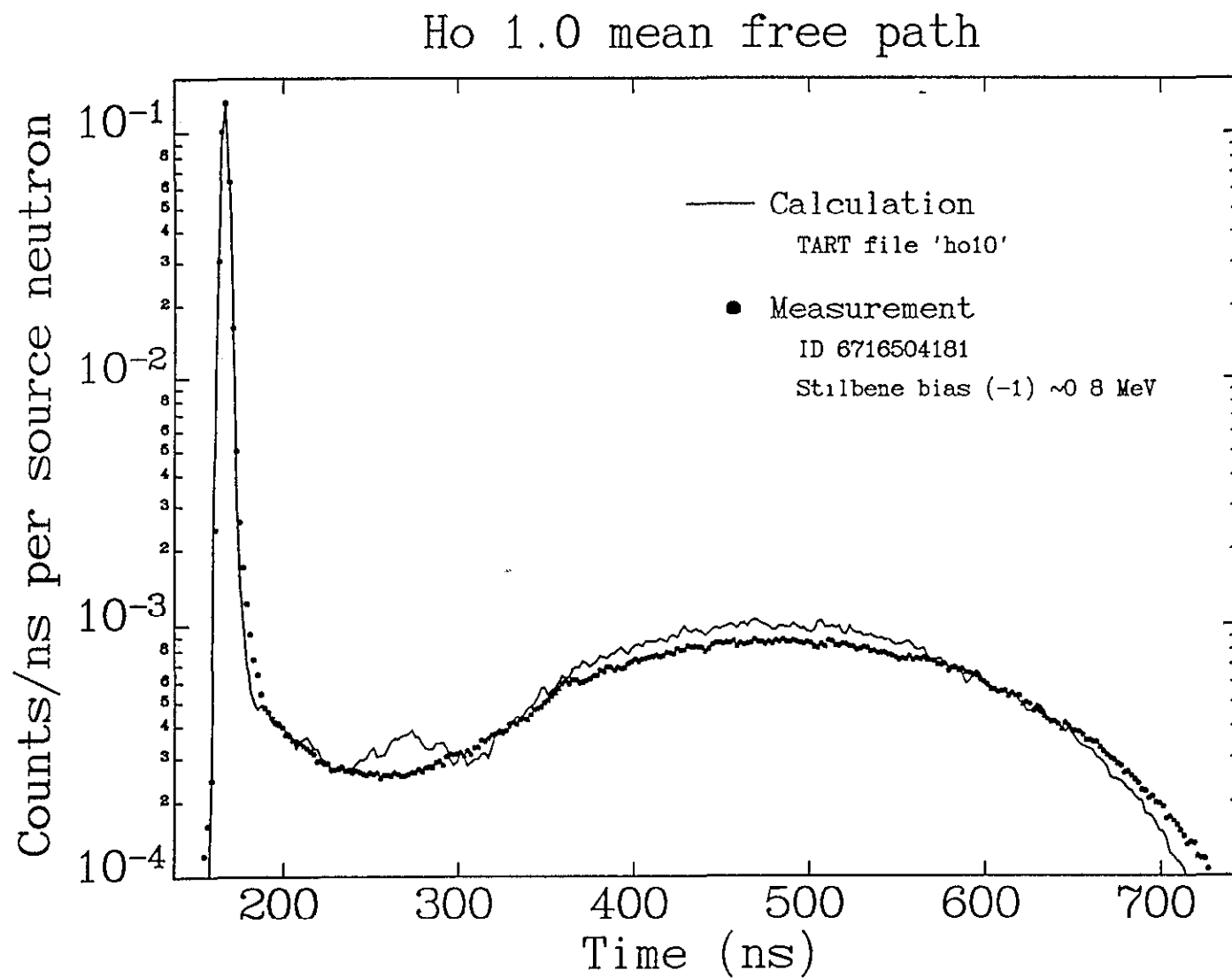




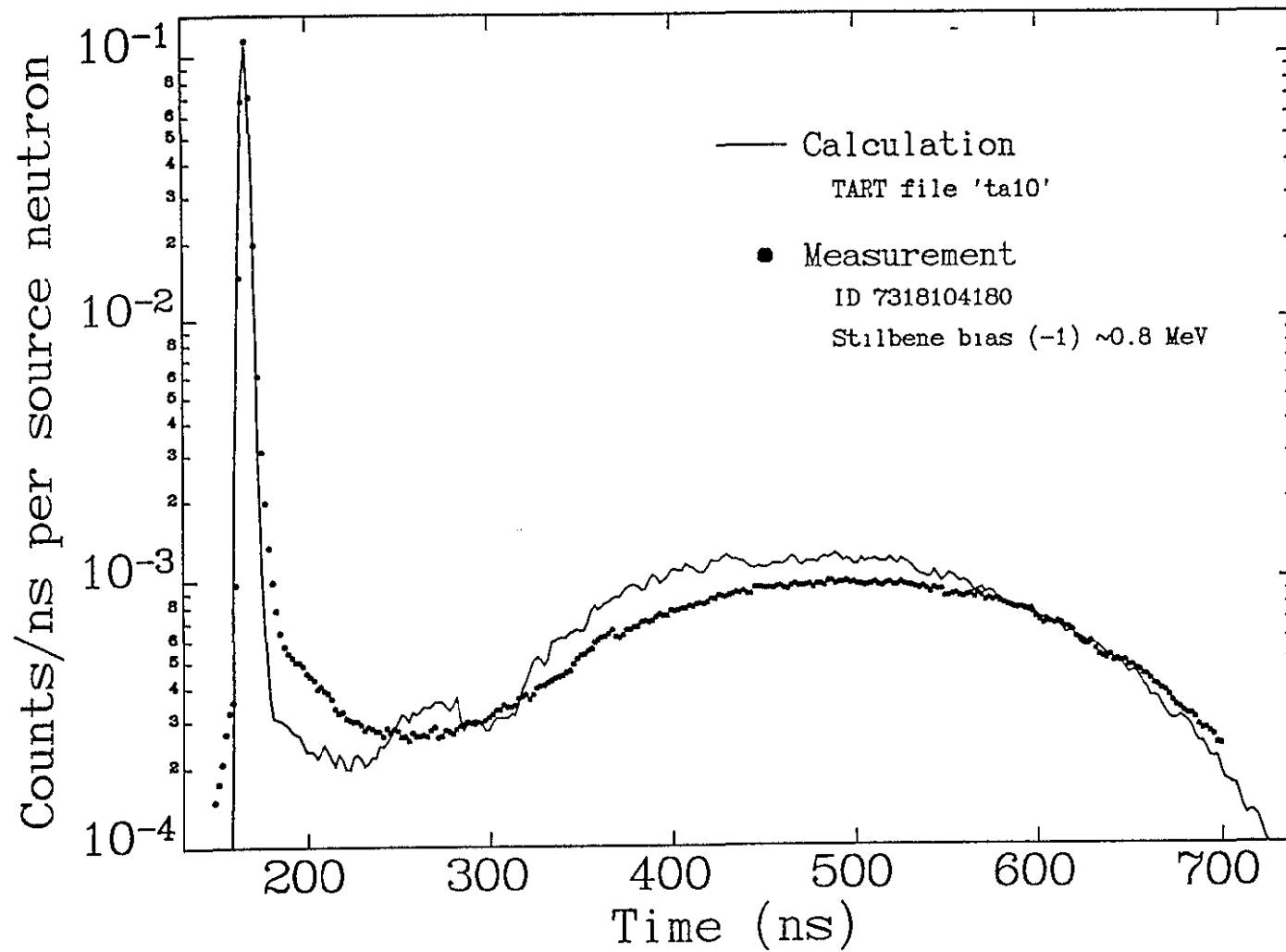


Sn 1.0 mean free path

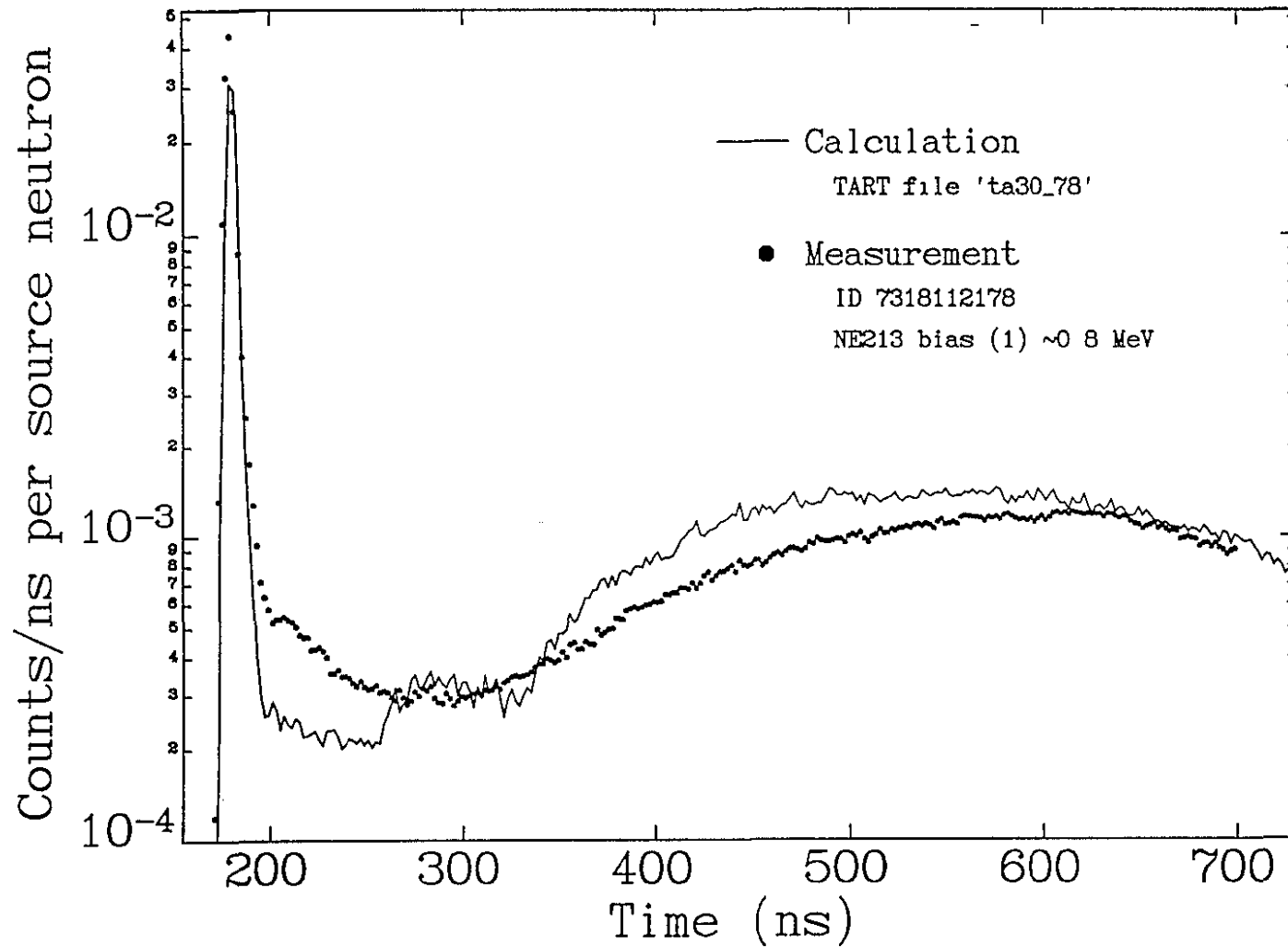




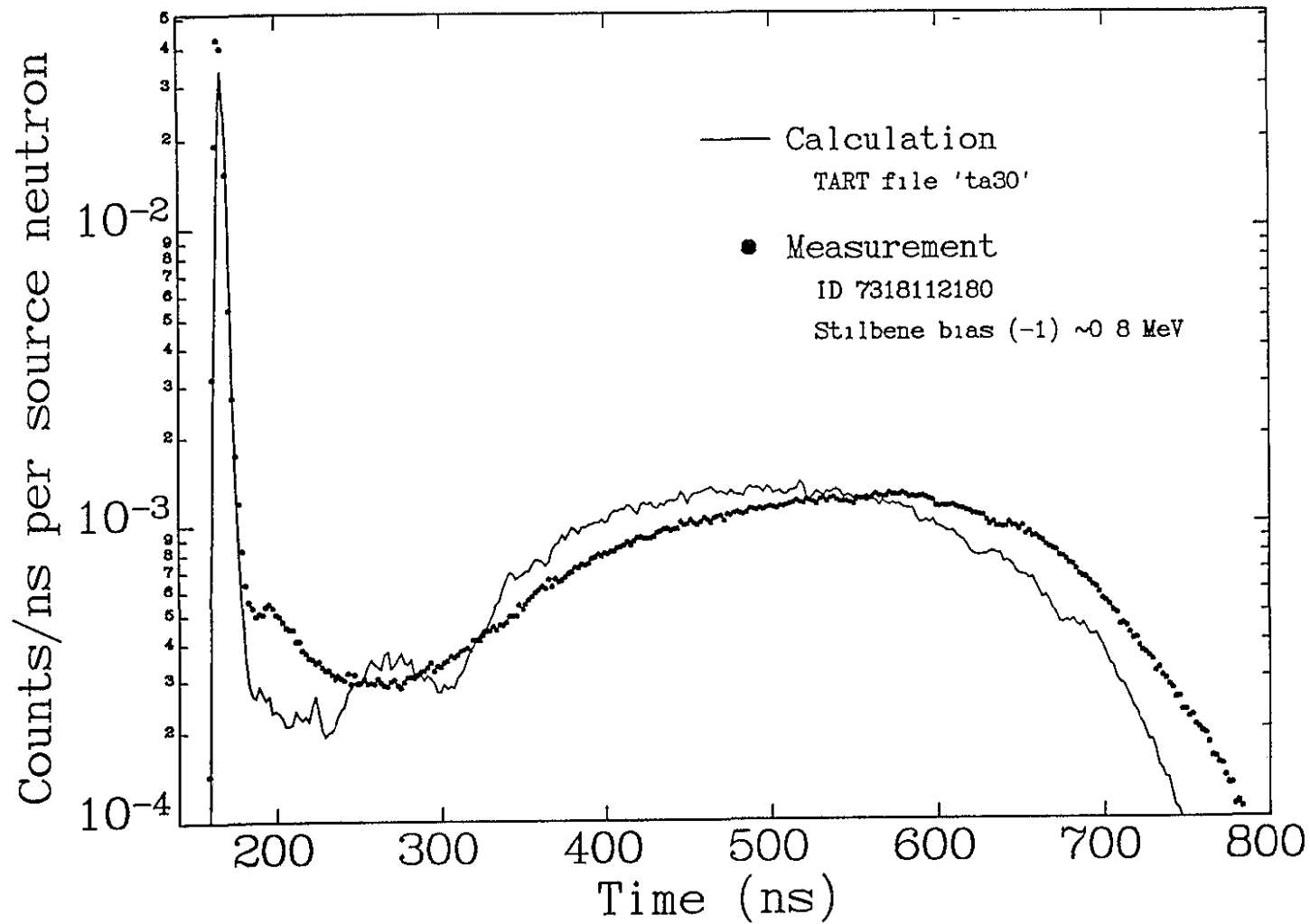
Ta 1.0 mean free path



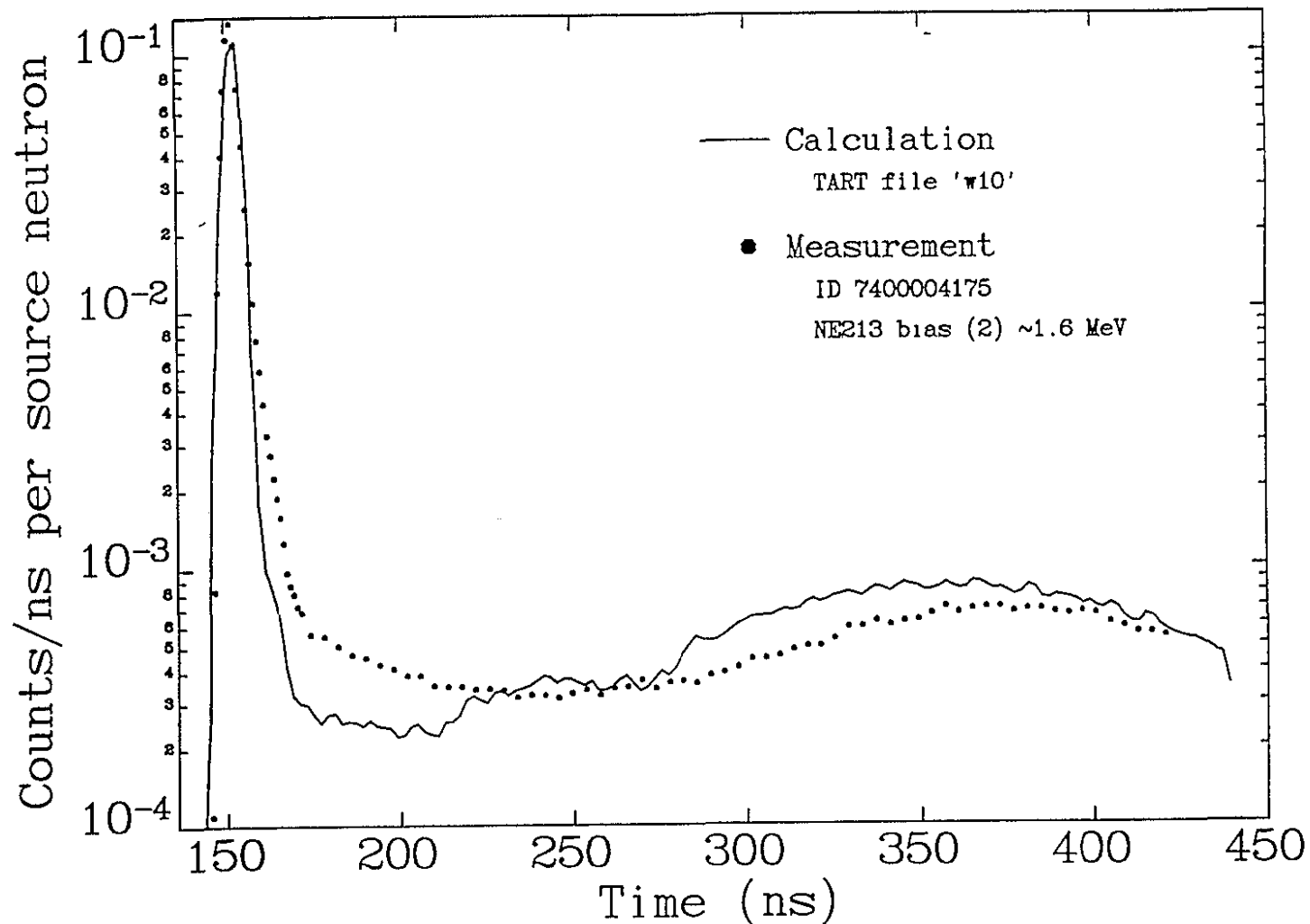
Ta 3.0 mean free path



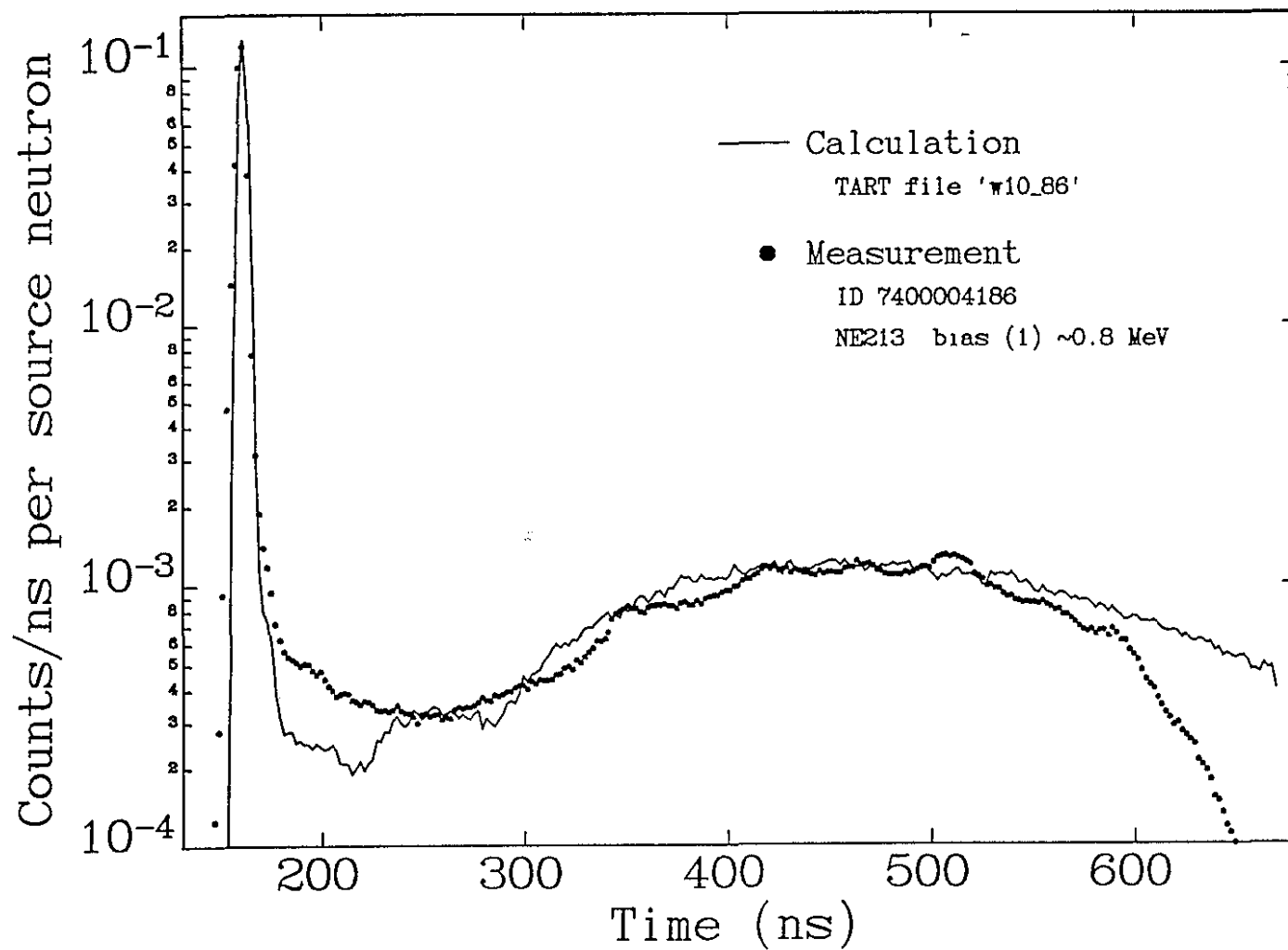
Ta 3.0 mean free path

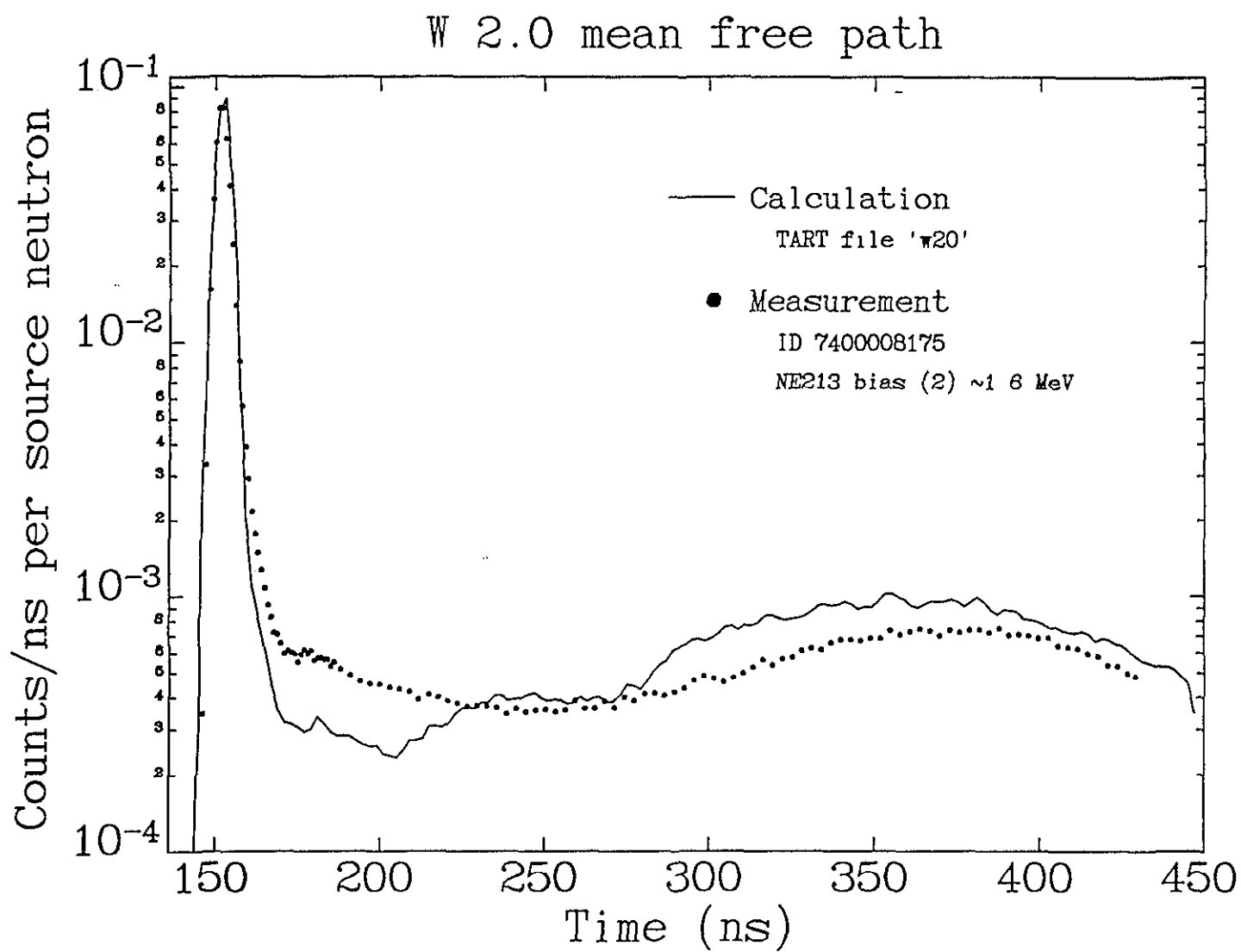


W 1.0 mean free path

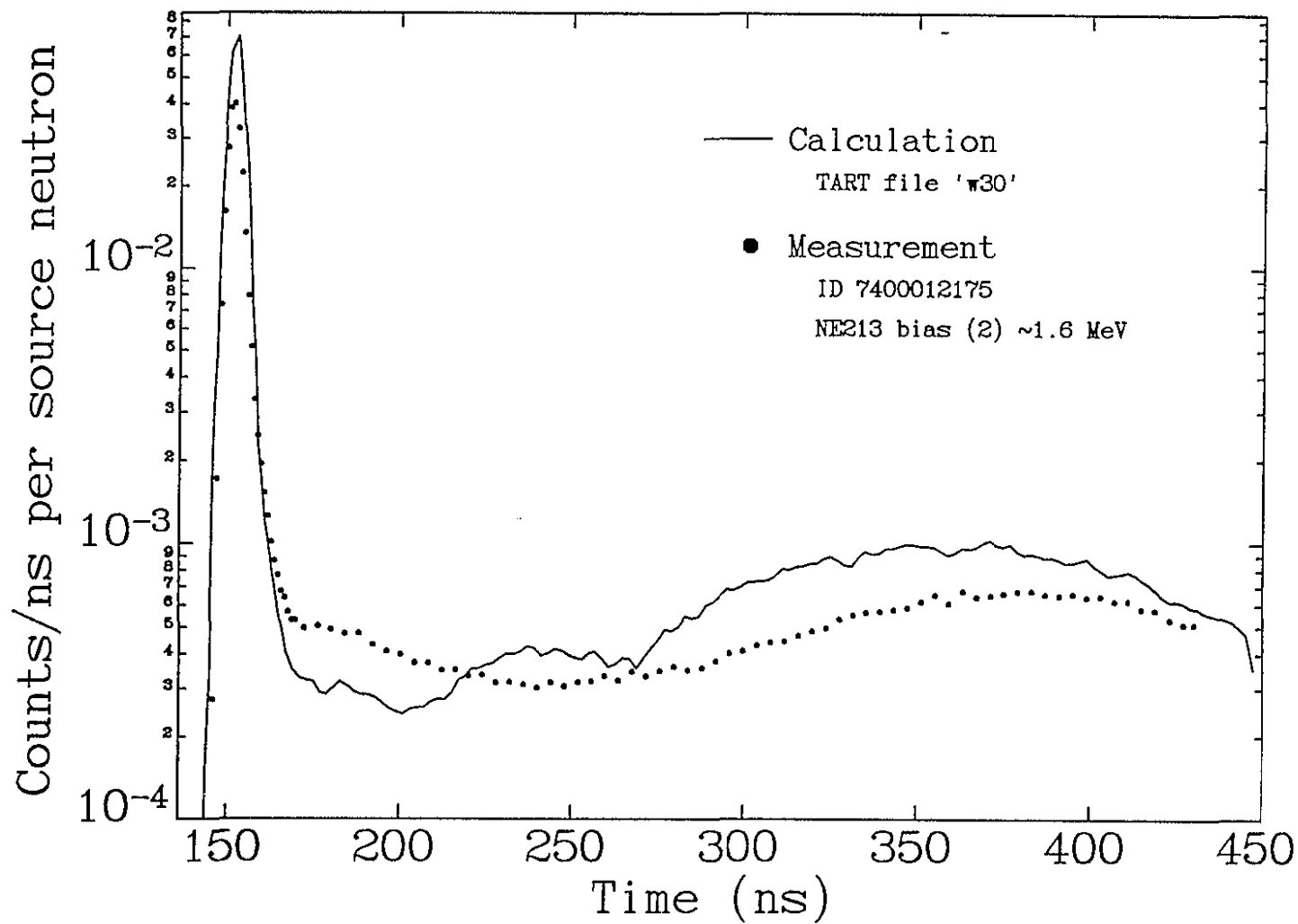


W 1.0 mean free path

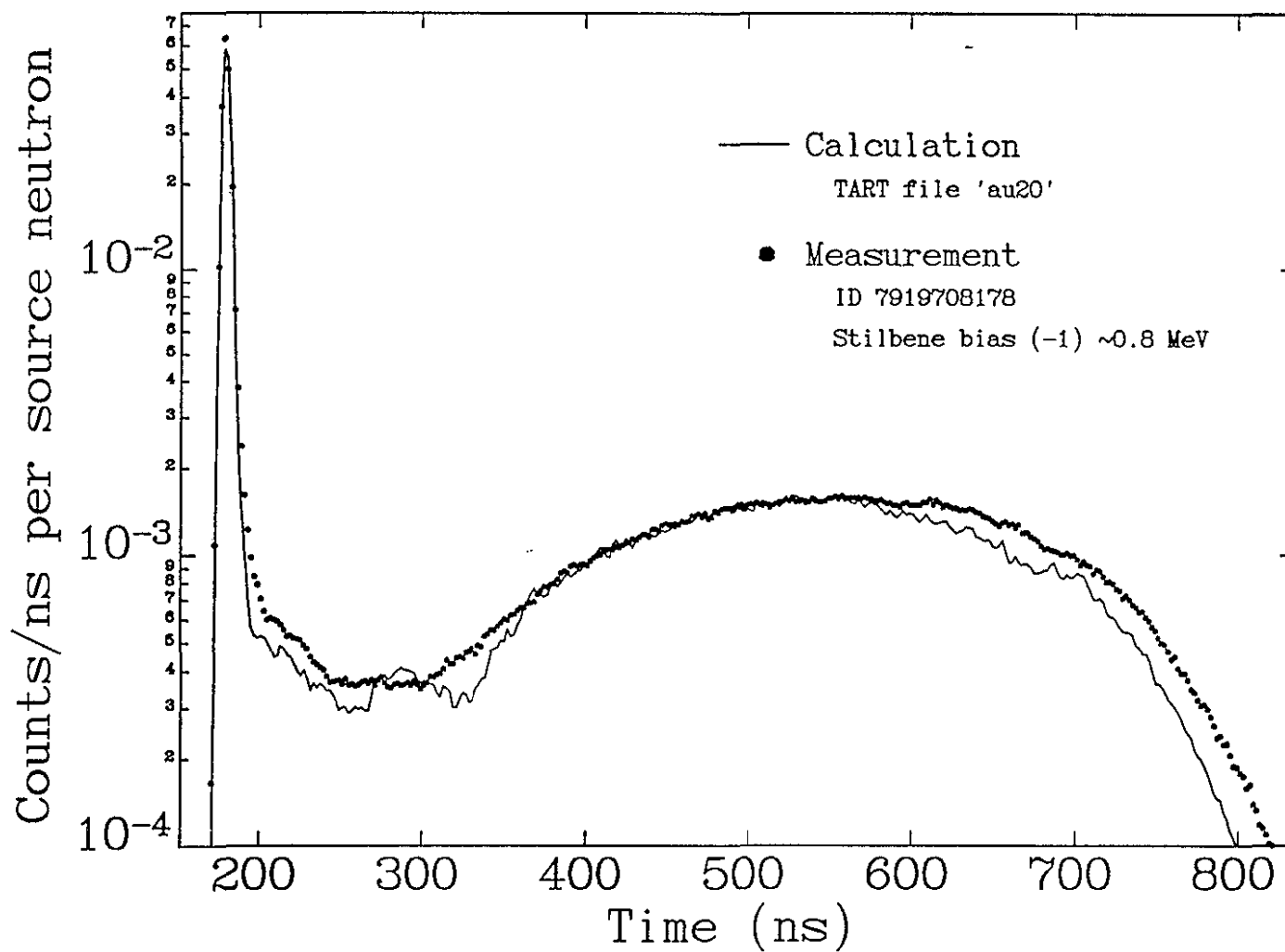




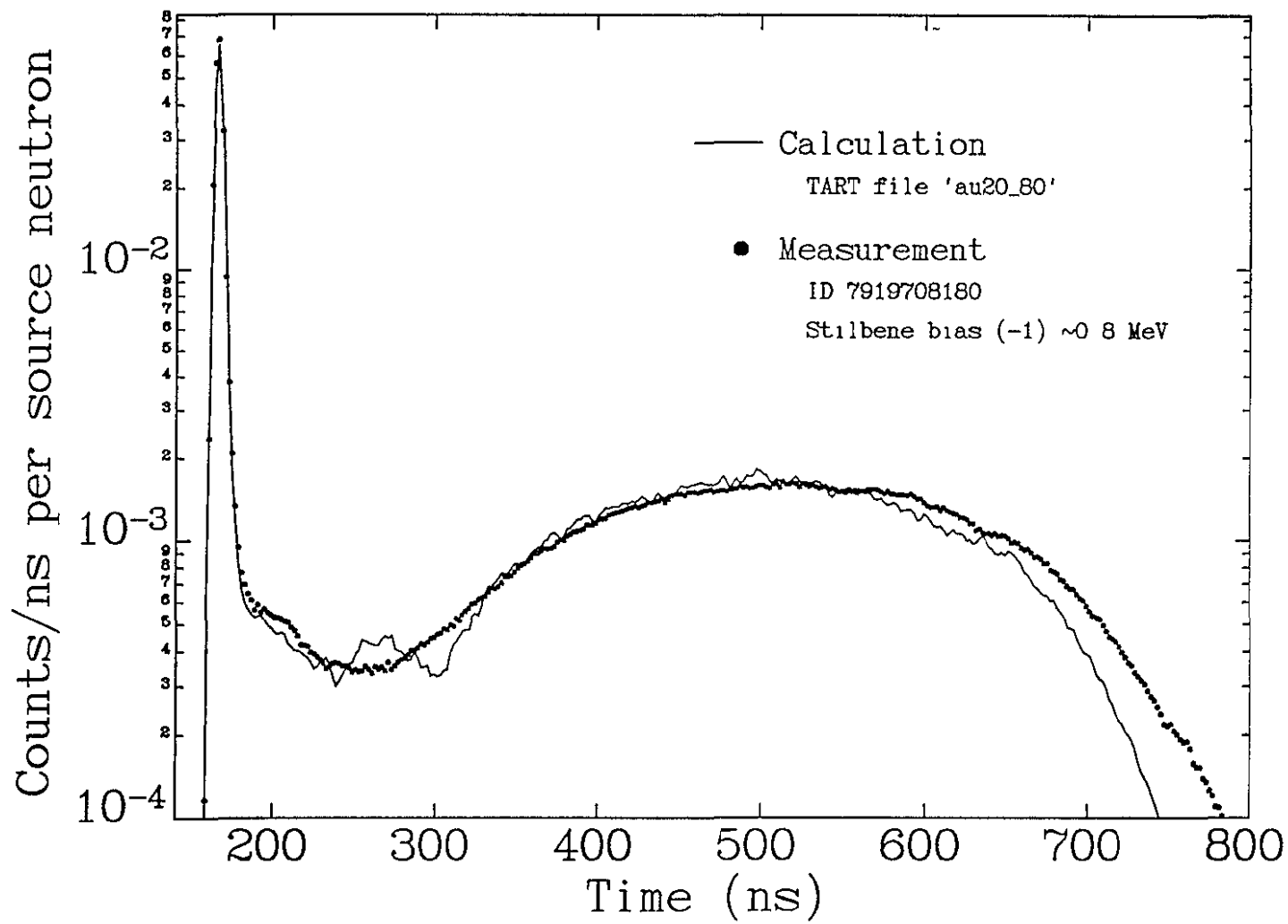
W 3.0 mean free path

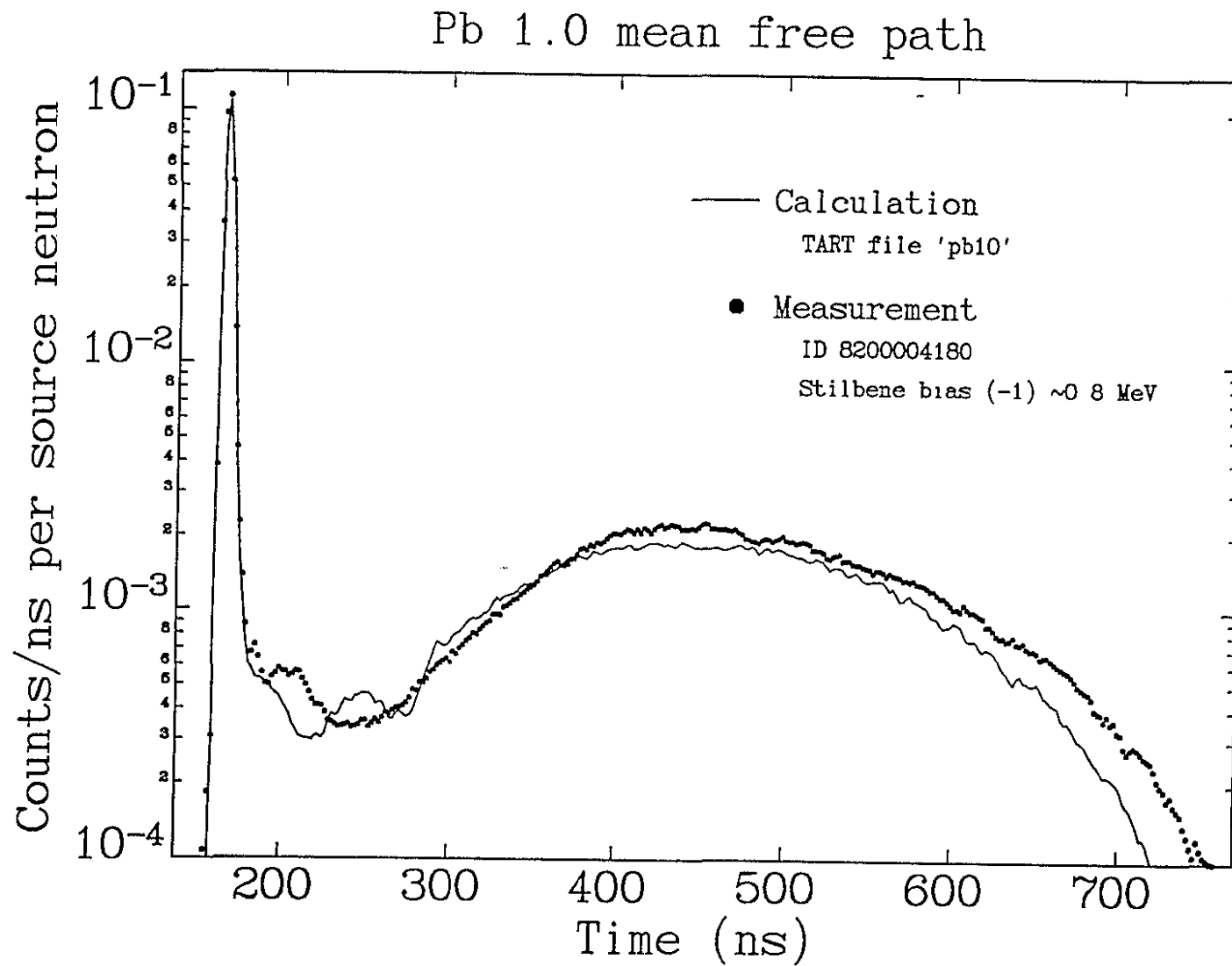


Au 2.0 mean free path

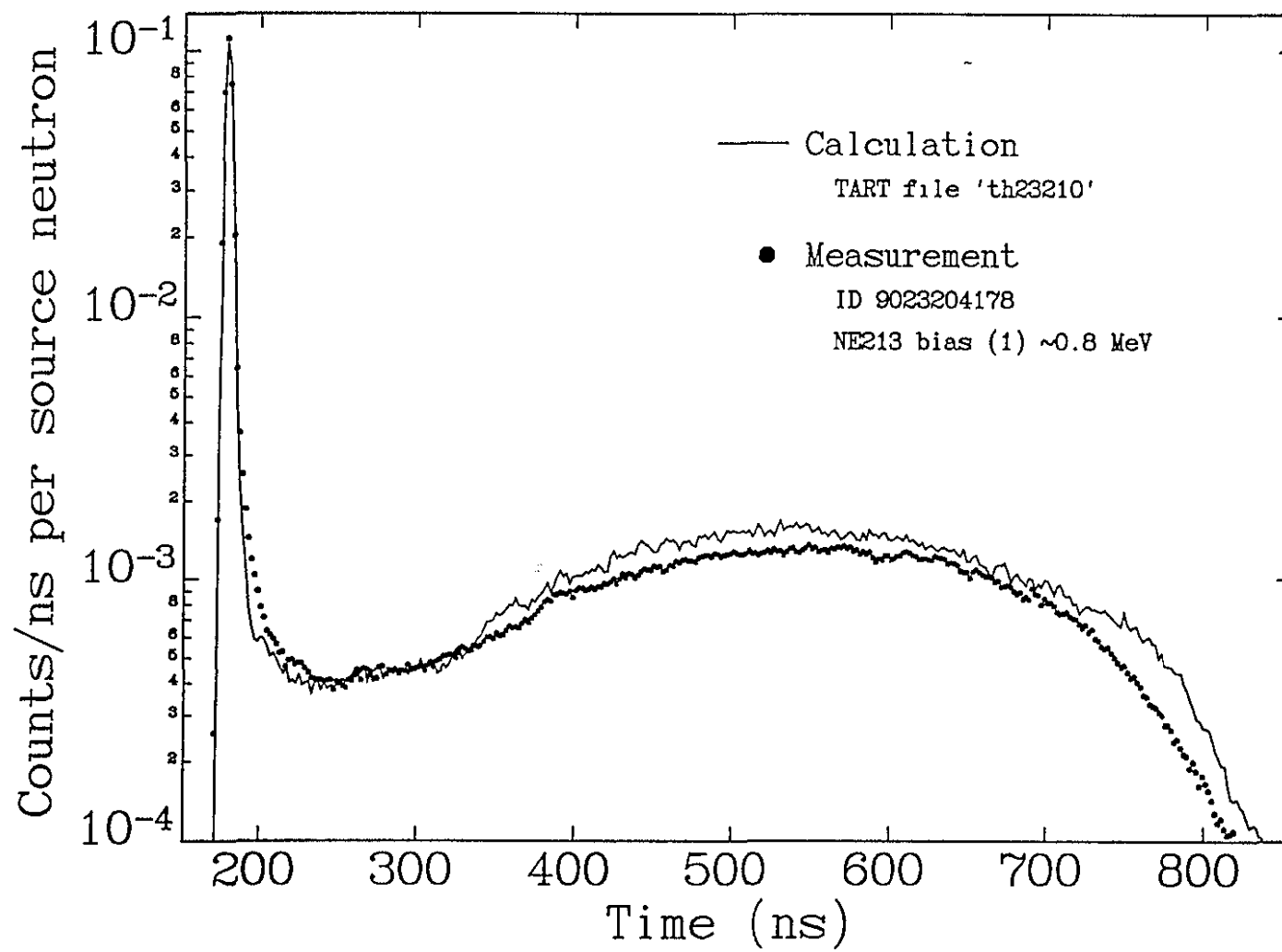


Au 2.0 mean free path

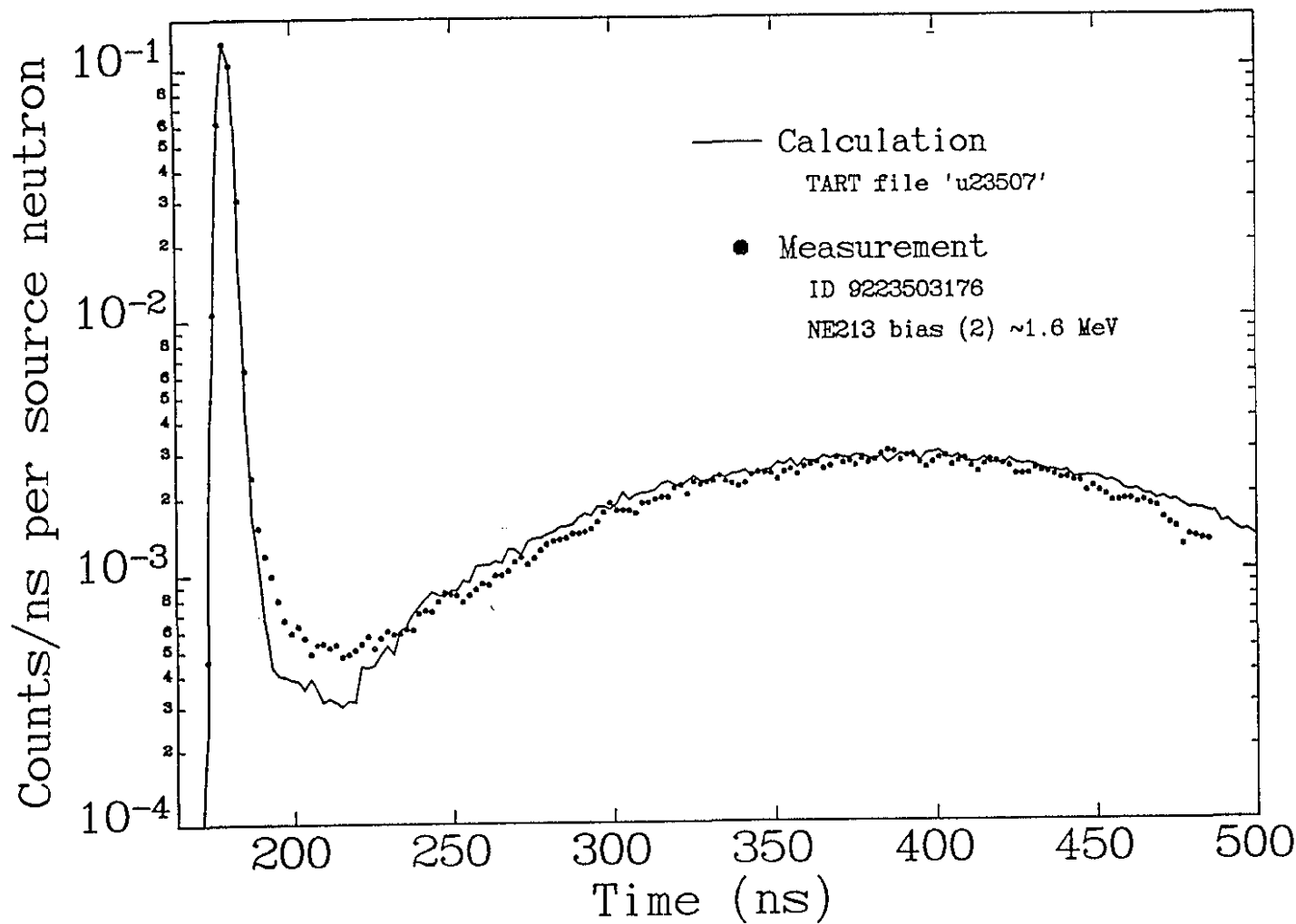


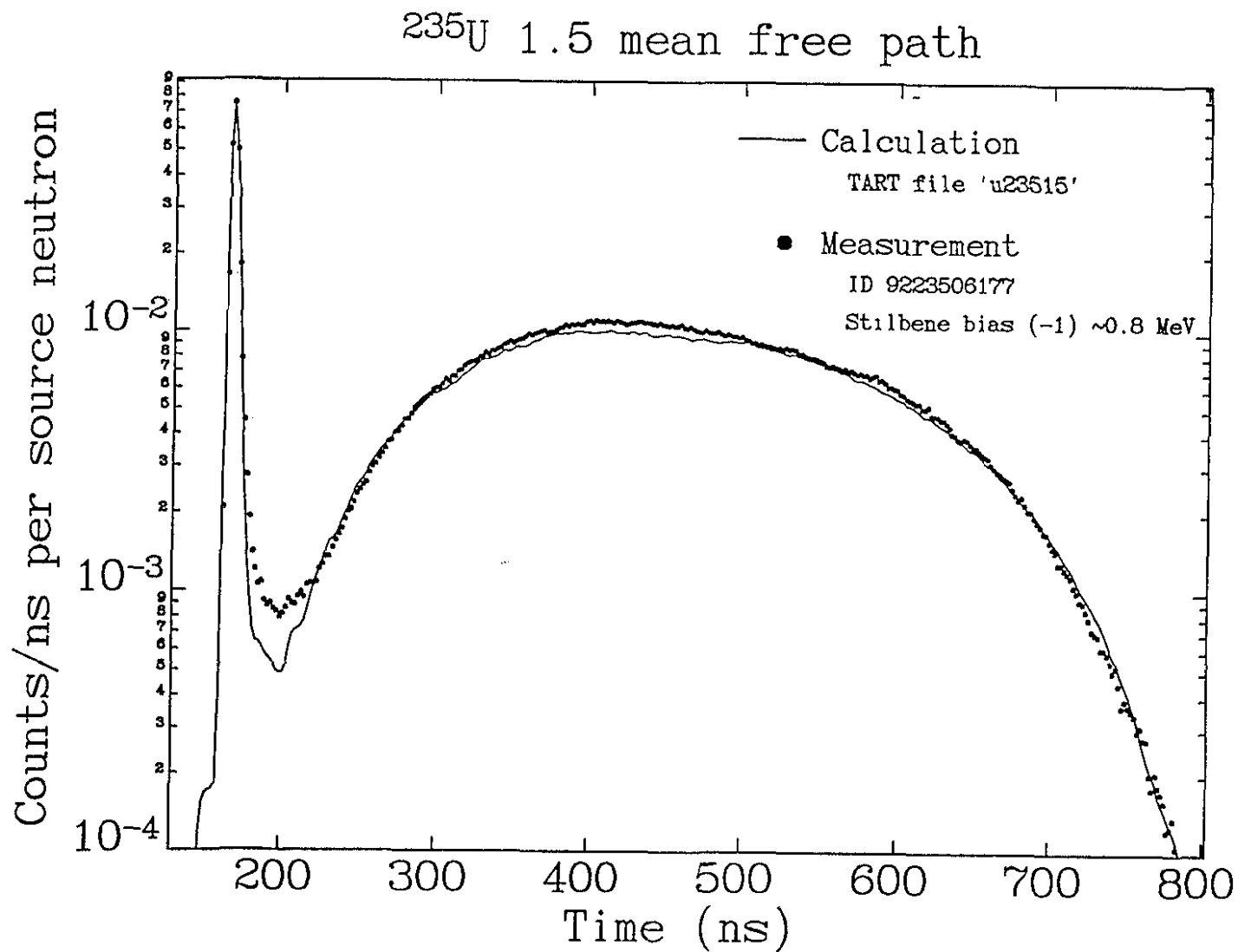


Th 1.0 mean free path

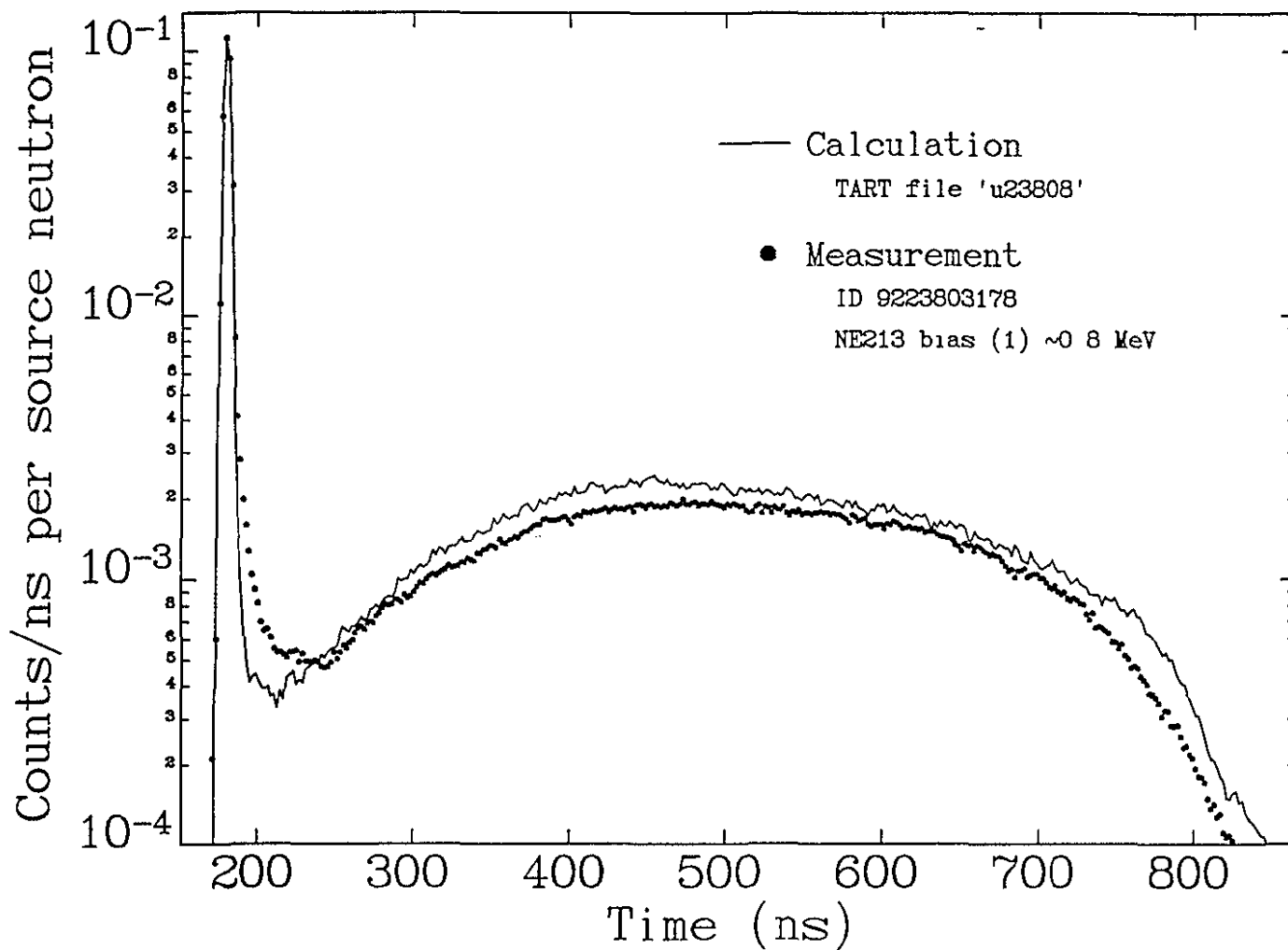


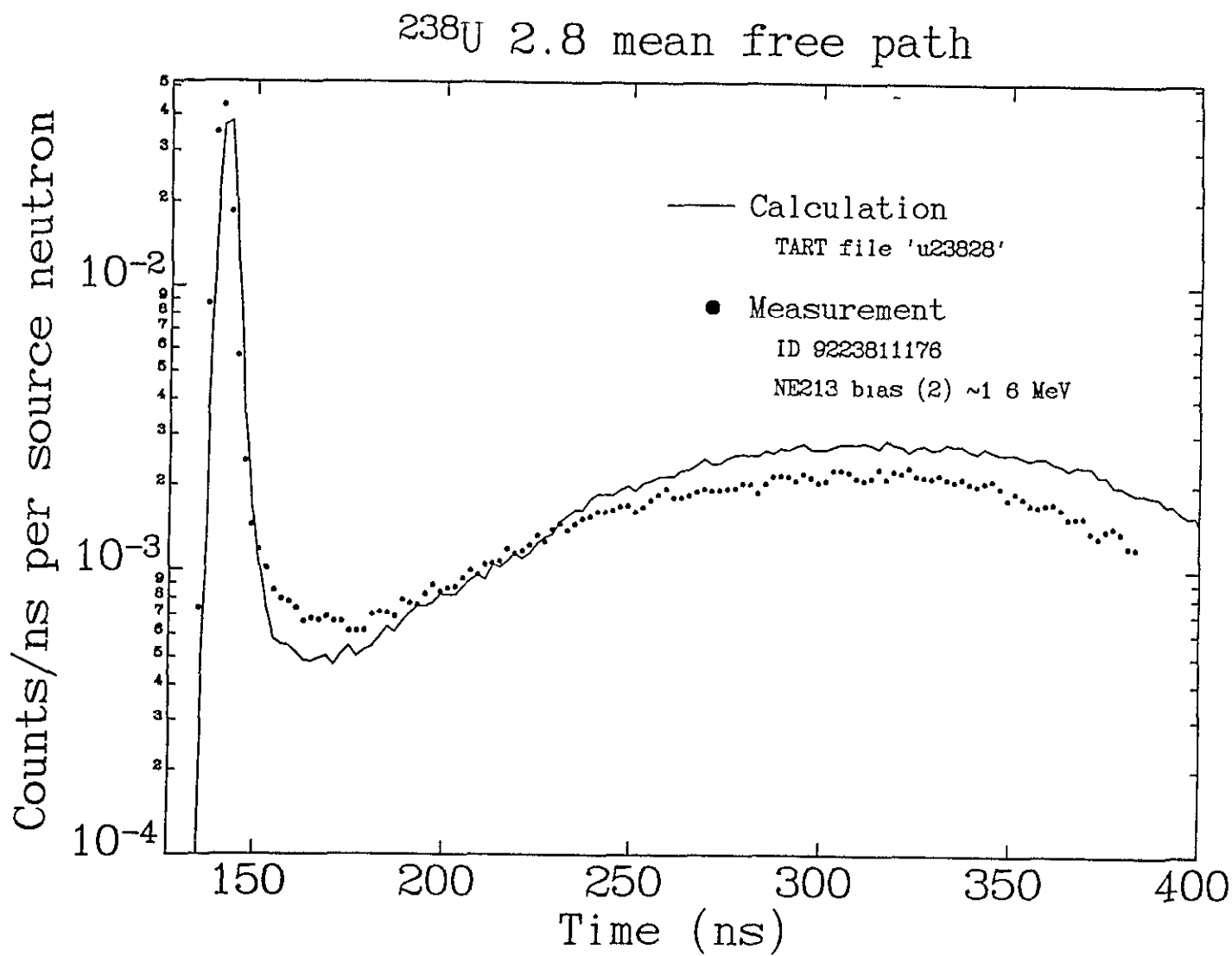
235U 0.7 mean free path



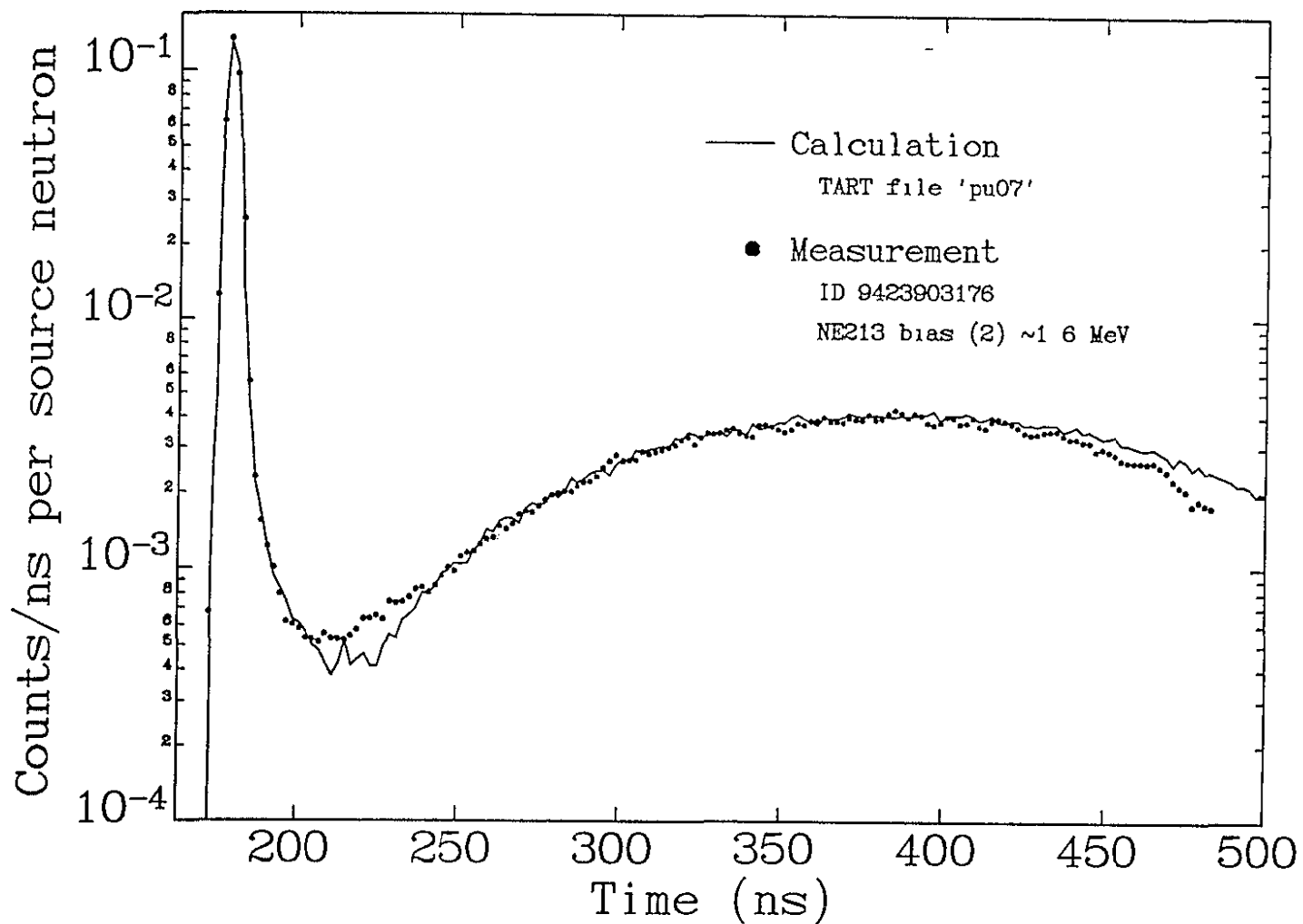


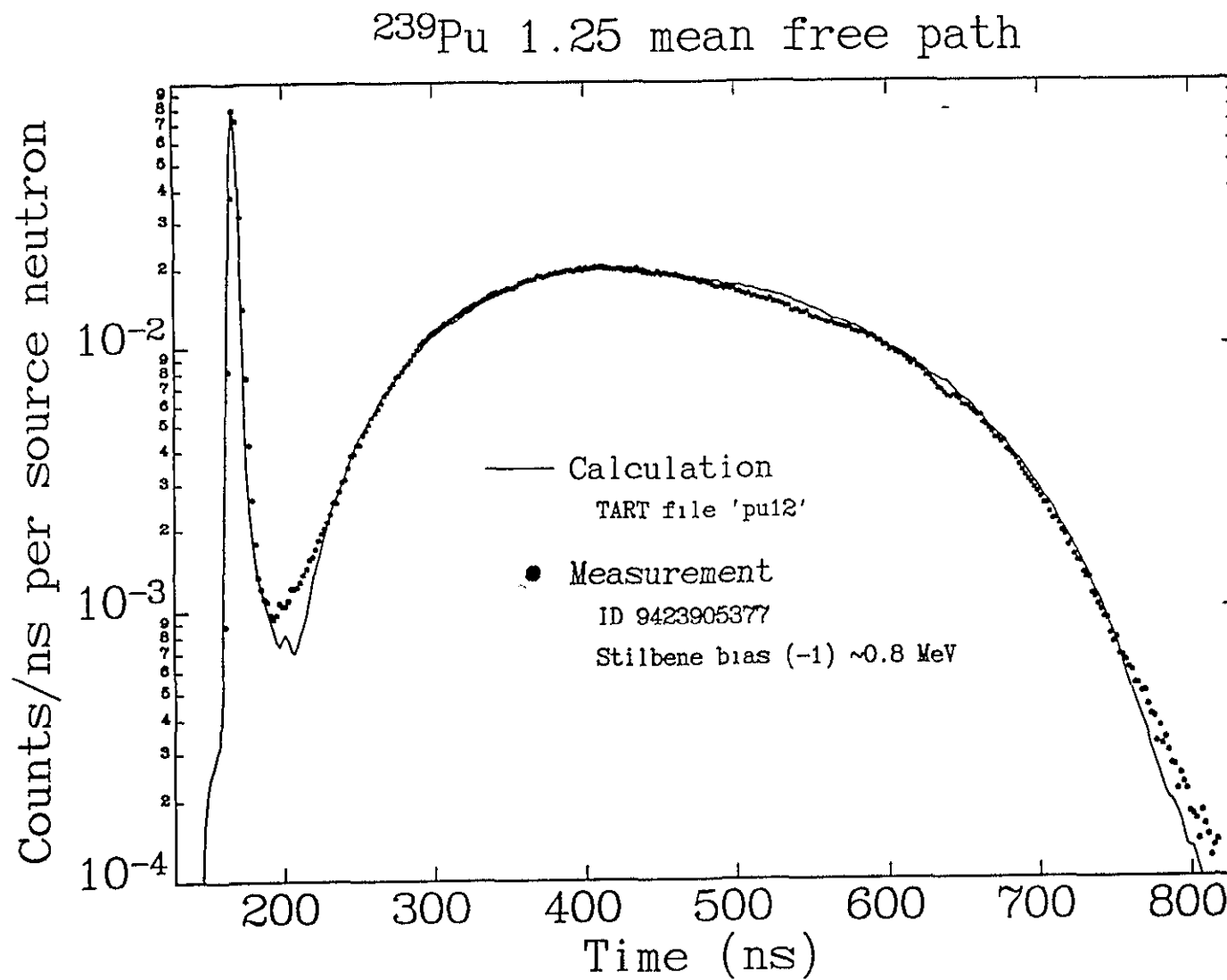
^{238}U 0.8 mean free path





^{239}Pu 0.7 mean free path





Technical Information Department • Lawrence Livermore National Laboratory
University of California • Livermore, California 94551